Structural development and interfacial engineering of hard coatings by HIPIMS

(High Power Impulse Magnetron Sputtering)

Dipl.-Ing. Jörg Ulrich Paulitsch

being a thesis in partial fulfilment of the requirements for the degree of a

Doctor of Montanistic Sciences (Dr.mont.)

Leoben, January, 2010

This thesis was supported by the Austrian Federal Government and the Styrian Provincial Government, represented by Österreichische Forschungsförderungsgesellschaft mbH and Steirische Wirtschaftsförderungsgesellschaft mbH, within the research activities of the K2 Competence Centre on "Integrated Research in Materials, Processing and Product Engineering", operated by the Materials Center Leoben Forschung GmbH under the frame of the Austrian COMET Competence Centre Program in cooperation with the Systec SVS Vacuum Coating Technologies GmbH.

Affidavit

I declare in lieu of oath, that I wrote this thesis and performed the associated research by myself, using only literature cited in this volume.

Leoben, January 2010

Jörg Paulitsch

Acknowledgements

First of all I want to express my sincerest gratitude and appreciation to Paul Mayrhofer who did not only give me the opportunity to carry out this PhD work but also provided me support and guidance I needed throughout the whole project. Thanks for being such a great teacher, and even more importantly, for becoming such a great friend in the last three years. I owe you a lot!

I thank Professor Reinhold Ebner and Dr. Richard Schanner, Researching and Managing Directors of the Materials Center Leoben Forschung GmbH, for giving me the chance to work on my PhD within the MCL Project.

I also want to express my gratitude to the Systec SVS Vacuum Coating Technologies GmbH for supporting my work and letting me use such an exceptional coating plant as the Z700. Special thanks to Markus Schenkel who spent a lot of time with me in front of the Z700 discussing the "Yes and No" of the HIPIMS deposition, for introducing me to the night-life of Karlstadt and showing me the right way how to snowboard.
I also extend my appreciation to Professor Wolf-Dieter Münz who supervised me in my first year in Karlstadt.

Many thanks to all the people from the Thin Film Group for making the last three years so enjoyable and so much fun for me. Special thanks to my office-mates Florian Rovere, Martin Moser and Richard Rachbauer for surviving the arctic temperatures in winter and for tolerating the permanent sound of the fan in summer; to Claudia Walter, Marisa Rebelo Figueiredo, Robert Franz and Rostislav Daniel for encouraging and acompanying me in trying new sport activities; to David Holec for letting me win at volleyball and tennis, never getting upset for teaching me how to speak English and especially for correcting my Styrian way of writing an English thesis. Special thanks to Joachim Haberl und Michael Zuber for supporting me throughout my studies and being friends for more than a decade. I also want to thank Martin Pfeiler-Deutschmann for being a college,

roommate and primarily for being a friend (you hit the bull's eye with the formulation in your thesis).

Furthermore, I want to thank my student co-workers Robert Hollerweger and Katharina Grundner for not quitting as soon as they had to prepare yet another TEM sample.

I also want to thank Reinhilde Stopar, Ulrike Egger, Simone Fink, Katrin Pongratz and Elisabeth Wolkenstein for watching over my financial in- and outputs and giving me a hand at all kinds of troubles, as well as all technical stuff who helped me within these three years.

Ganz besonders möchte ich auch jenen Personen danken die abseits der Arbeit und Universität immer für mich da waren: meiner Familie ein großes Dankeschön dass sie mich über die ganze 10 Jahre meines Studiums der Materialwissenschaften immer unterstützt haben und meiner Petra, die es trotz meiner stattlichen Erscheinung immer wieder geschafft hat mich aufzufangen und wieder aufzurichten wenn einmal nicht alles nach Plan verlief.

Contents

1 Introduction

One of the oldest and most important inventions of the mankind is the fabrication of a wheel, a circular device that is capable of avoiding sliding friction by a rolling movement around its axis. Nevertheless, only since Nikolaus August Otto, the wheel has been used as a part of transportation systems which people now can hardly imagine to live without, like cars, bikes and trucks. As the car tuning, the race sport or the forwarding community demonstrate, the development of engines directs towards an increased power-output combined with reliability and longevity.

The material surface and its performance are of a great importance since any interaction between two parts, e.g. a piston and a cylinder, takes place via their surfaces. Consequently, surface modifications are needed to achieve materials with demanded requirements for special technical applications like in the automotive industry. One possibility to achieve increased surface performances is to coat materials (called substrate) with thin films. The advantage of a film deposition is the combination of often quite different properties of the film and the substrate, e.g. hard corrosion and wear resistant films in combination with ductile, shape-giving substrates. Such protective films are often based on transition metal nitrides and/or carbides which extend the life-time and increase the efficiencies of e.g. high speed steels or cemented carbide tools.

The development and improvement of various deposition techniques to increase the life-time of machining parts, tools, and engineering components in automotive applications is the focus of many investigations. The coatings are usually produced by deposition from the gaseous state by evaporation of a certain material. The two common techniques are the chemical vapour deposition (CVD) and the physical vapour deposition (PVD) technique. Both of these techniques have their advantages and disadvantages [1-4]. This thesis is focusing on the PVD deposition.

The PVD techniques can be divided into two main systems, which are the direct current magnetron sputtering (DCMS) and arc evaporation. They differ in several aspects like the system arrangement or the plasma generation. Nevertheless, the main difference between

sputtering and arcing is the ionization density of the sputtered species: up to ~ 95 % during the arc evaporation compared with < 2 % during the sputtering [4; 5]. The major drawback of the arc deposition is that a large amount of macro-particles (droplets) from the target material can be easily formed due to the high energies and temperature loads in the arc spot. These are subsequently incorporated in the coating and thereby can decrease its performance. In sputtering, the particles are ejected by an ion bombardment of the substrate material and hence droplet formation can be avoided. On the other hand, the low ionization rate during the sputtering reduces the growth kinetics which can lead to coatings with deteriorated mechanical and tribological properties.

The high power impulse magnetron sputtering (HIPIMS) technology, which utilizes high power densities during magnetron sputtering, combines the advantages of the arc evaporation and sputtering, a high ion density without droplet formation. Therefore the HIPIMS technique shows high potential for growing superior quality hard coatings with increased wear and corrosion resistance for engineering components like in the automotive industry. Nonetheless, the low deposition rate of the HIPIMS process, usually around one third compared with DCMS, decreases the potential for industrial applications due to prolonged deposition times and increased operation expenses.

Hence, during this thesis the influences of the HIPIMS technology on the interlayer development, coatings structure and resulting properties, as well as possibilities to increase the deposition rate by depositing multilayer coatings using a simultaneous HIPIMS/DCMS deposition technique will be investigated and optimized for the usage in industrial applications. The first part of this thesis gives an overview on the theoretical background of the film deposition and an overall summary of the main results from more than 140 deposition runs. The second part contains four publications and shows the scientific output of the individual studies.

2 Thin film growth

It is well known, that thin films may have properties quite different from the bulk material. The microstructural characterisation includes analyses of grain size, phase composition, coating morphology and crystallographic orientation. Numerous publications and textbooks concentrate on the thin film growth and the fundamentals of the structure evolution [6-11]. The following chapters summarize briefly the main principles of these.

2.1 Structure and film evolution mechanisms

After evaporation of a neutral or charged atom from a target material using a certain PVD process (i.e. direct current magnetron sputtering), it is directed towards the substrate. When the atom hits the substrate surface it might be either bounced off or adsorbed depending on the transfer energy. If the transfer energy is sufficient the atom is bonded in a weakly adsorbed state known as physisorption and becomes a so-called adatom. The adatoms diffuse on the substrate surface and may desorb or, by condensation with several other adatoms, form small clusters. These clusters are called nuclei and the process of cluster formation is called nucleation [12]. After nucleation, the nuclei grow to form coherent films and to develop their structures, which means the films' crystallography and topography [13; 14]. Figure 2.1 schematically shows the processes from the atom arrival to the cluster formation, nucleation and film growth.

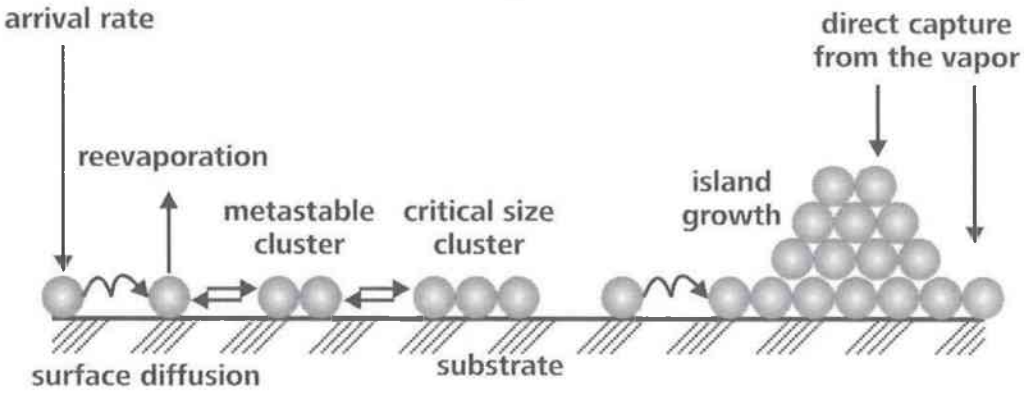

Figure 2.1: Schematic processes of nucleation and film growth modified after [8].

In general there are three types of film growth as shown in Figure 2.2: (1) an island growth (Volmer-Weber), (2) a layer growth (Frank-van der Merwe) and (3) a mixed layer-island growth (Stranski-Krastanov). Within these three processes the surface energy γ plays a crucial role, in particular the relationship between the surface energy of a substrate surface γ_s, of a film surface γ_f and of a substrate-film interface γ_i. If $\gamma_f = \gamma_i + \gamma_s$ then the formation of a layer-by-layer structure would increase the surface energy, hence island growth is dominant due to decreasing energies (Volmer-Weber). For $\gamma_f + \gamma_i < \gamma_s$ the total surface energy can be decreased by the substrate surface being evenly covered by the film, hence the coating will grow layer-by-layer (Frank-van der Merwe). The mixed layer-island growth (Stranski-Krastanov) changes from the initial layer-by-layer to island growth, which occurs at a critical layer thickness depending on the changing film and substrate surface energies. Nevertheless, the mechanisms driving the transition from the layer-by-layer to the island growth are not yet fully understood [14].

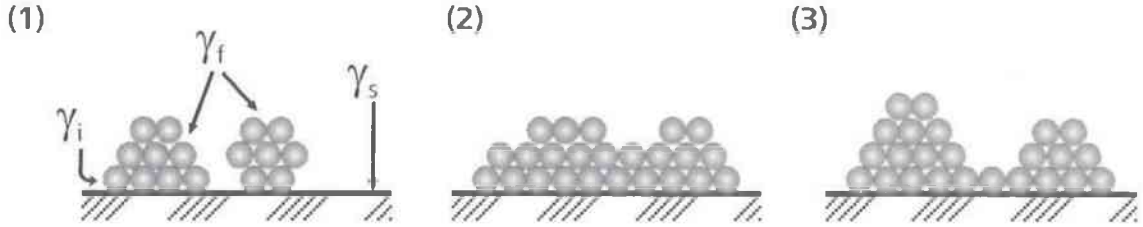

Figure 2.2: The three types of film growth: (1) Volmer-Weber island growth, (2) Frank-van der Merwe layer growth and (3) Stranski-Krastanov layer-island growth modified after [14].

2.2 Structure zone models

The three types of growth described above are only valid in an idealized case when the main surface diffusion of adatoms is sufficient so that they can minimize the surface energy. In such case the nucleation is not kinetically limited and the equilibrium state can be reached. On the other hand, the film growth can be conducted by quenched growth, which is a film formation without surface diffusion of the adatoms and they stick where they land [14]. The real film growth corresponds to an intermediate state between the quenched growth and the three types described above.

A limiting factor for growing dense coatings is the shadowing effect caused by the surface roughness, which is the geometric interaction between the surface topography and the angle of incident of the arriving adatoms. The shadowing effect results in formation of voids which can be partially suppressed by increasing the energy at deposition, hence increasing diffusion which could further enable even recrystallisation [15; 16].

Consequently the film forming processes like surface diffusion, nucleation and film growth are strongly depending on the mobility of the arriving atoms. Since the adatom mobility is related to the melting temperature (T_m) of the deposited material [2; 17], a correlation between T_m and T_s (deposition/substrate temperature) can be observed which influences the film growth. The ratio T_s/T_m is called homologous temperature. Its importance for the resulting film structure was recognized by Movchan and Demchishin and is summarized in a three zones (zone 1-3) structure zone model (SZM) [18]. Thornton added the gas pressure to the SZM of Movchan and Demchishin and observed an additional zone, called the transition zone (zone T) [19], see Figure 2.3a.

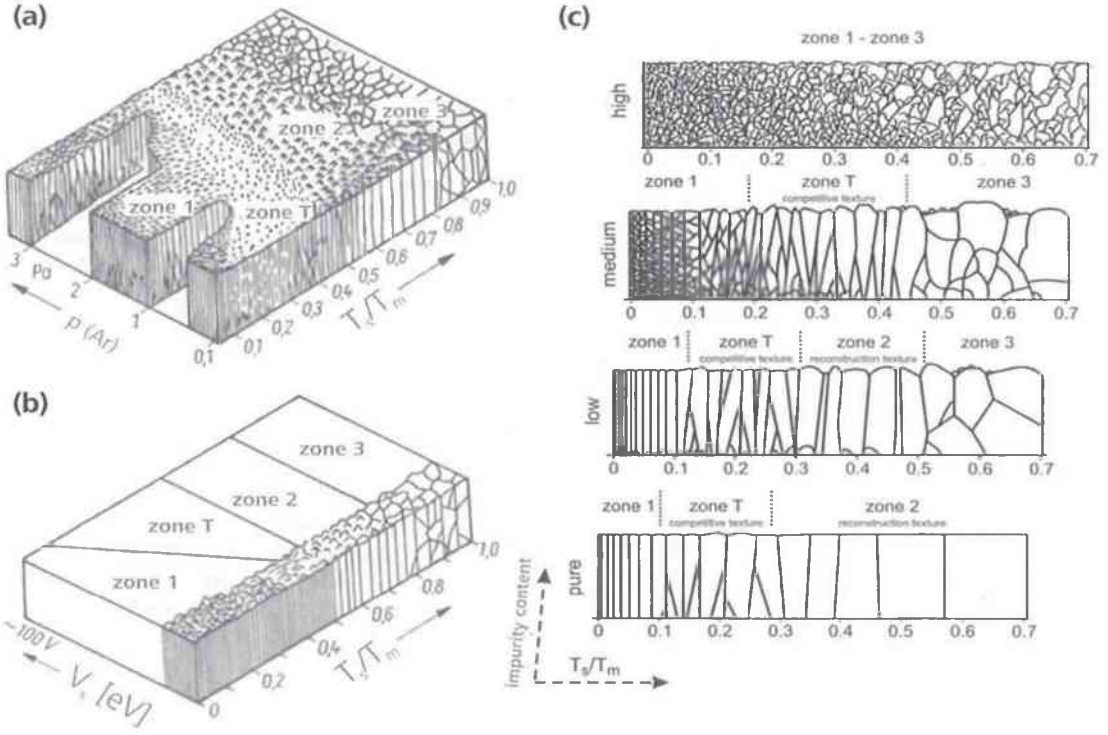

Figure 2.3: Structure zone models (SZM) (a) including the gas pressure by Thornton et al., (b) including the ion bombardment by Messier et al. and (c) including impurities during film growth by Barna and Adamik [7; 19; 20].

The characterisation of each zone is as follows [18; 20-22]:

- Zone 1 describes a porous structure, where the initial structure of crystallites is poorly defined. The crystallites diameter increases with increasing T_s/T_m implying higher activation energy and higher atom mobility.
- Zone T is the transition zone between zone 1 and 2 corresponding to higher densities and fine fibrous grains due to a limited surface diffusion.
- Zone 2 consists of columnar grains separated by dense boundaries. Shadowing at deposition is compensated by an increased surface diffusion.
- Zone 3 consists of equiaxed recrystallized grain structure due to the possibility of bulk diffusion.

As mentioned before, Thornton et al. also discussed the influence of the gas pressure on the evolution of the zones, in particular on the zones 1 and T. By increasing the pressure during the deposition the mean free pathway of the atoms decreases which results in an increased number of interactions between the vapour flux and working gas atoms. This effect, called the gas scattering, is decreasing the atom energy and hence decreasing the adatom mobility on the surface [2]. Since the zones 1 and T are mainly influenced by the adatom energy and mobility, the transition between these two zones is pushed to higher temperatures for increased pressures. Gas scattering has almost no influence on the zones 2 and 3, as it is balanced by the thermally activated adatom mobility due to the increased homologous temperatures.

The influence of the bias voltage on the structure formation is shown in Figure 2.2b, indicating a shift of the zone T to lower temperatures for increasing bias voltage. This can be explained by the increased adatom mobility for higher energy of the arriving atoms. This strong influence of the bias voltage on the growth conditions is even emphasised if the PVD processes make use of high ion distributions as for example in arc evaporation or high power impulse magnetron sputtering [20].

Furthermore, Barna and Adamik investigated the influence of impurities on the structure evolution and zone formation, see Figure 2.2c. Impurities, introduced by insufficient cleaning of the substrate, insufficient base pressure etc., can influence the adatom mobility and thus change the film forming processes. For high concentrations of

impurities, this results in blocking of the crystal growth by a periodicaly developing coverage of the whole crystal surface. Consequently no grain growth can take place and the film is composed of randomly oriented crystallites [7].

2.3 Ion bombardment

When adatoms arrive on the substrate surface they may have a certain degree of mobility to nucleate and condense [23]. The nucleation density of the adatoms on the surface (substrate or mode of grown film surface) is indicating the interfacial contact area and hence the degree of the interfacial voids. Therefore, high nucleation densities are required to deposit dense coatings with good adhesion [24]. The nucleation density depends on the kinetic energy, and hence mobility, of the arriving atoms. By higher energy of the arriving particles, neutral or ionized specimen, the nucleation density is increased but also surface defects or changes in the surface chemistry may be introduced [23]. Figure 2.4a schematically illustrates the possible effects of the impinging of energetic ions and Figure 2.4b indicates the resulting defects generated during the ion bombardment [24-26]. As mentioned in chapter 2.1, particles which arrive on the surface can immediately re-evaporate or adsorb and diffuse. When the incoming ions posses enough energy they may knock out atoms from their lattice positions in the substrate. These knock-out atoms create secondary collisions resulting in cascades of colliding atoms. The atomic motion along the trajectory leads to lattice rearrangements and material transport, i.e. point defects, interstitials and vacancies are created [25].

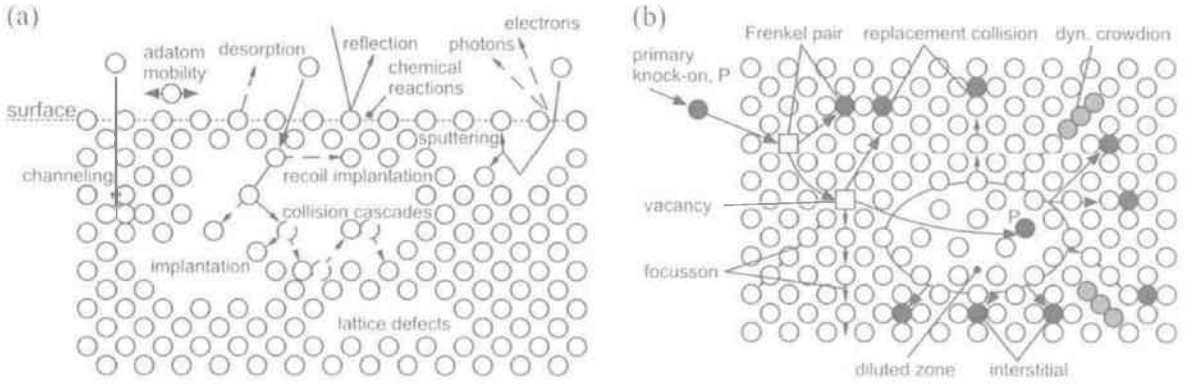

Figure 2.4: (a) effect of ion bombardment on the growing film and (b) possible generated defects [27].

In magnetron sputtering these arriving high energetic particles are generated from the sputtering gas and mainly consist of back-scattered inert gas neutrals or inert and reactive gas ions like Ar^+ or N^+ [28]. For arc evaporation or high power impulse magnetron sputtering (HIPIMS) the arriving particles contain of a high amount of ionized metal species. Multiple ionized atoms can also be generated in the HIPIMS technique, which results in high energy levels when attracted towards the substrate using high negative bias voltages [29-31]. Such HIPIMS generated ions may have enough energy to physically implant, as due to their high energy the lattice atoms appear to be reduced and the lattice seems to be empty in certain directions. Such a situation, called channelling, can influence several atom layers below the surface, or by using bias voltages around -1000V (e.g. during HIPIMS etching, see chapter 4.3) to depths around 30 nm [29]. This implantation into surface near regions is utilized in this thesis, as the HIPIMS process is used as pre-treatment step (etching) to clean the substrate prior to all depositions.

Of further interest is a deposition using an ion bombardment to modify the film structure, morphology and resulting properties. As shown in the SZM of Thornton et al. the energy of arriving particles influences the transition from the zone 1 to the zone T [19]. Similarly to an increase in bias voltage, an increase in ion ratio of the plasma improves the nucleation and the resulting morphology of the coatings. Nevertheless a higher bombardment by energetic ions produces larger residual stresses as well as high defect densities. Therefore, depositions using high densities of low-energy ions (e.g. small bias voltages) are required to deposit coatings with enhanced mechanical and tribological properties [32-34].

3 Thin film synthesis

Various techniques have been developed to deposit coatings with specific properties. They differ in the state of matter of the depositing material, i.e. deposition from gaseous, liquid or solid state, and in the deposition mechanism, i.e. mechanical, chemical, physical or thermal depositions. The main focus of this work is on physical vapour deposition (PVD) techniques. The following chapters illustrate the most important aspects of the individual PVD techniques.

3.1 Physical vapour deposition (PVD)

In general, the PVD processes are based on the transfer of a material into the gaseous state. Evaporation of materials is conducted by thermally loading employing direct resistance, radiation, electron beam, laser beam and arc discharge (evaporation), or by a transfer of a momentum (sputtering) [5; 10]. In the sputtering processes, gas ions (mainly Ar^+ ions) generated by a glow discharge bombard the target material (cathode) and detach atoms from the surface near regions of the target. These atoms move in a line-of-flight direction towards the substrate colliding with a few atoms/molecules of the working gas or some molecule artefacts of the evacuated chamber. In all PVD processes, the vapour source is characterized by a spatial flux distribution. The flux density decreases with increasing target-to-substrate distance [35]. Furthermore, the angle of impingement of the sputtered particles has influence on the film growth and the resulting properties, especially for non-symmetric substrates. Consequently, multi-source arrangements, application-specific cathodes (e.g. post cathodes or hollow cathodes apparatus) or multi-fold substrate rotation have to be used during depositions.

Nevertheless, the PVD techniques provide a lot of advantages as compared with other deposition techniques, e.g. the chemical vapour deposition (CVD): versatility in composition, the substrate temperature can be varied within wide limits from subzero to

high temperatures, possibility to deposit high purity coatings, adjustable surface bonding, and excellent surface finishing of the coated material etc. [5].

3.1.1 Magnetron sputtering

As mentioned before, the evaporation of the target material is conducted by sputtering its surface. Figure 3.1 shows schematically the arrangements for a simple direct current (dc) diode system, which consists mainly of two facing electrodes. The cathode, also known as target, is connected to the negative potential of the dc supply to sustain the glow discharge [13; 36]. The substrates are mounted on the facing anode, and can be either grounded, negatively or positively charged via the bias voltage. The evaporated atoms during the dc diode sputtering leave the target with a certain energy level (in the range of 5 eV) and undergo gas scattering while traversing the plasma. The resulting collision cascades do not only reduce the kinetic energy of the sputtered atoms but also scatter particles away so they do not hit the substrates, which results in low deposition rates of such dc planar diode sputtering systems.

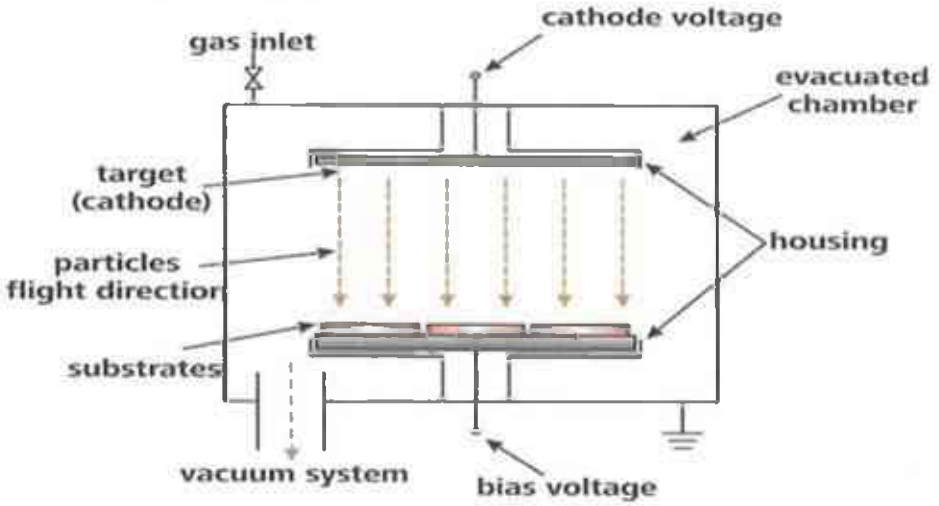

Figure 3.1: Schematic assembly of a dc diode sputtering system after [13]

To overcome the drawback of a low deposition rate, magnetic fields are applied, usually generated by permanent magnets behind the target. This arrangement is known as direct current magnetron sputtering (DCMS). The magnets create a magnetic field parallel to the target and perpendicular to the electric field resulting in a concentration of electrons near

the cathode and in an increase of the ionization of the working gas due to higher concentrations of charged species. A drawback of the DCMS deposition technique is the concentration of the charged and sputtered atoms at certain surface areas, due to the magnetic fields, resulting in formation of the sputtering wear track. As a consequence, the utilisation of the target material in DCMS is low.

Another advantage of the DCMS over the dc diode sputtering is the possibility of low pressures during deposition. In the dc diode sputtering, a low working pressure results in a small number of electron-ion collisions, hence the secondary electron yield is too low to sustain ionization in the discharge. Furthermore, with increasing pressure by increasing gas flow rates, the number of collisions increases, which lowers the energy levels. Since the electrons do not gain sufficient energies to ionize the gas atoms, the discharge is quenched [2]. In contrast, the magnetron sputtering technique provides the possibility of film deposition even at low pressures with increased deposition rates compared to dc diode sputtering, due to the shift of the minimum working pressure to lower values for a self-sustaining glow discharge [2; 5; 13; 37]. This effect is illustrated in Figure 3.2, which shows the Paschen curves for magnetron and non-magnetron (dc diode) discharges in argon, and displays the discharge threshold voltage V_s as a function of the Ar gas pressure p and the distance d between the electrodes. The shift to lower pd values and the increase in the width range of the latter indicates a more stable process of the magnetron sputtering technique compared with the non-magnetron technique [37].

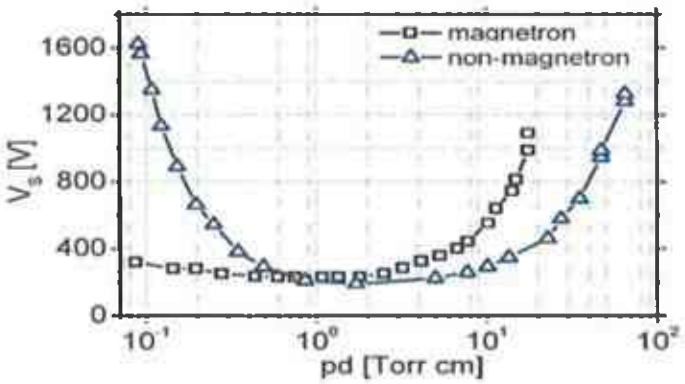

Figure 3.2: Paschen curve of a magnetron and non-magnetron sputtering system as a function of discharge threshold voltage V_s against Ar pressure p multiplied with the electrode distance d modified after [37].

In an idealized system, all magnetic fields loop between the outer and inner magnets; hence the magnetic arrangement is balanced against each other. This type of configuration is called a conventional balanced magnetron (CBM). The discharge is confined by the magnetic field, thus the bombardment with energetic species of the facing anode is minimal [38]. Consequently, the performance of the resulting film is not optimal as the bombardment of charged particles is essential to deposit coatings with outstanding mechanical and tribological properties (see chapter 2.3) as thereby the film structure and morphology can be improved. This problem can be overcome by changing the magnetic field configurations to increase the escape probability of energetic species and thus increase the growth kinetics and the resulting morphology of the film [2; 39-43]. Such adjustment is a so-called unbalanced magnetron (UBM) arrangement and has been investigated for industrial implementation in numerous publications [44-48].

An unbalanced magnetron system is utilized in this thesis for the deposition of hard coatings. Figure 3.3 shows its schematic arrangement and the magnetic field direction of the two facing unbalanced magnetron cathodes as used in the Z700 coating plant (see also chapter 4.4.3).

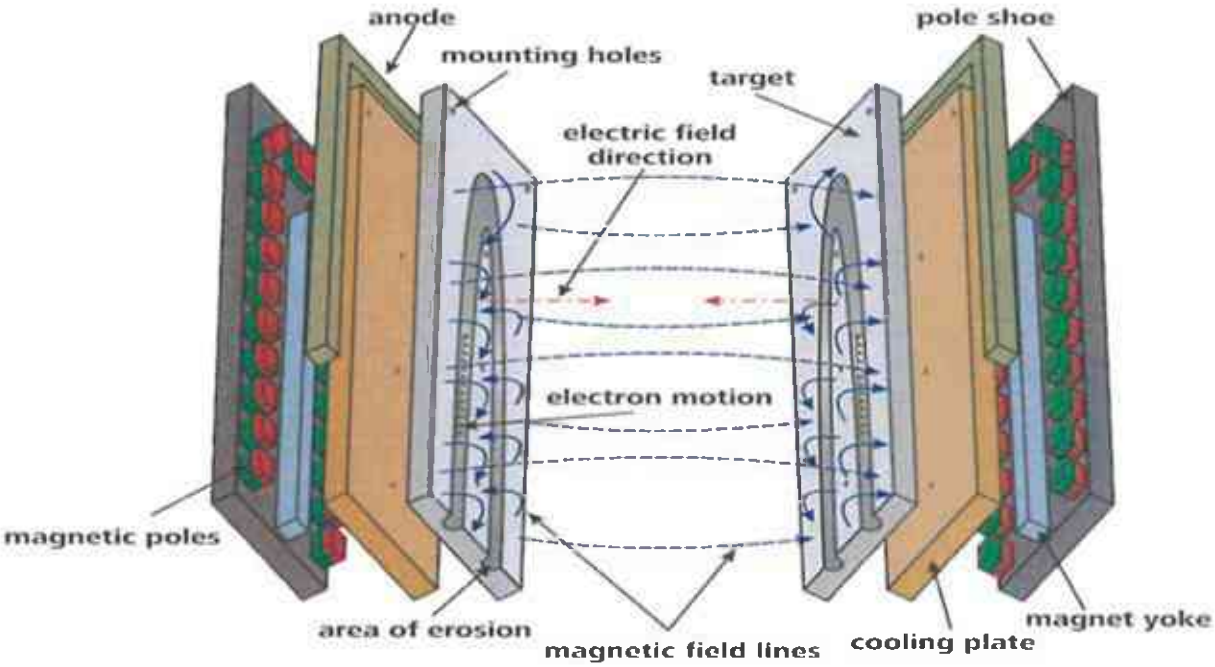

Figure 3.3: Image of two facing PK500 targets used in the Z700 coating plant. The image is illustrating the electric field lines and the magnetic field arrangement.

Each cathode consists of a pole shoe which is carrying the permanent cube-sized magnets and a yoke which is closing the magnetic field in the sputtering area. The target is mounted on a water-cooled platform which is housed by the chamber wall (anode). The distance between the housing (anode) and the target matches with the area of the dark space that is generated during sputtering in front of the target. In the dark space the electrons have too low energy levels to ionize the gas atoms. The electron energy level increases with the distance from the target till the charging is high enough to start the ionization cascades [2]. Therefore the distance between anode and target is shorter than the dark space area to avoid sputter effects at the target etches, but big enough to inhibit short-circuit between the cathode and anode.
The permanent magnets of the two facing cathodes are arranged to achieve a closed field in-between the two targets, as illustrated by the different north/south pole adjustment of the two cathodes in Figure 3.3. Consequently, an increased bombardment of the energetic discharge carriers on the substrate surface, mounted in the middle of the two facing cathodes, is achieved.

3.1.2 Pulsed dc sputtering

The DCMS technique is successfully used for a wide range of applications. Nevertheless dc sputtering cannot be used to sputter nonconductive targets and insulators such as silicon or BN, due to the charge accumulation on the target surface. This difficulty can be overcome by using a pulsed dc or radio frequency (rf) sputtering [49-51]. With pulsed DCMS the powering of the target is alternated between negative and positive voltages, as presented in Figure 3.4. During the negative pulse, the target is operating comparably to conventional DCMS systems, as the ions are attracted to the target to eject atoms out of the target surface. On the other hand, electrons are attracted to the target during the positive pulse to discharge the charged areas [52]. The magnitude and duration of the negative pulse is greater than the positive one in Figure 3.4. Such type of pulsed DCMS is called asymmetric bipolar pulsed DCMS. Same sized negative and positive shaped pulses are called unipolar pulsed DCMS.

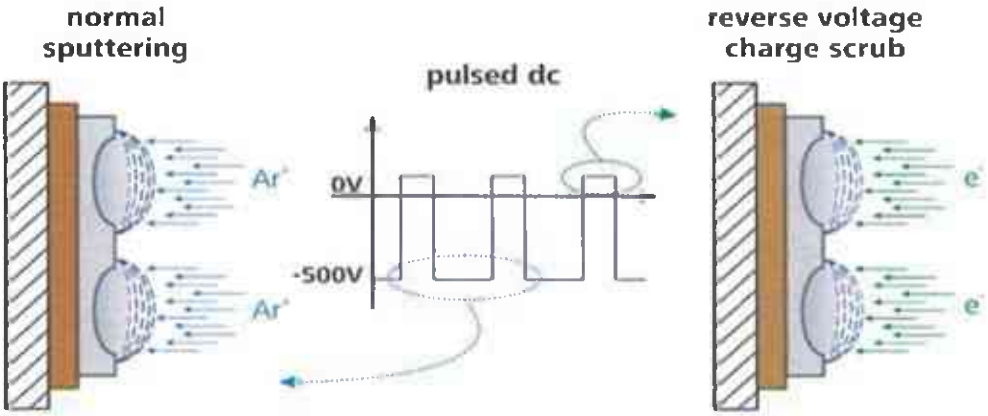

Figure 3.4: Schematic of an asymmetric dc pulse modified after [52]. The image indicates the sputtering of Ar ions during negative pulse, and the discharging due to the electron attraction during the positive pulse.

The pulsed DCMS method is also used to decrease the arc affinity on the target due to offset charge build ups on the surface, as the process provides two more degrees of freedom: the pulse frequency and the duty cycle (negative pulse time divided by the cycle time) [52]. Studies on adjustments of the duty cycle to decrease the arc formation on the target surface during sputtering were done by Kelly et al. and Carter et al. [53; 54]. On the other hand, a disadvantage of the pulsed DCMS technique is, when compared with DCMS, that the pulsing introduces a reduction of deposition rate.

3.1.3 Cathodic arc evaporation (CAE)

Arc evaporation is a PVD technique which utilizes high currents (tens to hundreds of amps) combined with a low dc voltage (in the range of some ten volts) gas discharge. The arc erosion is generated by a touch of two metal electrodes which are immediately separated to a small distance. A small luminous spot is formed at the cathode, which then passes the high current density region and ignites the arc. The spot where the arc touches the target is the so-called arc spot. Figure 3.5 illustrate the principle arrangement of a cathodic arc evaporation (CAE) system and the microscopic events at the arc spot. Arc spots have a short life-time as they are moving rapidly on the target surface, because of which unwanted thermally loads can be avoided. The high current density in the arc spot

concentrates at roughness tip (asperities of the target) and their surrounding areas which leads to evaporation (mostly ions) and melting (droplets) of the area. These molten zones exhibit new tips and the process can start again. The high temperature and the explosion-like processes in the arc spots lead to the high ion densities in the plasma [2; 13].

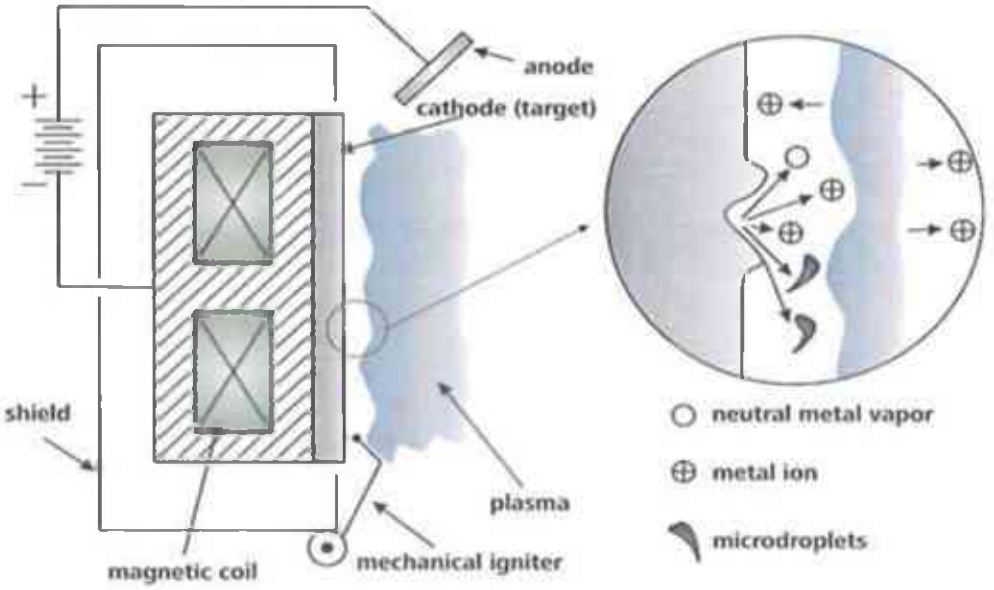

Figure 3.5: Schematic of an arc evaporation system and the microstructural events in the arc spot (after [2]).

The arc which erodes the target moves randomly on the target surface, hence this technique is called a random arc. Consequently the utilization of the target is in general good but the arc spot can rest on a certain point on the target for a longer time which causes extensive melting and hence damaging of the cathode. Furthermore, a special housing surrounding the target has to be mounted (mostly rings of BN) so that the arc cannot leave the target and damage the vicinity. To achieve a uniform sputtering of the target and a uniform film deposition the arc is steered magnetically, resulting in a material erosion in a series of flash evaporation events. This kind of cathodic arc evaporation is called a steered arc [2].

The CAE techniques exhibit deposition rates comparable to DCMS combined with an ionization rate of the vapour flux > 95 %. Nevertheless the main drawback of these techniques is the formation of droplets which are incorporated in the coatings and result in an increased surface roughness and thus deteriorated tribological properties. This can

be overcome by employing several filtering systems which decrease the droplet incorporation, but at the cost of decreased deposition rates and increased residual stresses [5].

3.1.4 Arc bond sputtering (ABS™)

The arc bond sputtering technique (ABS™) is a method which combines the advantages of the UBM sputtering technique with the CAE ones. It has been shown that there are distinct differences in the microstructure of TiN coatings depending on the deposition technique and the preparation of the interface between the film and substrate [55; 56]. The CAE technique is used as substrate pre-treatment due to the high ion to neutral plasma density. Similarly to the HIPIMS process (see also chapter 4.3) the high ion bombardment during etching together with high substrate bias voltages leads to some implantation effects in depths around 200 Å and recrystallization of zones as deep as 1600 Å [57-59]. For the deposition of the TiN coatings, the UBM method was conducted, as it is utilized in a wide range of industrial applications. Combined with the higher adatom mobility due to the arc etching, coatings with a dense morphology and increased mechanical and tribological properties can be obtained. The ABS™ is more and more replaced by the combination of HIPIMS and UBM, since no additional arc source is needed in the plant, as the HIPIMS process can be used on simple magnetron cathodes [60-62]. Another step forward is the combination of high ion density processes like HIPIMS with processes with increased deposition rates (UBM). There are investigated in this thesis and utilized for industrial applications (see chapter 4.4).

4 High power impulse magnetron sputtering (HIPIMS)

High power impulse magnetron sputtering (HIPIMS) [31], also known as high power pulsed magnetron sputtering (HPPMS) [63; 64], is a new PVD deposition technique with the advantage of high ion densities of the sputtered material. For conventional dc magnetron sputtering (DCMS), the maximum power to feed the supplies is limited by the heating of the target material caused by the high ion bombardment of the ionized gas molecules. To prevent the drawback of an increased thermal load at high power levels, a cooling period is needed. Consequently pulsing the dc powering is used to increase the plasma ion density without overheating the target during sputtering. Conventional pulsed sputtering operates in the kHz range, which results in increased powering of the cathode and increased ion dissipation compared to DCMS. For example, the ion current density of biased substrates at conventional dc sputtering is less than 10 mA/cm² [31; 38]. Whereas for conventional pulsed dc sputtering glow discharges with power densities around 900 W/cm² can be obtained [31]. The HIPIMS process is comparable to pulsed dc sputtering processes with the advantage of high electrical power densities which can be obtained by decreasing the duty cycles (on-time divided by the cycle time) of the pulse, which allows increased power levels during deposition, resulting in electron densities in the range of 10^{19} m^{-3}, and peak power levels around 1-3 kW/cm² [31; 65; 66].

4.1 Electrical parameters

The HIPIMS power supplies are based on artificial pulse-forming units. Depositions in the Z700 coating plant are carried out using AC Zielonka Poland power supplies and pulsing units. Figure 4.1 shows the principle setup of the HIPIMS powering system in a simplified block diagram. The arrangement is comparable with the basic mesh pulse forming network described by [65; 67]. The power is fed by a dc power supply unit which is directly connected via a dc link to the pulsing unit. The pulses are generated by charging and discharging a capacitor in a repetitive manner, through a thyristor switch. The capacitor is discharged over the electrodes of the sputtering device through cable

inductance, which are in series with the magnetron discharge. This impedance matching circuit reduces the rate of the current rise, and is reducing arc formation on the target surface due to the increased peak output, protects the power supply components [65; 67], and improves the stability of the pulsed plasma.

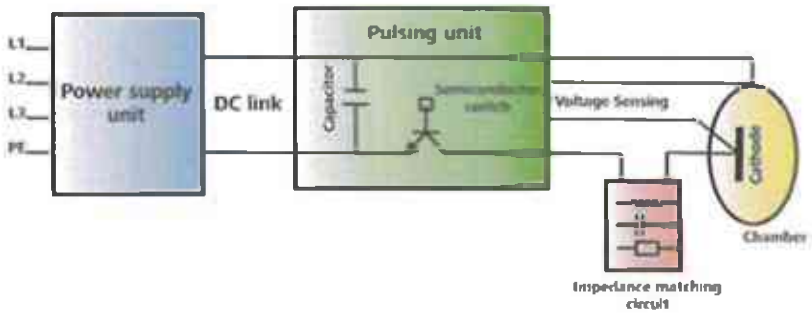

Figure 4.1: Schematic of a simplified block diagram for discharging a HIPIMS plasma.

An example of a generated pulse shape is shown in Figure 4.2. Kouznetsov et.al. observed a time delay of 50 µs for the ignition of a magnetron discharge for high power discharges, with peak powers around 0.6-2.8 kW/cm² at gas pressure around 0.065 Pa [31]. This typical wave form of current and voltage are also shown by Macák et al. [66], where the voltage increases at the beginning of the pulse to values in the kV range and subsequently drops to several hundred volts, which accompany an increase in the target current.

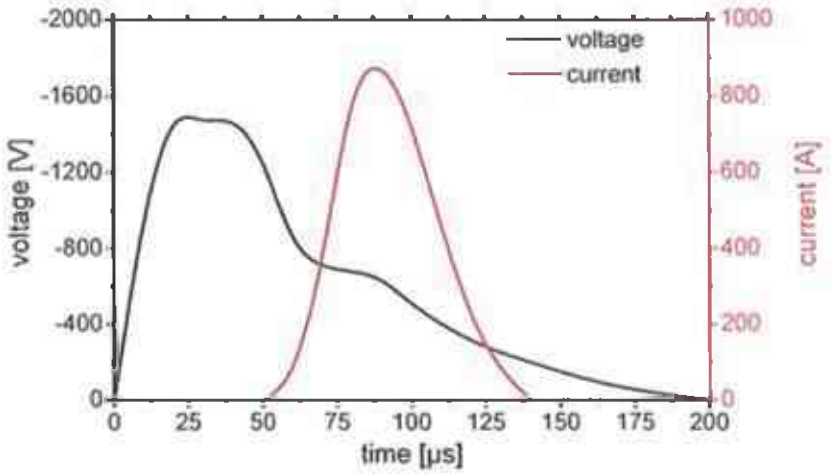

Figure 4.2: Time evolution of voltage and current of a HIPIMS generated pulse (modified after [31]).

These pulse shapes depend strongly on the power supply itself, the powering of the pulsing unit, the magnetic field configuration, the target material, the gas type and the working pressure. Concerning the gas pressure, it has been shown that by decreasing pressure during deposition the time of the plasma ignition increases [68]. This is demonstrated by an increased time difference between the maximum of voltage and current. Gudmundsson et al. [68] showed that a decreasing argon pressure has similar effect as a shortening of the pulse length of a conventional rectangular pulse, see Figure 4.3. The time delay of the plasma ignition is increasing with decreasing the working pressure; for example, the time delay is increasing from around 10 µs at pressures > 1.33 Pa to around 40 µs at gas pressures < 0.07 Pa (see Figure 4.3). Musil et al. introduced a three regime characterization for pulsed dc: (1) the plasma build up, (2) stationary plasma and (3) decaying plasma [69]. For pulse length < 100 µs the second regime (stationary plasma) cannot be reached and the pulse building regime (stage one) is dominant. Consequently, the pulse shape of the HIPIMS process is comparable to those of conventional pulsed sputtering processes with decreased pulse length and pressures see Figure 4.2, but with the advantage of high current densities resulting in high ion dissipation.

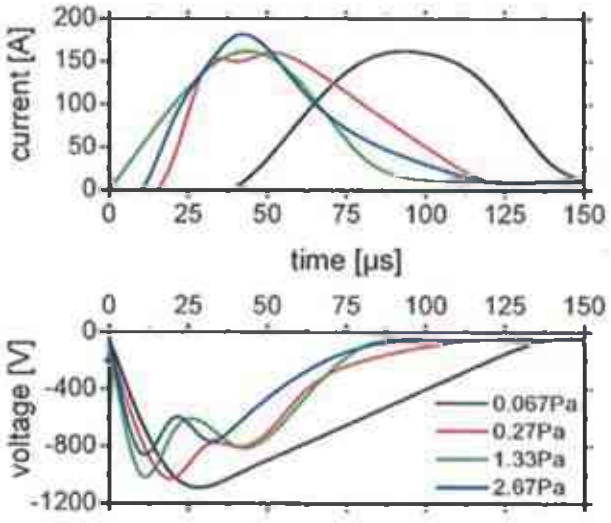

Figure 4.3: Current and voltage pulse shape of a conventional pulsed dc magnetron sputtering system at different pressures (modified after [68]).

Since the configuration and performance of the HIPIMS power supplies is essential for the process itself numerous investigations focus on their development. The main differences of these supplies, apart from internal electrical design, are the frequency, duration time and the maximum peak power, which is limited by the maximum voltage and current loads.

The first supplies developed for HIPIMS applications had repetition frequencies of 5-20 Hz and pulse durations of 2-10 ms with maximum peak powers around 400 kW [70]. Kouznetsov et al. deposited coatings using a frequency of 50 Hz and a pulse width of 50-100 µs (resulting in duration steps of 19.95-19 ms) with increased maximum peak power around 2 MW [31], resulting in metal ion ratios in the plasma around 70 %. Christie et al. reported on deposition supplies with frequencies of 500 Hz, pulse widths of 100-200 µs and maximum peak powers of 3 MW. [65]. A further increase in peak power to values around 6 MW with frequencies from 0-100 Hz and pulse widths up to 200 µs were obtained by Ehiasarian et al. [71]. Additional modifications of the HIPIMS power supplies, focusing on duration time and frequencies as well as on the arc suppression, are reported by [72; 73]. As can be seen, the trend for the HIPIMS deposition is leading towards frequencies < 500 Hz, duration times < 200 µs and increased peak powers levels, which results in increased plasma ion densities.

Depositions in the Z700 coating plant were carried out using supplies which can operate in frequencies ranges from 0 to 1000 Hz, pulse durations from 1-200 µs and maximum peak power levels up to 18 MW (limited by maximum voltage of 3 kV and maximum current of 6 kA). Due to the high energy in the HIPIMS pulse in the MW range and the increased probability of arc formation on the target, an arc handling for HIPIMS depositions is required [31; 65; 74]. The AC HIPIMS power supplies, utilized in this thesis, use sensing arc detection with adjustable detection criteria, controlled by the maximum peak current and the voltage/current cross detection, to decrease the occurrence of arcing on the target.

4.2 Plasma evolution

Dc magnetron sputtering is a well established PVD technique with the main drawback of a low ion density in the plasma. Furthermore, the generated ions at DCMS are mainly gas ions with typical densities of 10^9 cm^{-3} [30; 75]. Such a low ion density results in depositing underdense coatings, whereas a deposition with a low-energy ion bombardment is beneficial for production of dense defect-free coatings [34; 76]. Arc evaporation on the other hand reaches metal ion densities in the range of 10^{18} cm^{-3} but with the drawback of droplet formation. The HIPIMS technique provides high ion densities > 10^{13} cm^{-3}, reported by [30; 66; 68; 77], with the advantage of a droplet-free process and a significant amount of metal ions (up to 70%) in the generated vapour flux [31].

Figure 4.4 indicates the I-U characteristic of a conventional magnetron discharge and a HIPIMS discharge. As the axis marking is double logarithmic the linear I-U characteristic follows the power law $I = k \cdot U^n$, where n is indicating the slope of the curve, and k is the intersection with the y axis [30]. The current-voltage characteristics for the glow discharge exhibit different modes of the glow discharge: the sub-normal glow, the normal glow, the abnormal glow and the transition region to the arc, see Figure 4.4a [37]. For sputtering the first half of the abnormal glow discharge area is used, as it indicates an easy increase of the current density by a simple increase in the target powering. For conventional magnetron sputtering the n value is between 5 and 15 [78]. Ehiasarian et al. evaluated an n value of 8 for conventional DCMS sputtering of a rectangular target at gas pressure around 0.4 Pa, see Figure 4.4b. An inspection of the HIPIMS I-U characteristics (same pressure range, but cylindrical cathode) reveals two regimes: at currents below 600 $mAcm^{-2}$ the exponent is approximately 7, which corresponds to the abnormal glow discharge at DCMS but with a shift to higher target current densities, while by increasing the current to values above 600 $mAcm^{-2}$ the exponent changes to values around 1. The system is at higher currents (n=1) working in an operation mode where a minimal increase of voltage is not followed by an enormous increase of discharge current (second half of the abnormal state area). In the normal and abnormal glow discharge area the number of electrons and ions produced is the same and the plasma is self-sustained. Consequently,

as all atoms in the plasma are already charged [37], saturation is adjusted and the current density is more or less constant with increasing voltage. A further increase in target powering will result in the transition from an abnormal glow discharge to an arc formation, where an increase in current density is combined with a decrease in the target voltage due to the ignition of an arc spot. An additional effect of the sudden change in the n value of a HIPIMS glow discharge is, that due to the changing magnetic field at high current densities the secondary electrons accelerated in the sheath cannot be trapped, which results in an increased ion collision probability [30]. Nevertheless the HIPIMS process seems to be more sensitive in the change from the abnormal to the transition glow discharge zone, compared to DCMS.

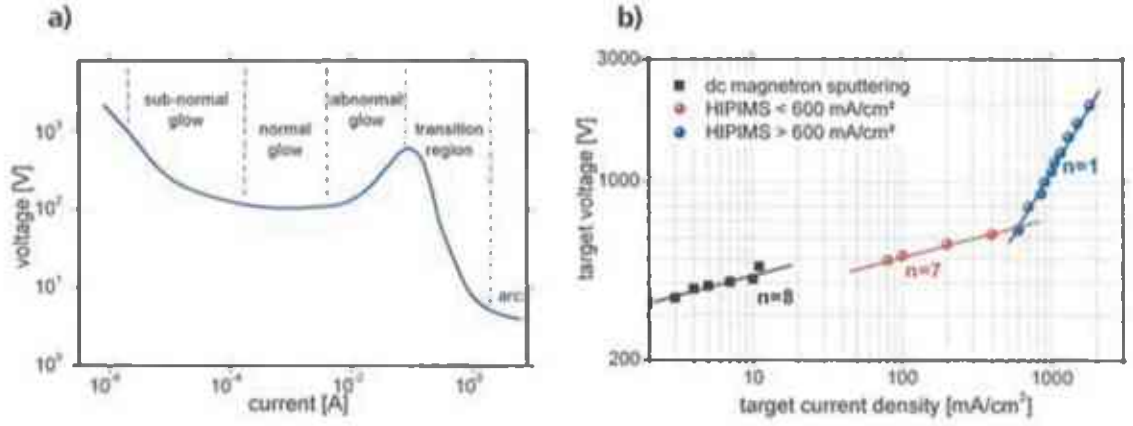

Figure 4.4: (a) voltage-current characteristic of a DCMS glow discharge (after [37]) and (b) voltage-current characteristic of a DCMS glow discharge compared to a HIPIMS glow discharge (after [30].

It is well known that the plasma ionization rate depends on the dwell time of the sputtered particles in the sheath of the plasma [75]. Sputtered atoms evaporate from a target material with a certain energy level (typically a few electron volts) and travel across the generated plasma. The dwell time is the time particles need to cross the sheath and it is directly connected to the plasma density [30]. During the HIPIMS discharge the sputtered atoms evaporate with the same energies compared with the dc sputtering, but they have to penetrate a denser sheath due to the high discharge power, which results in increased collision cascades and hence a higher ionisation of the sputter flux is obtained. Furthermore, the high metal ion density in the sheath and the high discharge voltage during HIPIMS pulsing causes an attraction back to the target surface, giving rise to a self-

sputtering [30]. The model of Christie et al. is illustrating the schematically particle pathways and self-sputtering effects during a HIPIMS deposition and will be described in chapter 4.3 [65].

Investigations on an ionized particle evolution in the plasma were done by the group of Ehiasarian [30] using time resolved optical emission spectroscopy (OES). According to these OES spectra, Ar ion emission was detected 10 µs after powering the cathode in the HIPIMS mode, followed by an evolution of single ionized Cr atoms. Another 40 µs later the high density plasma was adjusted. These results demonstrate two stages of the HIPIMS plasma generation. The first stage is the emission of Ar neutrals after applying a certain power at the HIPIMS cathode. Within these 10 µs of the first stage, the Ar neutrals are replaced by ionized Ar atoms by glow discharge. It can be seen that in the OES spectra, also Cr neutral atoms are measured at this stage of an increasing number of Ar ions in the plasma. The Ar ions start to sputter the target surface and to evaporate neutral metal atoms. This stage is the main part of the conventional dc magnetron sputtering. HIPIMS depositions exhibit also a second stage, which is the evolution of ionized metal atoms due to collision cascades in the plasma. These alter the plasma configuration from Ar ion dominant to a highly metal ionized plasma [30; 67]. Due to the high collision probability, the raised plasma density, and the increased evaporation energies during self sputtering, also twice ionized metal atoms are detected, in case of Ehiasarian et al. [30] Cr^{2+} (see Figure 4.5). These multiple-ionized species increase the energy level, resulting in a high-energy substrate etching as well as in increased adatom mobility during film deposition.

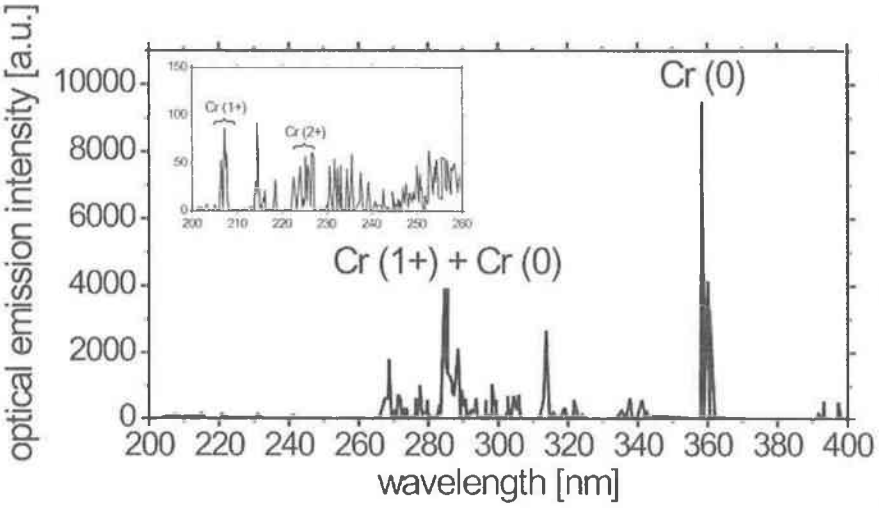

Figure 4.5: OES spectra of a HIPIMS sputtered Cr in Ar atmosphere indicating multiple ionizations (modified after [30]).

4.3 Field of applications, state of the art

The main challenge of all PVD techniques in general is the control of the deposition direction. Consequently highly ionized plasmas are of interest for these purpose [79; 80]. The advantage of the HIPIMS deposition is the ease of controlling the metal ions direction by the bias voltage applied at the substrate. Kouznetsov et al. [31] obtained dense morphology from HIPIMS sputtering even for extreme conditions like film deposition on surfaces perpendicular to the target or a film deposition in narrow trenches. Figure 4.6 shows a focused ion beam image of HIPIMS deposited Cu [31]. A void free deposition of copper on the substrate surface (parallel to the target surface) and narrow trenches (1 μm^2 of area and 1 µm in depth) can be observed, with columnar growth predominately from the bottom [31].

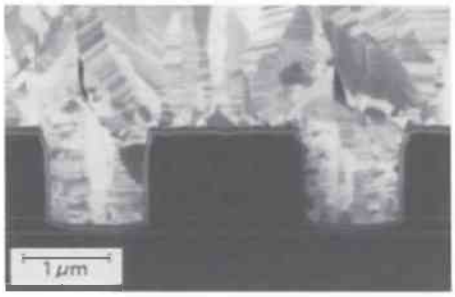

Figure 4.6: Focused ion beam image (secondary electron image) of HIPIMS sputtered Cu [31].

To enhance the deposition conditions and emphasize the advantages of the HIPIMS process over the conventional dc magnetron sputtering technique, Alami et al. [81] carried out Ta film deposition on surfaces 90° tilted to the target. These investigations are similar to those of Kouznetsov et al. with the difference of changed dimensions of the trenches. The Si substrates were placed along a whole shaped substrate holder with drill holes in area 1 x 1 cm^2 and 2 cm in depth. The holders were positioned in a way, that openings of the trenches were facing the target material [81]. Figure 4.7a and c demonstrate HIPIMS Ta coatings with a dense fibrous morphology and a growth direction perpendicular to the tilted surface. On the other hand, Figure 4.7b and d show deposited Ta films on surfaces perpendicular to the target, sputtered by the conventional DCMS technique. The SEM images indicate an open columnar morphology with a film growth direction tilted towards the target material by an angle α. This results in decreased performances of the coatings and in non-uniform film thickness along the drill holes due to shadowing effects during dc deposition.

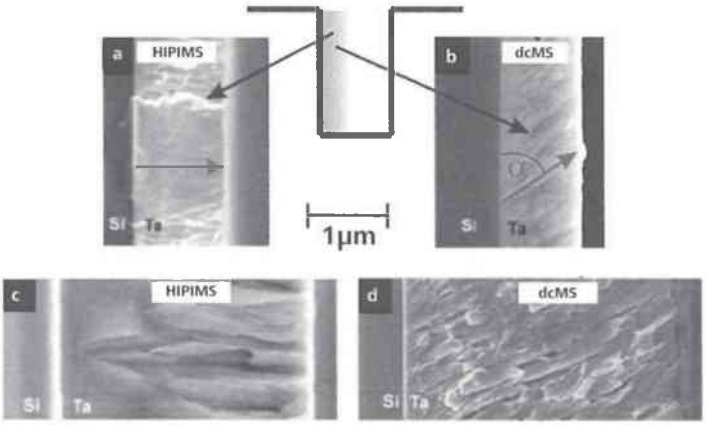

Figure 4.7: SEM images of the comparison between HIPIMS (a,c) and DCMS (b,d) sputtered Ta films on surfaces tilted 90° to the target [81]

Further investigations on the HIPIMS deposition and resulting film properties were done by DeKoven et al., who deposited C films [82], or Sproul et al. who investigated the possibility to deposit oxide films with enhanced optical characteristics [83] and HIPIMS CrN coatings were analyzed by Ehiasarian et al. [29]. Figure 4.8 shows a TEM micrograph of a HIPIMS deposited CrN film, showing a dense fibrous structure with crystallite diameters up to 1 µm [29]. Such film morphology results in increased mechanical properties, e.g. hardness values around 25 GPa, and improved wear properties, e.g. friction coefficients decreased to values around 0.45 and sliding wear coefficients around 10^{-16} m^3/Nm [84-86]. Comparable results are observed in paper I using the hybrid HIPIMS/DCMS technique.

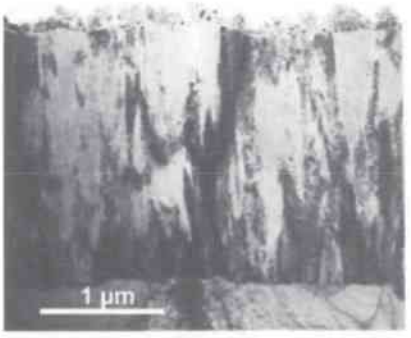

Figure 4.8: TEM image of a HIPIMS CrN coating [29].

Furthermore, Ehiasarian et al. [29] demonstrated that the HIPIMS process enables the possibility of metal ion etching to improve the adhesion of the growing film to the substrate, and to increase the growth kinetics. In conventional dc magnetron sputtering units the substrate bombardment intended to clean the surface and to increase the adatom mobility at deposition, is mainly conducted by high-energy argon gas ions. For HIPIMS etching, a large fraction of ions are metal ions from the target material like Cr^+ and Cr^{2+} or Ti^+ and Ti^{2+} [29; 87]. Due to the high metal ion ratio and the high bias voltage used during etching (around -1000 V) implantation effects occur, see Figure 4.9a. Cross-sectional transmission electron microscopy (X-TEM) investigations of HIPIMS Cr etched substrates revealed a gradual change in the Cr content between substrate and deposited CrN coating near the substrate-film interface [29; 88; 89]. Comparable results of HIPIMS etched steel substrates are shown in paper IV, indicating an implantation depth around 20

nm. This high-energy bombardment and the implantation of metal species in the substrate leads to improved adhesion as well as to increased adatom mobility, and thus proved to be beneficial for the growing film [4; 29; 73; 88]. Figure 4.9b shows scratch tests on CrN coatings, deposited after HIPIMS Cr etching, with thicknesses around 2 µm. The curves demonstrate the maximum load values during scratch testing, indicated by the sudden increase in the friction force due to a total delamination of the coating. The green area represents the minimum load value (> 70 N) of CrN coatings with excellent adhesion to the substrate material [3]. HIPIMS deposited and etched CrN coatings in this thesis exhibit perfect adhesion, as they reach normal loads > 70 N before delamination occurs.

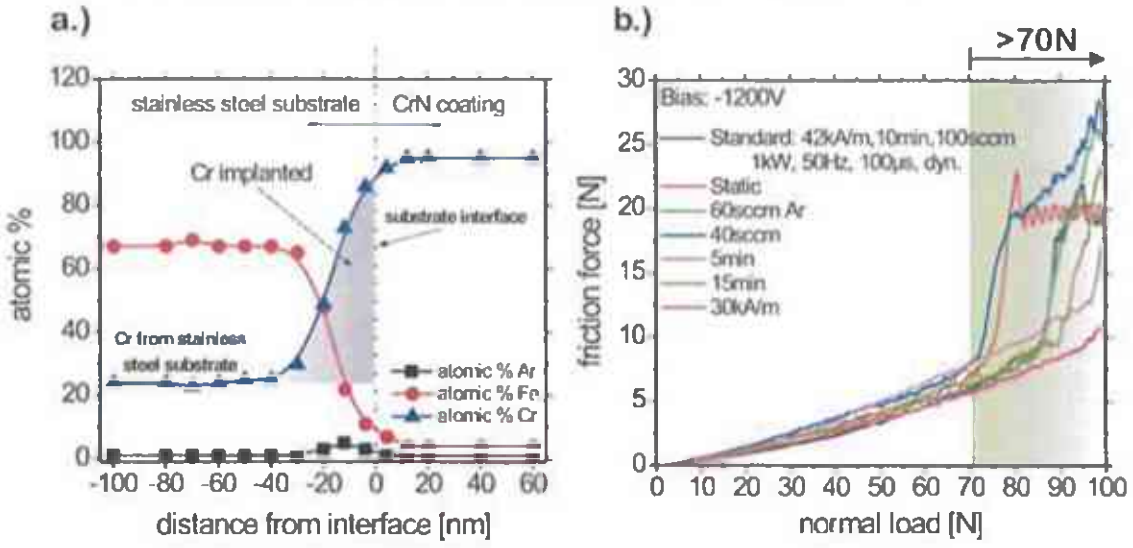

Figure 4.9: (a) X-TEM image of a HIPIMS Cr etched steel substrate indicating an implantation depth around 30 nm (modified after [29]) and (b) scratch tests on HIPIMS etched (using different parameters) and HIPIMS deposited CrN coatings (unpublished results).

The HIPIMS technology provides a lot of advantages such as high ion densities, high metal ion ratios, droplet free depositions, simple adjustment to magnetron sputtering units etc. The main drawback of the HIPIMS process is its low deposition rate compared with the conventional DCMS. For example, Bugaev et al [70] reported on reduction of the deposition rate by a factor two at Ti deposition when compared to DCMS. As mentioned before, Christie et al. [65] described the low deposition rate and high ionization efficiency of a HIPIMS deposition in a theoretical model, which is shown in Figure 4.10.

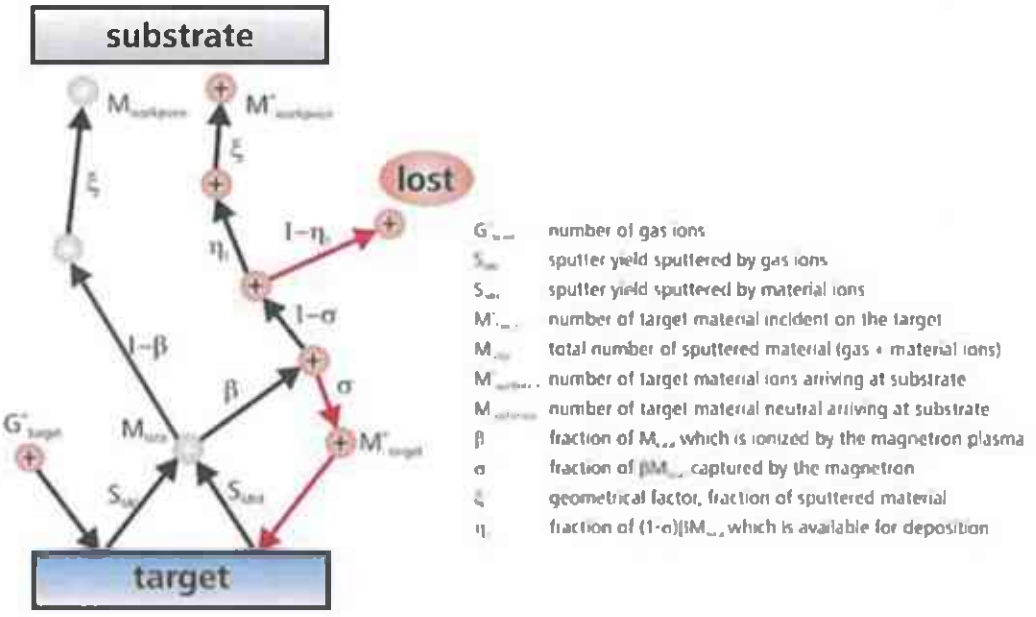

Figure 4.10: Model of the theoretical pathways at HIPIMS sputtering, modified after [65].

The total number of evaporated atoms M_{total} is divided into two contributions: neutral atoms, which cross the sheath heading to the substrate almost without being influenced by the magnetic field and by colliding with any other atoms (1-β), and ionized particles generated by collisions (β). Due to the magnetic field and the high voltage discharge at the cathode, numerous metal ions cannot penetrate the sheath and are backtracked to the target, which results in the self-sputtering (σ). Metal ions which were able to cross the sheath are attracted to the substrate (η) or get lost and have no contribution to the growing film (1-η). Consequently the low deposition rate of the HIPIMS process is a combination of the low on-time of the plasma, due to the required decreased duty cycles at pulsing, and the increased probability of attracting the ionized metal species back to the cathode. These can then result in self-sputtering events, which for Ti, Cr and other metals is smaller than the Ar sputtering event. Hence the deposition rate decreases. Helmersson et al. evaluated the interrelation between the deposition rate and the relative sputtering yield (ratio between the self-sputtering yield S_S and the Ar yield S_{Ar}) of different target materials for HIPIMS and conventional DCMS (see Figure 4.11) [67].

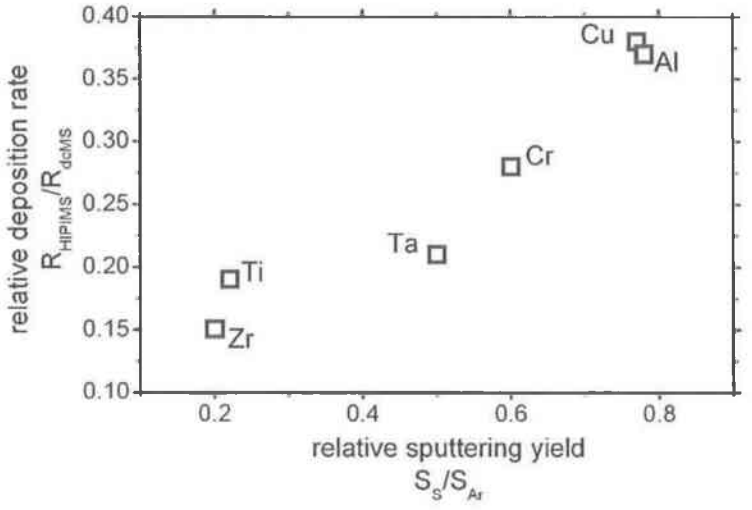

Figure 4.11: The relative deposition as a function of the relative sputtering yield (S_S self-sputtering yield, S_{Ar} argon sputtering yield) modified after [67].

Due to the prolonged deposition times and increased production costs, industrial applications are limited. Consequently up to now the HIPIMS process is mainly used for substrate pre-treatment, to clean the surface from impurities such like oxides, and to increase the film adhesion. Papers I and II compare the deposition rates and the film properties depending on substrate rotation variation during HIPIMS and DCMS deposition and indicate the hybrid HIPIMS/DCMS deposition as a solution to grow coatings with increased properties and deposition rates.

4.4 Selection of target material and film deposition

In particular for automotive applications, the quality of the sputtered films is crucial. Consequently, the development of droplet free coatings with dense morphology is of great interest. The HIPIMS process is known to be beneficial in this case, as it provides for example droplet free high metal ionised plasmas. Conventional dc magnetron sputtered CrN and TiN hard coatings have been thoroughly investigated and are known for their unique properties such as high hardness or good wear resistance. Therefore great

attention has been paid to the investigation and improvement of these hard coatings [1; 27; 34; 90-100].

4.4.1 Chromium nitride (CrN_x) hard coatings

CrN_x coatings are well established as hard coating, due to the wide range of their applications like cutting, casting and cold forming parts, or automotive applications such as machine, motor and hydraulic tools. Depositions of these coatings, focusing on PVD techniques, are done by arc evaporation, reactive or non-reactive dc magnetron sputtering or arc bond sputtering (ABS™). An advantage of the CrN_x coatings, apart from their mechanical and tribological properties, is the possibility of deposition temperatures below 200°C [101]. This adds the option to deposit films on substrate materials which are not thermally stable at temperatures above 200 °C, or depositions of the end product, where no thermal treatment of the bulk material is wanted.

Regardless of the deposition technique, various phases of CrN_x were identified depending on the partial pressure of N_2 [1; 101; 102]: Cr, Cr(N) solid solution, Cr_2N, Cr_2N + CrN and CrN. Figure 4.12 shows the relation between the chemical composition and the N_2/Ar gas flow ratio in dependence on the ion energy and the resulting indentation hardness of DCMS CrN_x films. The plot clearly demonstrates that by changing the nitrogen gas flow rate (i.e. by changing the nitrogen partial pressure during deposition) all phases can be easily formed [1].

The focus for high power impulse dissipation was to form stoichiometric CrN coatings. CrN coatings were preferred due to their superb sliding wear performance when compared with the brittle Cr_2N films, and because of the wide range of gas flow ratios from ~0.45 up to ~1.2, see Figure 4.12. The variability of the nitrogen partial pressure is simplifying the deposition of multilayered coatings, especially when combining CrN films with TiN films in a multilayered arrangement, see Chapter 4.4.4.

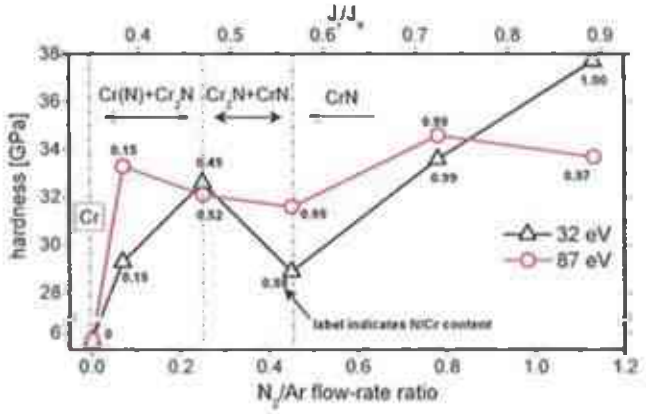

Figure 4.12: Hardness as a function of the N_2/Ar gas flow rate and J/J_a of DCMS CrN indicating the chemical composition [1].

4.4.2 Titanium nitride (TiN_x) hard coatings

Similar to CrN coatings, also TiN hard coatings show function-specific properties in applications such as wear protective coating for cutting tools, machining industry, automotive applications, and due to their goldish colour, also as decorative hard coating. Matthews et al. [90] investigated deposition of two-phase Ti + Ti_2N and Ti_2N + TiN coatings, which turned out to have improved wear properties when compared with a single phase TiN. Nevertheless, the hardest Ti-N based coating is the single phased cubic δ-TiN [103]. Deposition of the cubic TiN is strongly influenced by the N_2/Ar gas ratio during deposition. By increasing the nitrogen content the chemical composition changes from a solid solution of N_2 in α-Ti to the cubic δ-TiN phase. Formation of the required goldish coloured δ-TiN, which indicates to have increased mechanical properties, appears to be very sensitive to variations in the nitrogen partial pressure. An increase of the nitrogen gas flow rate, at deposition, results in the formation of the off-stoichiometric phase, which exhibits a brown colour due to the increased surface roughness and decreased mechanical and tribological properties. Figure 4.13 illustrates the resulting hardness of the sputtered films as a function of the nitrogen gas flow ratio. The plot contains three Ti-N coatings deposited with different parameters like substrate temperature or bias voltage, detailed information on the process is given in [104; 105].

Independent on the process parameters, all three curves have a maximum in hardness, which should correspond with the goldish stoichiometric cubic δ-TiN as it is the hardest phase in the Ti-N system. The sudden decrease in hardness by increasing the N_2/Ar gas flow ratio is caused by the off-stoichiometry combined with the increased influence of the substrate (see Oliver and Pharr [106]), as the deposition rate decreases and consequently, by using same deposition times, also the film thickness.

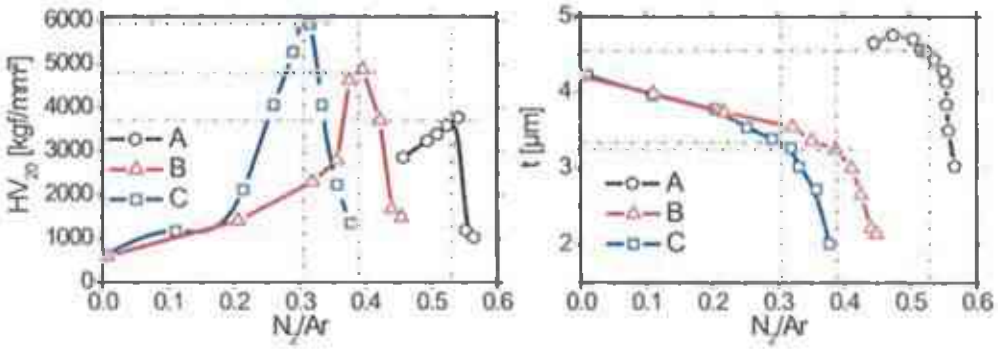

Figure 4.13: Hardness and film thickness as a function of N_2/Ar of TiN films deposited with different parameters (modified after [104; 105].

Furthermore, the high power discharge of the HIPIMS process occurs to be even more sensitive to the Ti target material, resulting in increased target surface arcing for nitrogen partial pressures higher than the values to deposit stoichiometric TiN. It is envisioned that arcing during HIPIMS is extremely sensitive to the poisoning of the target. Detailed information on the HIPIMS and DCMS deposition of TiN is given in Chapter 4.4.4.

4.4.3 Z700 coating plant

The coatings investigated in this thesis were deposited using a Z700HPM PVD coating plant, manufactured by the Systec SVS vacuum coating technology Karlstadt, Germany. Figure 4.14a is a schematic image of the Z700 and Figure 4.14b shows a cross-sectional top view of the used facility. The main data of the coating plant is as follows:

- coating chamber: Ø = 700 mm
- coating chamber height: 900 mm
- substrate load: Ø = 500 mm

- substrate load height: 400 mm
- substrate load weight: max. 500 kg
- cathodes types: 1 – 6 DCMS, HIPIMS or arcing sources
- cathode version: PK500 or HAK500
- target version: bolted or bonded type
- target size: (l x w x h) 488 x 87.5 x 6 mm (PK500)
- HIPIMS power supply: 2 KV / 2 KA pulse per cathode
- DCMS power supply: 5 – 8 KW dc per cathode
- arc power supply: 50 V / 100 A per cathode
- substrate power supply: 5 KW dc and pulsed dc
- pumping system: T1600 + WAU501 + SV200 or SV300
- gas inlet system: 3-5 MFC

For this project four cathodes of the coating plant were used, out of which the cathodes number one and two operate exclusively in HIPIMS mode, and cathode three in DCMS mode. Since the HIPIMS process can be easily adjusted to various magnetron sputtering systems, cathode number four can operate in DCMS or in HIPIMS mode by employing a change over switch system. However, using cathode four in HIPIMS mode disables completely cathode two because they have a shared HIPIMS power supply. Cathodes two and three are mounted on a so called mini chamber. The mini chamber can be easily moved in and out of the chamber. Figure 4.14a indicates the working chamber with the mini chamber removed, which offers the possibility to deposit large sized samples. Depositions in this project were carried out only with using the mini chamber, providing the advantage of two pairs of facing cathodes and hence an easy way for a multilayer deposition. As mentioned before, up to six cathodes can be used in the Z700, but for the investigations in this thesis the two cathodes, which can be fixed in the chamber door, were not mounted. The samples are mounted on substrate holders eight cm away from the target. Depending on the selection of individual rotation modes of the substrate holder carousel (platform rotation and rotation of the substrate holder pylons can be controlled independently of each other) various rotation modes, up to a three-fold rotation, can be achieved.

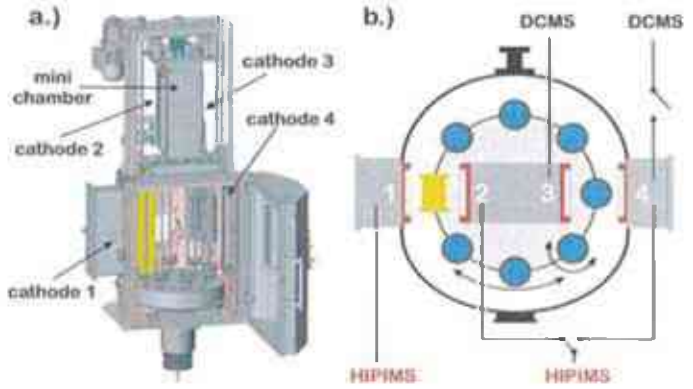

Figure 4.14: (a) schematic of the Z700 coating plant with removed mini chamber, and (b) cross-sectional top-view of the Z700.

4.4.4 HIPIMS deposition

All depositions carried out using the Z700 coating plant included the following pre-treatment steps:

I. samples were cleaned in an alcohol and acetone ultrasonic bath.

II. chamber was pumped down to pressures below $5 \cdot 10^{-5}$ mbar to start with

III. thermal cleaning of the substrates at 450 °C for 30 min (CrN_x deposition) and 650 °C for 60 min (TiN deposition).

IV. Ar ions sputter cleaning of the target material with a gas flow rate of 100 sccm. The powering of the target during etching was set on the same values as used during the individual depositions.

V. glow combustion for 8 min using an Ar gas flow rate of 500 sccm and a bias voltage of -1000 V, using two- and three-fold substrate rotations. At glowing, the targets three and four were operating in DCMS mode with a target powering of 180 V.

VI. samples were ion etched using the Cr target and a one-fold substrate rotation in front of the HIPIMS operating cathode (mainly cathode 1 or 4). This cathode 1 or 4 was with 1 kW, a frequency of 50 Hz and a duration time of 100 µs. The Ar gas flow rate was kept constant at 100 sccm. The bias voltage was ramped within a minute from -600 V to -1000 V. Total etching time used was 10 min.

As has been mentioned in chapter 4.3 an arc and droplet free plasma during HIPIMS deposition is required. Consequently all deposition parameters for the different targets have to be developed by indicating the frequency and duration time of a HIPIMS deposition in order to achieve controlled processes. Parameter detection for HIPIMS depositions have to be carried out if the used targets are varying as follows:

- material: e.g. Cr, Ti, TiAl
- different surface roughness of same materials
- different grain size of same materials
- manufacturing: i.e. hot isostatic pressing (HIP), electro slag remelting (ESR), binding elements etc.
- different purity of same materials

Figure 4.15 shows a HIPIMS generated plasma during CrN deposition, demonstrating an arc free process. Generation of arcs in the sputter track are sometimes not visible with the naked eye during deposition and the monitoring of the system can be too slow or not sensible enough to measure the rapid changes in the current densities. Due to this a check of the target material surface after HIPIMS deposition is essential to exclude any kind of discrete arcing on the surface. The HIPIMS plasma shown in Figure 4.15 indicated no evidence of any kind of discrete arcs on the target surface.

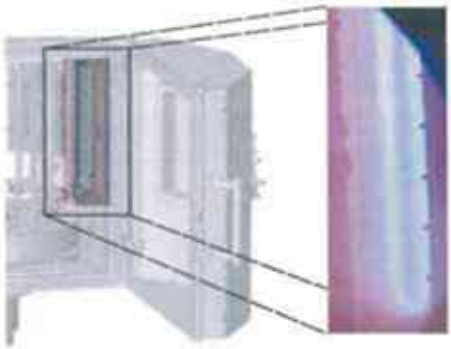

Figure 4.15: HIPIMS generated CrN plasma, using a dc powering of 5.5 kW, a frequency of 75 Hz and a duration of 150 µs.

Table 4.1 and Table 4.2 present a short summary of the CrN and TiN parameters for HIPIMS and DCMS deposition. The Ar/N_2 gas flow rate was set to a value corresponding to stoichiometric coatings. The powering of the DCMS cathode was to achieve comparable thicknesses to the HIPIMS deposition, evaluated at static deposition. The

powering of the HIPIMS cathode was at maximum values, where water cooling of the target material is still sufficient and no thermal load of the target, which would result in arcing and droplet formation or in the worst cases large-area melting, occurs. The magnetic field was set to 42 ± 2 kA/m, due to the unpredictable and not fully understood influence on the plasma yield.

Table 4.1: **Summary of the deposition parameters to deposit stoichiometric HIPIMS and DCMS CrN coatings and for the deposition of multilayered CrN/CrN coatings with the hybrid HIPIMS/DCMS deposition technique.**

Name	Hz/duration [Hz/µs]	Powering [kW] HIPIMS/UBM	Ar [sccm]	N_2 [sccm]	Bias [V]	Magnetic field [kA/m]	Temp. [°C]
HIPIMS CrN	75/150	5.5	100	200	-80	42±2	RT
DCMS CrN	-	2.0	100	200	-80	42±2	RT
HIPIMS/DCMS CrN/CrN	75/150	5.5/2	100	200	-80	42±2	RT

Depositions of multilayer CrN coatings were carried out also by using the hybrid HIPIMS/DCMS deposition technique where cathode three is operating in DCMS mode and cathode four in HIPIMS mode. This deposition arrangement was chosen to increase the deposition rate, due to the DCMS technique, as well as to increase the adatom mobility caused by the increased metal ion ratio generated by the HIPIMS technique.

Table 4.2: **Summary of the deposition parameters to deposit stoichiometric HIPIMS and DCMS TiN coatings and for the deposition of multilayered CrN/TiN coatings with the hybrid HIPIMS/DCMS deposition technique.**

Name	Hz/duration [Hz/µs]	Powering [kW] HIPIMS/UBM	Ar [sccm]	N_2 [sccm]	Bias [V]	Magnetic field [kA/m]	Temp. [°C]
HIPIMS TiN	300/100	5.5	100	7	-80	42±2	450
DCMS TiN	-	4.0	100	24.5	-80	42±2	450
HIPIMS/DCMS CrN/TiN	75/150	5.5/4	100	75	-80	42±2	450

Table 4.2 indicates that no hybrid HIPIMS/DCMS deposition, comparable with the CrN/CrN deposition, was achieved for TiN. As mentioned in Chapter 4.4.1, depositions of stoichiometric CrN coatings, compared to TiN deposition, can be conducted in a wide range of N_2/Ar gas flow ratio without any change in the hardness values. Figure 4.16 shows the hardness over N_2/Ar gas flow rate for single HIPIMS and DCMS deposited TiN and CrN coatings. As can be seen, the N_2 gas flow ratio for the stoichiometric CrN deposition is in the same range for both techniques, HIPIMS and DCMS, between one and two. On the other hand, TiN depositions exhibit two different gas flow ratios for the deposition of stoichiometric TiN coatings: 0.065 to 0.075 by using the HIPIMS technique and between 0.25 and 0.3 for the DCMS technique. Due to the affinity to arcing on the Ti target by increasing the gas flow ratio to values above 0.1 at HIPIMS deposition, and the deposition of non-stoichiometric films by decreasing the gas flow ratio below 0.2 at DCMS deposition, no hybrid HIPIMS/DCMS TiN deposition could be achieved.

On the other hand, an increase in the gas flow ratio above 0.3 during the UBM TiN deposition exhibits no arcing on the target surface and no significant changes in the hardness values, and thus enables a deposition of multilayered CrN_{HIPIMS}/TiN_{DCMS} coatings, see Table 4.2.

Papers I to IV demonstrate the advantages of the hybrid HIPIMS/DCMS generated multilayered CrN/CrN and CrN/TiN coatings.

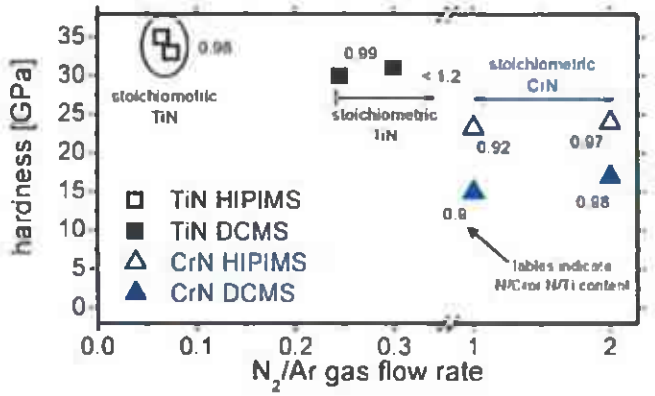

Figure 4.16: Hardness as a function of the N_2/Ar gas flow rate of DCMS and HIPIMS CrN and TiN coatings indicating the chemical compositions (unpublished results).

5 Coating characterisation

Chemical compositions, morphology, mechanical and tribological properties of the deposited coatings were studied. The following chapters summarize the main destructive and non-destructive evaluation methods used in this thesis.

5.1 Hardness

The hardness is commonly defined as the resistance of a material against plastic deformation caused by the penetration of a harder material like diamond [2; 107]. Indenters differ in their shape and thus in their area of application, for example a pyramidal shape (Vickers) or spherical shape (Brinell). These indenters are mostly used for micro- and macro-hardness measurements, thus normal loads from below 2 N to above 30 N. The three-sided Berkovich indenter is the most popular geometry for the nanoindentation testing ($P < 50$ mN), due to its sharper tip as compared to the four-sided Vickers pyramidal indenter [108; 109]. Figure 5.1a shows a cross-section of an indentation illustrating the parameters used for the calculation, as well as the real depth of the indentation and the projected area after unloading due to elastic relaxations [106].

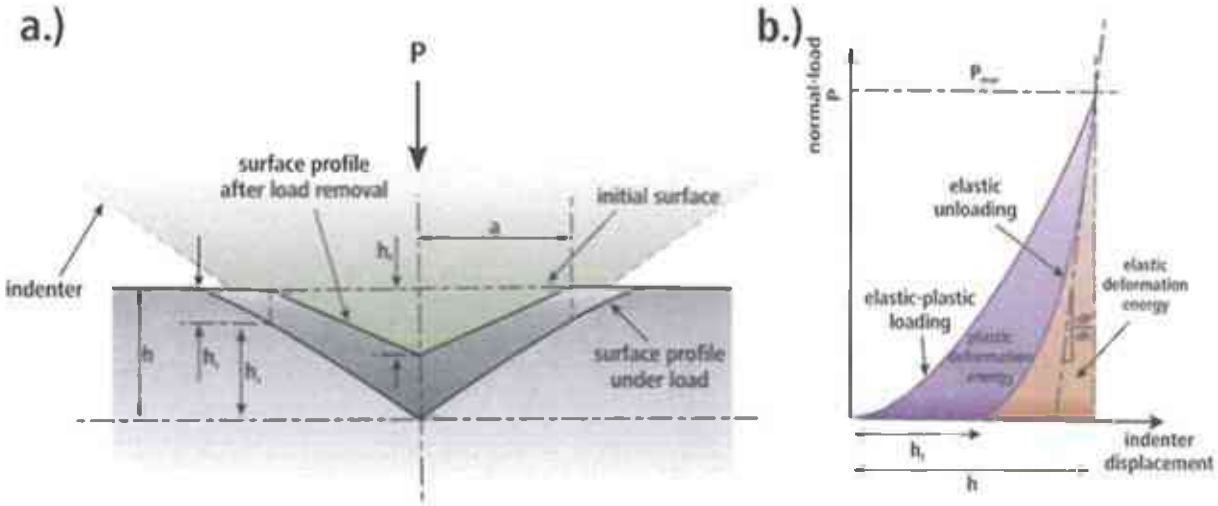

Figure 5.1: (a) Schematic of an indentation with a Berkovich indenter modified after [106] and (b) the resulting load-displacement curve after [110].

The most important difference between the micro hardness and the hardness measured by the nanoindentation is the evaluation of the indentation depth. Commonly the depth after the micro-indentation is evaluated by measuring via optical devices of the projected area, which is the surface profile after unloading (see Figure 5.1a) and recalculate the hardness using the dimensions of the indenter. This is possible since during the micro- and macro-hardness measurements the difference between the elastic and plastic deformation is neglible small and hence the resulting calculation error is small. For the nanoindentation, the difference between the plastic and elastic deformation is too big and thus a recording of the load versus indenter displacement is required, see Figure 5.1b. From the recorded indenter displacement curves the hardness values as well as the elastic moduli can be evaluated. Detailed information on the evaluation and calculation of the hardness and elastic modulus are given in [106; 108; 109].

5.2 Wear

Tribology is the science addressing the damage or removal of a material due to sliding, rolling or impact motion caused by a counter facing material, which results in a deformation of one or both of the material surfaces. These interactions take place at the moving interface and is controlled by the friction, wear or lubrication behaviour [111; 112].

5.2.1 Adhesive wear

Adhesive wear occurs when two nominally flat materials are in a sliding contact. This can be obtained in a dry atmosphere or under lubricious conditions. However, the contact between the two real surfaces occurs at the small asperities in the interface and results in adhesion which is more or less a bonding of the two surfaces, and is shared due to sliding. The bonding between the two materials can be strong enough to cause detaching of fragments, mostly from the softer material, and subsequent re-attachment on the other material during sliding testing [112]. Several mechanisms of the materials detachment

during sliding testing have been proposed and are summarized in [112]. Nevertheless, pure adhesive wear measurements are difficult to conduct due to the influence of asperities during sliding testing.

The sliding wear measurements reported in this thesis were obtained by a ball on disks tribometer (BOD). Figure 5.2 shows a schematic image of the CSM tribometer for measurements at RT. The Al_2O_3 counterpart ball, which is held stationary while the tested material rotates, has a diameter of 6 mm and indicates the required flat contact area for the adhesive testing. The alumina ball was chosen, because of its higher wear resistance than the deposited coatings and shows nearly no wear. Consequently, the shape of the ball is constant during testing and no change of the contact area and resulting normal load occurs. The normal load and the test distance were varied from 1 to 5 N and from 100 to 5000 m. Changes in the rotation speed and the number of overruns per spot have no influence on our coatings performance during testing.

The friction coefficient (μ) is defined as the ratio of the friction force (F_f) and the applied normal load (F_N): $F_f = \mu F_N$. The friction coefficient μ is independent of the sliding velocity and the normal load but it is influenced by the real contact area, as due to the surface roughness only a contact of the asperities occurs. If the applied normal load is low the deformation of the asperities is elastic, the contact is still only due to surface roughness. On the other hand, if the load is high the asperities can be detached and cause abrasive wear during the sliding testing. Consequently, the used BOD test apparatus evaluates a combination of the adhesive and abrasive mechanisms during the measurements.

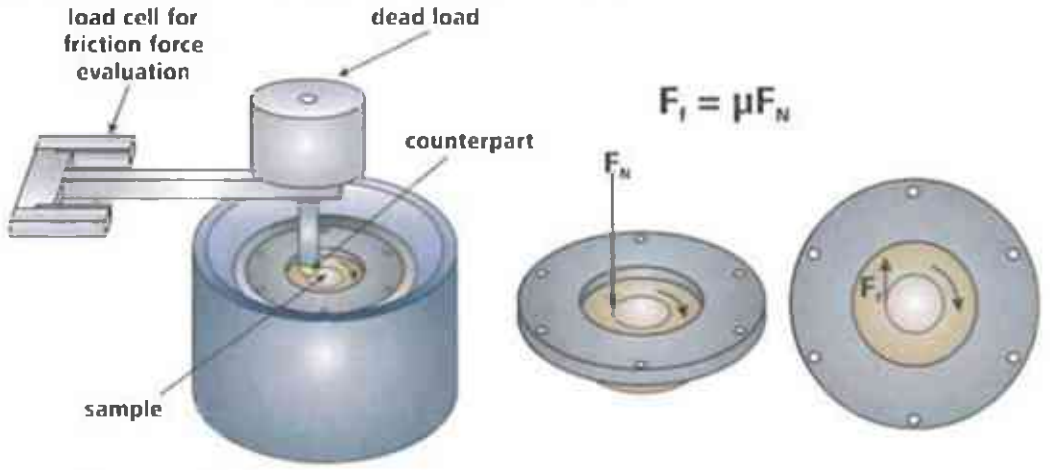

Figure 5.2: Schematic of a CSM BOD measuring system.

5.2.2 Abrasive wear

Pure abrasive wear occurs when hard particles or hard asperities groove on a surface and cause damage of the interface by a plastic deformation or fraction. The most common test to measure the abrasive wear resistance is to introduce hard particles (the abrasives) in-between the interface of the testing material and the counterpart. The abrasive wear measurements strongly depend on the size and shape of the particles as well as on their hardness and their amount [111; 112].

The measurements carried out in this thesis are conducted with a simple ball cratering setup (see Figure 5.3), using a hard steel ball with a diameter of 25.4 or 30 mm and an aqueous suspension of Al_2O_3 granulate with particle sizes of 4 µm. The normal load was approximately 0.45 N (measured with a load cell during the testing) and the total distance of the test was 50 m. The amount of the abrasives was determined by the mixing ratio of the Al_2O_3 powder and distilled water. The calculations of the abrasive wear coefficient followed [113].

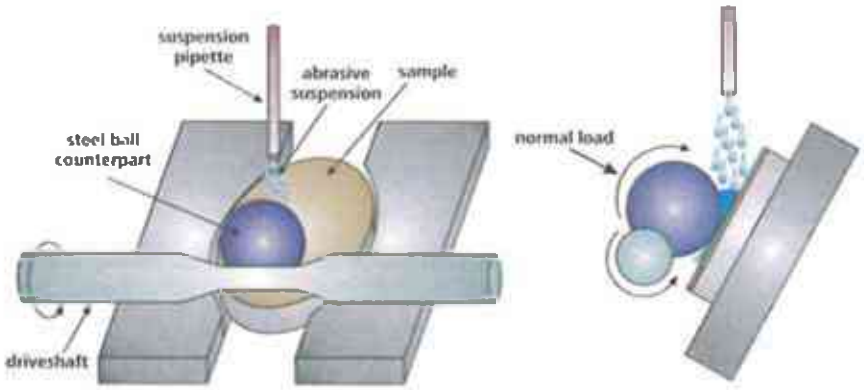

Figure 5.3: Schematic of a CSM ball cratering measuring system.

5.3 X-ray diffraction (XRD)

The X-ray diffraction (XRD) is a non-destructive method to determine the structure, phase composition and texture by comparing the evaluated peaks with known standards. The XRD method is based on the correlation between lattice plane spacing and the wavelength (λ) of the X-ray. Emitted beams with high intensities due to a constructive interference along certain directions are detected when the incident X-rays impinge at

certain diffraction angles (θ). Consequently, for each system of lattice planes described by the lattice plane spacing parameter d, the diffraction condition known as Bragg's law ($n \cdot \lambda = 2 \cdot d \cdot \sin\theta$), n is an integer, is fulfilled only for special values of the diffraction angle θ [2; 107; 114]. Further information on the XRD and measurement methods is given in [115; 116].

XRD measurements carried out in this thesis were mostly done in the Bragg-Brentano mode or glancing angle mode. By using glancing angle (grazing incident), the angle (θ) of the incident beam is fixed at 4 ° to minimize the penetration depth of the X-rays into the material. Consequently, for 2 µm thick coatings on steel and silicon substrates the peaks of the substrate materials are not visible in the XRD scan, which results in an easier identification of the film structure.

5.4 Scanning electron microscopy (SEM)

Scanning electron microscopy (SEM) is a standard technique and commonly used to characterize structure and morphology as well as chemical composition of materials. The SEM uses thermally emitted electrons from a cathode filament and focuses them into a high energetic electron beam to detect the materials surface. The typical size of such a beam is in the range of 10 Å in diameter. The emitted focused electron beam is interacting with the material, as the electrons loose energy by an interaction with the sample lattice due to inelastic collisions. This scattering of the surface results in a tear drop shaped interaction area. The generated signals include secondary electrons, backscattered electrons and X-rays [2].

The secondary electron mode is the most commonly used to image the material surface. The number of detected secondary electrons is affecting the brightness of the image and is accountable for the three dimensional shaped illustration of this mode. The backscattered electrons and the X-ray monitoring are used to detect different chemical compositions. The backscattered electrons provide difference in the brightness of the image due to the size (increasing atomic number results in a brighter contrast in the

image) of the materials elements, and the X-ray mode is used to identity the chemical composition of the material [2].

The secondary electrons monitoring and the energy dispersive X-ray spectroscopy (EDX) were used to evaluate the structure and morphology as well as the chemical composition of the deposited coatings in this thesis.

5.5 Transmission electron microscopy (TEM)

Similarly to the SEM, the transmission electron microscopy (TEM) uses the interaction of a focused electron beam with the sample. As the name implies, the sample has to be thin enough to allow transmission of electrons and to provide structural information. A series of magnetic lenses positioned above and below the sample are used to direct the signal to a detector, usually a fluorescent screen or a video camera [114].

The common methods used to get information about the samples structures are the bright-field imaging, the dark-field imaging, the lattice imaging, the diffraction, the X-ray spectroscopy or the electron energy loss spectroscopy [2]. Detailed information on the different TEM techniques are given in [117; 118].

The TEM cross-section imaging is used to investigate the film to substrate area and the layer-by-layer growth of the multilayer CrN/TiN arrangement in this thesis. Coatings on silicon or steel substrates were thinned in a transverse direction. The thinning of the samples were done by hand grinding and polishing (up to a grain size of 0.25µm of the lubricious polishing suspension) on both sides to a thickness of around 30 – 50 µm. To achieve a transmittable area the samples were further ion polished using a precise ion polishing system (PIPS) with an ion incident angle of 4 °.

5.6 Secondary ion mass spectrometry (SIMS)

In the secondary ion mass spectrometry (SIMS) a solid specimen is bombarded in vacuum by high energetic narrow beam of ions, called primary ions. These impacts cause sputtering of the surface and ejections of small atom clusters which can be neutrals or

charged particles. As the name implies, in this method charged ions, the so-called secondary ions, are used and are subsequently accelerated towards a mass spectrometer. There they are separated according to their mass-to-charge ratio and counted. The measured secondary ions number are converted to concentrations and compared with known standards [114].

The SIMS measurements carried out in this thesis are concerning on the implantation effects of the HIPIMS etching process. The incorporation of chromium and titanium into the substrate near surface regions and the evaluation of the effective implantation depth after etching in an industrial sized unit are evaluated by a time-of-flight SIMS (ToF-SIMS) assisted by an optical profilometer to evaluate the sputter-depth after the SIMS measurement.

6 Summary of papers and contribution to the field

Paper I

High power impulse magnetron sputtering is a PVD technique with high ion dissipation but low deposition rates. We investigated the effect of hybrid HIPIMS/DCMS sputtered on the microstructure, the texture, the mechanical and the tribological properties as well as on the deposition rate of single-phase CrN coatings deposited at RT. The generated coatings are multilayered CrN_{HIPIMS}/CrN_{DCMS} as the substrate holder is rotating in-between two facing cathodes, one of which is operating in HIPIMS and the other one in DCMS mode.

Increasing the DCMS power from 0 to 5 kW while keeping the HIPIMS cathode power constant at a maximum value of 5.5 kW causes a change from a dense and almost equiaxed to an open columnar microstructure, and a transition from a preferred (200) orientation to a (111) dominated texture. These changes in the film morphology due to increased CrN_{DCMS} content result in decreasing the hardness values from ~25 to 7 GPa and increasing the sliding wear coefficients from $\sim 0.35 \cdot 10^{-16}$ to $1 \cdot 10^{-16}$ m^3/Nm and the abrasive wear data from $1.7 \cdot 10^{-13}$ to $8.6 \cdot 10^{-13}$ m^3/Nm. On the other hand the deposition rate increases linearly with the increasing DCMS content in the multilayered CrN_{HIPIMS}/CrN_{DCMS} coating from 23 to 65 nm/min.

Based on these results we can conclude that coatings with required mechanical and tribological properties combined with industrial useable deposition rates can be obtained by simple adjustments of the HIPIMS/DCMS bilayer period.

Paper II

The influence of deposition conditions on CrN and TiN coatings deposited in the HIPIMS and DCMS modes using 0-, 1-, 2- and 3-fold substrate rotation and sample temperatures around 150 and 400 °C are investigated in this paper. The results clearly demonstrate that HIPIMS allows for denser coatings with superior mechanical and tribological properties as compared with DCMS. To combine the benefits of HIPIMS and DCMS (especially the

higher deposition rate) investigations of hybrid CrN_{HIPIMS}/CrN_{DCMS} coatings were conducted as a function of the CrN_{DCMS} content. The effects of the different bilayer periods on structure, mechanical and tribological properties were also discussed in paper I, and emphasized the advantages of the hybrid deposition technique, like the increased wear resistance of the CrN_{HIPIMS}/CrN_{DCMS} coatings with different bilayer periods, which were around $1 \cdot 10^{-16}$ m^3/Nm and consequently at least two orders of magnitude lower than those of their monolithic CrN_{DCMS} counterparts.

Comparable results are obtained for HIPIMS and DCMS prepared TiN coatings. Hardness values of monolithic TiN_{HIPIMS} coatings around 35 GPa, using 0- or 1- fold substrate rotation and substrate temperatures T_s ~150 °C were obtained, compared with ~30 and 10 GPa for monolithic TiN_{DCMS} coatings when using 0- and 1-fold substrate rotation, respectively, and T_s ~400 °C.

To increase the performance of the monolithic TiN_{DCMS} coatings, depositions with an additional anode using substrate temperatures of ~150 and 400 °C were performed, resulting in hardness values of ~10 and 35 GPa, respectively. Furthermore, depositions of a monolithic TiN_{DCMS} film on top of a multilayered CrN_{HIPIMS}/TiN_{DCMS} base-layer, operating as a template, were carried out at ~400 °C, resulting in hardness values of this DCMS top-layer comparable with those of monolithic TiN_{HIPIMS}.

In conclusion, our results suggest that HIPIMS offers a higher versatility (by providing uniform and dense coatings) than DCMS when thermally sensitive materials need to be deposited and/or the deposition process needs to be up-scaled or substrate-rotations have to be changed for complex shaped specimens.

Paper III

Deposition of monolithic CrN and TiN coatings were carried out in HIPIMS and DCMS mode using 0- and 1-fold substrate rotations. As can be seen in paper I and II, the HIPIMS process provides coatings with excellent mechanical and tribological properties especially if a substrate rotation is used, when compared with DCMS.

TiN_{DCMS} coatings appear to be very sensitive if changing from static to dynamic depositions, as the hardness decreases from ~30 to 10 GPa with a simple change from 0-

to 1-fold substrate rotation, respectively. This drawback can be overcome if the TiN coatings are prepared by HIPIMS. TiN_{HIPIMS} show almost no influence of the changing deposition conditions as the hardness is ~39 and 34 GPa for 0- and 1-fold substrate rotation, respectively. Corresponding results for CrN coatings were obtained and are discussed in paper I and II.

Depositions of multilayered CrN_{HIPIMS}/TiN_{DCMS} coatings were carried out with variation of the DCMS content in the coating by increasing the power at the cathode from 4 to 7 kW, and show hardness values around 26 GPa, independently of the TiN_{DCMS} layer thickness. These values are higher than 12 GPa of the single TiN_{DCMS} and indicate that HIPIMS also influences the plasma conditions in front of the cathode operating in DCMS mode. Furthermore monolithic TiN_{DCMS} coatings yielded a pronounced (111) orientation as compared with the multilayered CrN_{HIPIMS}/TiN_{DCMS} which exhibited a dense structure and a strong (200) orientation, even for increased TiN layer thicknesses. Consequently, the sliding wear coefficients of the CrN_{HIPIMS}/TiN_{DCMS} coatings are in the range of $3.5\text{-}6 \cdot 10^{-16}$ m^3/Nm and hence at least two magnitudes lower as compared with $150 \cdot 10^{-16}$ m^3/Nm obtained for the monolithic layer TiN_{DCMS}.

These results clearly demonstrate that the combination of HIPIMS and DCMS enables preparation of dense coatings with excellent mechanical and tribological properties.

Paper IV

Multilayered CrN_{HIPIMS}/TiN_{DCMS} coatings with varying bilayer periods from 7.8 to 6.4 nm where the CrN_{HIPIMS} layer thicknesses were kept constant at 3.2 nm were deposited with 1-fold substrate rotation between two facing Cr and Ti targets operating in HIPIMS and DCMS modes, respectively. As already shown in paper III the hardness values are constant at around 26 GPa for all bilayer periods. Nevertheless during dry-sliding RT ball on disc (BOD) tests decreasing friction coefficients from ~0.7 to 0.35 are obtained, when the bilayer period decreases from 7.8 to 6.4 nm, respectively.

Further reduction of the friction coefficient can be obtained by introducing a third cathode operating in HIPIMS mode equipped with a Cr or Ti target to deposit CrN_{HIPIMS}/TiN_{DCMS} using a 2- and 3-fold substrate rotation. The friction coefficient μ in

ambient air conditions (relative humidity around 25%) decreases to values of ~0.25 or 0.05, when equipping the additional HIPIMS cathode with a Cr or Ti target (i.e. CrN/TiN/CrN or CrN/TiN/TiN), respectively.

Tests in different atmospheres (Ar, N_2, synthetic air) during BOD testing show, that if the relative humidity is decreased to values around 1% the friction coefficient of the CrN/TiN/TiN coatings increases from ~0.05 to ~0.7. On the other hand measurements in distilled water give friction coefficients comparable with those evaluated in ambient air conditions. Therefore we conclude that the friction coefficient of the multilayered CrN_{HIPIMS}/TiN_{DCMS} coatings is related to the relative humidity during testing. Measurements of the contact angle between a distilled water droplet and the as deposited coating surfaces were carried out indicating increased wettability of the coatings with decreased friction coefficients.

Based on these results we conclude that by combining the HIPIMS technology with the conventional DCMS technology to deposit multilayered CrN/TiN coatings, friction coefficients as low as 0.05 with hardness values of ~26 GPa and reasonable deposition rates can be simultaneously obtained even for multi-fold substrate rotations.

Contribution to the field

The HIPIMS process is a new PVD deposition technique which inheres the advantages of DCMS and arc evaporation. Consequently, HIPIMS has been a topic of many recent publications, discussing the plasma generation and configuration. Nevertheless, it is yet not common to use HIPIMS as an industrial deposition technique. CrN and TiN hard coatings are well investigated and used in many applications, e.g. in the automotive area. Therefore, they can serve as a perfect benchmark for investigations of the HIPIMS process at the industrial scale.

The HIPIMS process indicates to be very sensitive to the target material used which results in adjusting all the individual parameters (even when changing the target but not the material) to generate an arc-free plasma. Consequently, the estimated deposition parameters described in this thesis are of no general use, but rather exhibit a parameter range of possible frequencies and durations for an easier finding of the deposition

configurations. Nevertheless, the Z700 input values for depositing monolithic CrN_{HIPIMS} and TiN_{HIPIMS} coatings are investigated for static and dynamic depositions, and the films exhibit superior mechanical and tribological properties as compared with CrN_{DCMS} and TiN_{DCMS} coatings, respectively.

The HIPIMS process is known to have a low deposition rate, about one third of the DCMS deposition. To overcome this drawback we investigated the hybrid HIPIMS/DCMS deposition technique to obtain coatings with improved properties and at the same time with economically and industrially usable deposition rates. In case of the CrN_{HIPIMS}/CrN_{DCMS} coatings, the obtained deposition rate is three-times higher than that of monolithic CrN_{HIPIMS}, with the advantage of improved wear resistance compared with CrN_{DCMS}. On the other hand, increasing the deposition rate (by increasing the CrN_{DCMS} layer-thickness of the multilayered CrN_{HIPIMS}/CrN_{DCMS} coatings) leads to decreasing hardness values from around 23 to 7 GPa. Consequently, an application oriented choice of the bilayer period is possible, i.e. high deposition rate with increased wear properties or lower deposition rate with increased mechanical and tribological properties.

Additional, also TiN depositions using HIPIMS and DCMS with varying substrate rotations and temperatures T_s around 150 and 400 °C were performed. The results are comparable with those evaluated for CrN, but the difference between HIPIMS and DCMS were more pronounced due different growth kinetics of Ti based materials.

To improve the monolithic TiN_{DCMS} coating properties, we investigated the effects of an additional anode during the deposition at T_s ~150 °C, which resulted in hardness values comparable with monolithic TiN_{DCMS} when using temperatures around 400 °C. We also investigated template effects of the HIPIMS generated layers on the DCMS generated layers, resulting in increased performances. Consequently, we investigated the template effects of a multilayered CrN_{HIPIMS}/TiN_{DCMS} base-layer on a TiN_{DCMS} top-layer deposited at temperatures around 400 °C. The results indicate the positive effect of the base-layer on structure, mechanical and tribological properties of the top-layer.

Investigations of multilayered TiN_{HIPIMS}/TiN_{DCMS} coatings, comparable with CrN_{HIPIMS}/CrN_{DCMS}, could not be carried out in the Z700 since the difference in the N_2 partial pressure is too pronounced between HIPIMS and DCMS, which resulted in increased arcing on the

HIPIMS cathode or in the formation of under-stoichiometric coatings. As a consequent, depositions of multilayered CrN_{HIPIMS}/TiN_{DCMS} coatings were carried as the CrN_{HIPIMS} and the TiN_{DCMS} depositions require comparable reactive gas flow rates. The evaluated hardness values and the wear coefficients are in the range of the monolithic CrN_{HIPIMS} coatings independent to the TiN_{DCMS} layer-thicknesses (the range is defined by minimum and maximum powering of the Z700 coating plant), gaining the advantage of decreased friction coefficients to values < 0.1 as measured by a BOD tester at ambient air conditions. Consequently we have developed a low friction hard coating, which can compete with carbo-nitride or DLC coatings.

It has to be mentioned that the Z700 is a very unique coating plant due to its target arrangement (two pairs of two facing cathodes). Therefore, investigations in other deposition plants where the HIPIMS plasma is not directly interacting with the DCMS plasma, e.g. the Z1200, could be the terms of further studies.

Furthermore, plasma and resulting film properties as a function of the magnetic field strength of the HIPIMS powered cathode are of interest, as our investigations were conducted using fixed magnetic field strengths.

For industrial applications, depositions and substrate metal ion etching using a multi-fold substrate rotation are of interest, as in this thesis the etching was carried out in front of the HIPIMS cathode only by using 0- or 1-fold substrate rotation.

The work done in this thesis demonstrates, that the HIPIMS technique is very promising as it is capable of depositing coatings with superior properties for industrial applications, especially when our hybrid HIPIMS/DCMS technique is used.

7 Bibliography

[1] P.H. Mayrhofer, G. Tischler, C. Mitterer, Surface and Coatings Technology 142-144 (2001) 78.
[2] M. Ohring, The material science of thin films, Academic Press (1991).
[3] B. Warcholiński, A. Gilewicz, Z. Kukliński, P. Myśliński, Vacuum 83 (2008) 715.
[4] M. Lattemann, A.P. Ehiasarian, J. Bohlmark, P.A.O. Persson, U. Helmersson, Surface and Coatings Technology 200 (2006) 6495.
[5] R.F. Bunshah, D.M. Mattox, Deposition Technologies for Films and Coatings, Development and Applications, Noyes Publications, New Jersey (1982).
[6] P.B. Barna, Proc. Diagnostics and Applications of Thin Films (L. Eckertová, T. Ruzicka eds.) Institute of Physics Publishing (1992) 295.
[7] P.B. Barna, M. Adamik, Thin Solid Films 317 (1998) 27.
[8] J.E. Greene, Handbook of Crystal Growth (D.T.J. Hurle, ed.) 1 (1993) 640.
[9] J.E. Greene, Handbook of Deposition Technologies for films and coatings (R.F. Bunshah ed.) (1994) 681.
[10] Y. Pauleau, P.B. Barna, Protective Coatings and Thin Films, Kluwer Academic Publisher, Dordrecht (1997).
[11] I. Petrov, P.B. Barna, L. Hultman, J.E. Greene, Journal of Vacuum Science & Technology A 21 (2003) 117.
[12] C.A. Neugebauer, Handbook of Thin Film, (L.I. Maissel ed) (1983).
[13] B. Rother, J. Vetter, Plasma-Beschichtungsverfahren und Hartstoffschichten, Dt. Ver. für die Grundstoffindustrie (1992).
[14] D.L. Smith, Thin-Film Deposition, McGraw-Hill Inc. (1995).
[15] F.-W. Bach, T. Duda, Moderne Beschichtungsverfahren, Wiley-VCH (2000).
[16] R.A. Haefer, Oberflächen und Dünnschicht-Technologie, Teil I, Springer Verlag (1987).
[17] A.M. Brown, M.F. Ashby, Acta Metallurgica 28 (1980) 1085.
[18] B.A. Movchan, A.V. Demchishin, Phys. Met. Metallogr. 28 (1969) 83.
[19] J.A. Thornton, Annual Review of Materials Science 7 (1977) 239.
[20] R. Messier, A.P. Giri, R.A. Roy, Journal of Vacuum Science & Technology A 2(2) (1984) 500.
[21] J.A. Thornton, Journal of Vacuum Science & Technology 11 (1974) 666.
[22] J.A. Thornton, Journal of Vacuum Science & Technology 12 (1975) 830.
[23] J.E. Greene, Solid State Technology 30 (1987) 115.
[24] D.M. Mattox, Journal of Vacuum Science & Technology A 7 (1989) 1105.
[25] P.H. Mayrhofer, C. Mitterer, L. Hultman, H. Clemens, Progress in Materials Science 51 (2006) 1032.
[26] W. Ensinger, Nuclear Instruments and Methods in Physics Research, Section B 127-128 (1997) 796.
[27] P.H. Mayrhofer, Doctor thesis Montanuniversität Leoben (2001).
[28] S.M. Rossnagel, Journal of Vacuum Science & Technology A 7 (1989) 1025.
[29] A.P. Ehiasarian, W.D. Münz, L. Hultman, U. Helmersson, I. Petrov, Surface and Coatings Technology 163-164 (2003) 267.
[30] A.P. Ehiasarian, R. New, W.D. Münz, L. Hultman, U. Helmersson, V. Kouznetsov, Vacuum 65 (2002) 147.
[31] V. Kouznetsov, K. Macák, J.M. Schneider, U. Helmersson, I. Petrov, Surface and Coatings Technology 122 (1999) 290.

[32] C. Mitterer, P.H. Mayrhofer, E. Kelesoglu, R. Wiedemann, H. Oettel, Zeitschrift fuer Metallkunde/Materials Research and Advanced Techniques 90 (1999) 602.
[33] C. Mitterer, P.H. Mayrhofer, W. Waldhauser, E. Kelesoglu, P. Losbichler, Surface and Coatings Technology 108-109 (1998) 230.
[34] I. Petrov, L. Hultman, J.E. Sundgren, J.E. Greene, Journal of Vacuum Science & Technology A 10 (1992) 265.
[35] A.S. James, A. Matthews, Surface and Coatings Technology 61 (1993) 282.
[36] G. Kienel, Vakuumbeschichten 2, Verfahren und Anlagen, VDI Verlag Düsseldorf (1995).
[37] M. Konuma, Film deposition by plasma techniques, Springer Verlag (1992).
[38] B. Window, N. Savvides, Journal of Vacuum Science & Technology A 4 (1986) 453.
[39] B. Window, Surface and Coatings Technology 81 (1996) 92.
[40] J. Ganz, Metalloberfläche 45 (1991) 11.
[41] W.D. Sproul, Surface and Coatings Technology 49 (1991) 284.
[42] I. Ivanov, P. Kazansky, L. Hultman, J.E. Sundgren, Journal of Physics D: Applied Physics 27 (1994) 280.
[43] I. Petrov, F. Adibi, J.E. Greene, W.D. Sproul, W.D. Münz, Journal of Vacuum Science & Technology A 10 (5) (1992) 3283.
[44] A. Spencer, K. Oka, R. Howson, R. Lewin, Vacuum 38 (1988) 857.
[45] S. Kadlec, J. Musil, W.D. Münz, G. Hakanson, J.E. Sundgren, Surface and Coatings Technology 39-40 (1989) 487.
[46] S. Kadlec, J. Musil, V. Valvoda, W.D. Münz, H. Petersein, J. Schroeder, Vacuum 41 (1990) 2233.
[47] W.D. Münz, Proceedings, Annual Technical Conference - Society of Vacuum Coaters (1993) 411.
[48] W.D. Münz, B.V. Venlo, Proceedings, Annual Technical Conference - Society of Vacuum Coaters (1992) 240.
[49] P.D. Davidse, Vacuum 17 (1967) 139.
[50] B. Probyn, Vacuum 18 (1968) 253.
[51] G.N. Jackson, Thin Solid Films 5 (1970) 209.
[52] W.D. Sproul, D.J. Christie, D.C. Carter, Thin Solid Films 491 (2005) 1.
[53] P.J. Kelly, P.S. Henderson, R.D. Arnell, G.A. Roche, D. Carter, Journal of Vacuum Science & Technology A 18 (2000) 2890.
[54] D. Carter, H. Walde, G. McDonough, G. Roche, Proceedings of the 45th Annual Technical Conference Proceedings of the Society of Vacuum Coaters (2002) 570.
[55] G. Håkansson, L. Hultman, J.E. Sundgren, J.E. Greene, W.D. Münz, Surface and Coatings Technology 48 (1991) 51.
[56] W.D. Münz, J. Schroeder, H. Peterstein, G. Håkansson, L. Hultman, J.E. Sundgren, Proc. SURTEC Berlin (1989) 61.
[57] W.D. Münz, F.J.M. Hauzer, D. Schulze, B. Buil, Surface and Coatings Technology 49 (1991) 161.
[58] W.D. Münz, D. Schulze, F.J.M. Hauzer, Surface and Coatings Technology 50 (1992) 169.
[59] W.D. Münz, K. Vannisselroy, R. Tietema, T. Hurkmans, G. Keiren, Surface and Coatings Technology 58 (1993) 205.
[60] P.E. Hovsepian, A.P. Ehiasarian, A. Deeming, C. Schimpf, Vacuum 82 (2008) 1312.
[61] P.E. Hovsepian, A.P. Ehiasarian, U. Ratayski, Surface and Coatings Technology 203 (2009) 1237.
[62] P.E. Hovsepian, C. Reinhard, A.P. Ehiasarian, Surface and Coatings Technology 201 (2006) 4105.

[63] K. Sarakinos, J. Wördenweber, F. Uslu, P. Schulz, J. Alami, M. Wuttig, Surface and Coatings Technology 202 (2008) 2323.
[64] J. Böhlmark, Doctor thesis Linköping University (2005).
[65] D.J. Christie, F. Tomasel, W.D. Sproul, D.C. Carter, Journal of Vacuum Science & Technology A 22 (2004) 1415.
[66] K. Macák, V. Kouznetsov, J. Schneider, U. Helmersson, I. Petrov, Journal of Vacuum Science and Technology A 18 (2000) 1533.
[67] U. Helmersson, M. Lattemann, J. Bohlmark, A.P. Ehiasarian, J.T. Gudmundsson, Thin Solid Films 513 (2006) 1.
[68] J.T. Gudmundsson, J. Alami, U. Helmersson, Surface and Coatings Technology 161 (2002) 249.
[69] J. Musil, J. Leština, J. Vlček, T. Tölg, Journal of Vacuum Science and Technology, Part A: Vacuum, Surfaces and Films 19 (2001) 420.
[70] S.P. Bugaev, N.N. Koval, N.S. Sochugov, A.N. Zakharov, International Symposium on Discharges and Electrical Insulation in Vacuum, ISDEIV 2 (1996) 1074.
[71] A.P. Ehiasarian, R. Bugyi, 47th Annual Technical Conference Proceedings of the Society of Vacuum Coaters (2004) 486.
[72] S.P. Bugaev, N.S. Sochugov, Surface and Coatings Technology 131 (2000) 474.
[73] S. Konstantinidis, J.P. Dauchot, M. Ganciu, M. Hecq, Applied Physics Letters 88 (2006) 1.
[74] W.D. Sproul, D.J. Christie, D.C. Carter, F. Tomasel, T. Linz, Surface Engineering 20 (2004) 174.
[75] I. Petrov, A. Myers, J.E. Greene, J.R. Abelson, Journal of Vacuum Science & Technology A 12 (1994) 2846.
[76] L. Hultman, U. Helmersson, S.A. Barnett, J.E. Sundgren, J.E. Greene, Journal of Applied Physics 61 (1987) 552.
[77] J.T. Gudmundsson, J. Alami, U. Helmersson, Applied Physics Letters 78 (2001) 3427.
[78] S.M. Rossnagel, H.R. Kaufman, Journal of Vacuum Science & Technology A 6 (1988) 223.
[79] S.M. Rossnagel, J. Hopwood, Applied Physics Letters 63 (1993) 3285.
[80] S.M. Rossnagel, J. Hopwood, Journal of Vacuum Science & Technology B 12 (1994) 449.
[81] J. Alami, P.O.Ã. Persson, D. Music, J.T. Gudmundsson, J. Bohlmark, U. Helmersson, Journal of Vacuum Science & Technology A 23 (2005) 278.
[82] B.M. DeKoven, P.R. Ward, R.E. Weiss, D.J. Christie, R.A. Scholl, W.D. Sproul, F. Tomasel, A. Anders, Proceedings, Annual Technical Conference - Society of Vacuum Coaters (2003) 158.
[83] W.D. Sproul, D.J. Christie, D.C. Carter, Proceedings, 47th Annual Technical Conference - Society of Vacuum Coaters (2004) 96.
[84] A.P. Ehiasarian, P.E. Hovsepian, L. Hultman, U. Helmersson, Thin Solid Films 457 (2004) 270.
[85] J. Paulitsch, P.H. Mayrhofer, W.D. Münz, M. Schenkel, Proceedings, 50th Annual Technical Conference - Society of Vacuum Coaters (2007) 150.
[86] J. Paulitsch, P.H. Mayrhofer, W.D. Münz, M. Schenkel, Thin Solid Films 517 (2008) 1239.
[87] J. Bohlmark, M. Lattemann, J.T. Gudmundsson, A.P. Ehiasarian, Y. Aranda Gonzalvo, N. Brenning, U. Helmersson, Thin Solid Films 515 (2006) 1522.
[88] C. Schönjahn, L.A. Donohue, D.B. Lewis, W.D. Münz, R.D. Twesten, I. Petrov, Journal of Vacuum Science & Technology A 18 (2000) 1718.

[89] C. Schönjahn, A.P. Ehiasarian, D.B. Lewis, R. New, W.D. Münz, R.D. Twesten, I. Petrov, Journal of Vacuum Science & Technology A 19 (2001) 1415.
[90] A. Matthews, D.G. Teer, Thin Solid Films 73 (1980) 315.
[91] A. Matthews, D.G. Teer, Thin Solid Films 72 (1980) 541.
[92] J.E. Sundgren, Thin Solid Films 128 (1985) 21.
[93] L. Hultman, J.E. Sundgren, L.C. Markert, J.E. Greene, Journal of Vacuum Science & Technology A 7 (1989) 1187.
[94] J. Musil, S. Kadlec, J. Vyskočil, V. Valvoda, Thin Solid Films 167 (1988) 107.
[95] P.H. Mayrhofer, C. Mitterer, J. Musil, Surface and Coatings Technology 174-175 (2003) 725.
[96] P.H. Mayrhofer, G. Tischler, C. Mitterer, Galvanotechnik 92 (2001) 762.
[97] R.F. Bunshah, Thin Solid Films 107 (1983) 21.
[98] E.J. Bienk, H. Reitz, N.J. Mikkelsen, Surface and Coatings Technology 76-77 (1995) 475.
[99] A. Wilson, A. Matthews, J. Housden, R. Turner, B. Garside, Surface and Coatings Technology 62 (1993) 600.
[100] B. Navinšek, P. Panjan, I. Milošev, Surface and Coatings Technology 97 (1997) 182.
[101] T. Hurkmans, D.B. Lewis, J.S. Brooks, W.D. Münz, Surface and Coatings Technology 86-87 (1996) 192.
[102] T. Hurkmans, D.B. Lewis, H. Paritong, J.S. Brooks, W.D. Münz, Surface and Coatings Technology 114 (1999) 52.
[103] V. Poulek, J. Musil, V. Valvoda, R. Cerny, Journal of Physics D: Applied Physics 21 (1988) 1657.
[104] V. Valvoda, Surface and Coatings Technology 80 (1996) 61.
[105] V. Valvoda, R. Kužel, R. Černý, J. Musil, Thin Solid Films 156 (1988) 53.
[106] W.C. Oliver, G.M. Pharr, Journal of Materials Research 7 (1992) 1564.
[107] K. Nitzsche, Schichtmeßtechnik, Vogel-Fachbuch, Würzburg (1997).
[108] A.C. Fischer-Cripps, Surface and Coatings Technology 200 (2006) 4153.
[109] A.C. Fischer-Cripps, P. Karvánková, S. Veprek, Surface and Coatings Technology 200 (2006) 5645.
[110] H. Willmann, Doctor thesis Montanuniversität Leoben (2007).
[111] B. Bhushan, Modern Tribology Handbook, Volume One, CRC Press LLC, Florida (2001).
[112] B. Bhushan, Principles and Applications of Tribology, J. Wiley & Sons Inc, New York (1999).
[113] P. Berghofer, Diploma Thesis, Montanuniversität Leoben (2001).
[114] R.C. Brundle, C.A. Evans Jr., S. Wilson, Encyclopedia of Materials Characterization, Butterworth - Heinemann, Boston (1992).
[115] M. Birkholz, Elements of X-ray scattering, Wiley-VCH, Weinheim (2006).
[116] B.D. Cullity, S.R. Stock, Elements of X-ray diffraction, Prentice Hall, New Jersey (2001).
[117] G. Thomas, M.J. Goringe, Transmission Electron Microscopy of Materials, J. Wliey & Sons, New York (1979).
[118] D.B. Williams, C.B. Carter, Transmission Electron Microscopy - A Textbook for Material Science, Plenum, New York (1996).

8 Paper I

Mechanical and tribological properties of CrN coatings deposited by a simultaneous HIPIMS/UBM sputtering process

J. Paulitsch [a], P.H. Mayrhofer [b], W.-D. Münz, [c] M. Schenkel [c]

a Materials Center Leoben, A-8700 Leoben, Austria
b Department of Physical Metallurgy and Materials Testing, Montanuniversität Leoben, A-8700 Leoben, Austria
c SVS Vacuum Coating Technologies, D-97753 Karlstadt, Germany

Abstract

High power impulse magnetron sputtering (HIPIMS) is known to allow deposition rates which are approximately a third of conventional unbalanced magnetron (UBM) sputtering. To compensate this drawback at least partially while keeping the advantages of HIPIMS (e.g., increased ion bombardment during growth), a simultaneous combination of both processes is investigated. This paper presents first results on single-phase CrN grown at temperatures below ~150 °C on substrates which are mounted on a cylindrical holder that rotates between a HIPIMS and a conventional UBM sputtering cathode. Consequently, the substrates dive per rotation into a HIPIMS and a UBM generated plasma. With increasing the UBM sputtering power from 0 to 5 kW for the simultaneous HIPIMS/UBM deposition of CrN, while keeping the HIPIMS cathode power constant at 5.5 kW, the microstructure changes from dense to open columnar and (200) to (111) dominated orientation. Thereby, the hardness values decrease from 25±1 to 8±1 GPa, the sliding wear rate increases from 0.35 to $1 \cdot 10^{-16}$ m³/Nm and the abrasive wear rate increases from 1.7 to $8.6 \cdot 10^{-13}$ m³/Nm, respectively. Furthermore, an increase of the deposition rate from 23 to 65 nm/min is obtained. Our results demonstrate that the combined HIPIMS/UBM sputtering process is extremely versatile in preparing films with tailored microstructures and properties as well as deposition rates for individual applications.

Introduction

Magnetron sputtering is a well established physical vapour deposition (PVD) technique. The main drawback of conventional unbalanced magnetron (UBM) sputtering is its low degree of ionized species of the sputtered material. Usually a low ion to neutral ratio during deposition results in porous films with low adhesion to the substrate [1,2]. High power impulse magnetron sputtering (HIPIMS) is a novel sputtering technique, characterised by high power dissipation at the target, which allows a much higher ion to neutral ratio as compared to conventional UBM sputtering. Ionization rates >40% with also two-fold ionized metal species are reported for HIPIMS generated plasmas [3,4,5].The plasma condition with a high ion to neutral ratio has been successfully utilised as a substrate pre-treatment. The high ion bombardment improves the adhesion due to implantation of metal species into the surface-near substrate regions at high negative Bias voltages (up to -1200V) [5]. Furthermore, the intensive metal ion bombardment during deposition due to the high ion to neutral ratio of the HIPIMS process results in a densification of the growing film due to an increased adatom mobility. The main disadvantage of HIPIMS compared to DC magnetron sputtering is the lower deposition rate of up to a third compared to DC magnetron sputtering. Consequently, to compensate this drawback a simultaneous UBM and HIPIMS deposition is studied here.

The present paper investigates the effect of simultaneously deposited CrN films on their resistance to adhesive and abrasive wear, hardnesses and microstructure at various UBM cathode power during the combined HIPIMS/UBM sputtering process.

Experimental details

Deposition conditions

The depositions were performed in a SYSTEC Z700HPM PVD coating plant of SVS Vacuum Coating Technology Karlstadt, Germany. All substrates are mounted on a cylindrical holder with one fold rotation between two facing magnetron cathodes. The area of the magnetron sources are about 440 cm^2 each. Prior to deposition the substrates are thermally cleaned within the vacuum chamber at 450 °C for 30 minutes at a base pressure

below 1 mPa. During deposition no external heating was used, which results in substrate temperatures below 150 °C [6], to maximize the effects of the HIPIMS and UBM generated plasma conditions on microstructure and resulting properties of the prepared coatings.

To improve the adhesion of the coatings, the substrates are ion etched using a Cr target in Argon atmosphere and a Bias voltage of -1200 V, where surface near regions are also implanted by or during the HIPIMS pre-treatment step. The 100Cr6 disk substrates (diameter 3.5 mm, 0.5 mm height) are positioned at a distance of 5 cm to the target. The substrate holder rotates with seven rounds per minute during the etching and implantation process. Coating deposition was carried out simultaneously with HIPIMS and UBM sputtering. Therefore, the facing targets are fed by the HIPIMS and the UBM power supply. The gas flow mixture of Argon to Nitrogen was at a constant ratio of 1:2. During deposition, the rotation speed of the substrate holder was equal to the etching process at seven rounds per minute. The cathode power for the HIPIMS target was set constant at 5.5 kW whereas the UBM cathode power was varied between 0 and 5 kW. A substrate Bias of -80 volts was used for all deposition runs and the cathode frequency and pulse duration for the HIPIMS source was 75 Hz and 150 µs, respectively. The deposition time was appointed at 60 min to obtain a film thickness of 2 µm for a combined HIPIMS/UBM deposition at 2 kW UBM cathode power. For comparison also single UBM sputtered films with a constant cathode power of 2 kW are prepared.

Coating investigations

Scanning electron microscopy (SEM), using a Zeiss EVO 50 type, investigations of fracture cross sections were carried out on coated silicon (100) wavers. Chemical investigations of the prepared films are performed with energy dispersive X-ray spectroscopy (EDX). Structural and phase analyses are conducted by X-ray diffraction (XRD) in the Bragg-Brentano mode using a Siemens D500 equipped with a CuK radiation source. Hardness values are obtained by nanoindentation with a Berkovich indenter using a CSIRO UMIS 2 (ultra micro indentation system). For proper statistics at least 25 indents were carried out for each sample with maximum loads ranging from 10 to 35 mN. The results were calculated from the loading and unloading segments of the indentation curves after the

Oliver-Pharr method [7]. The sliding wear behaviour of the combined HIPIMS/UBM films were evaluated with an optical profilometer (Wyko NT1000) after ball on disk tests using a CSM tribometer equipped with an alumina ball of 6 mm as counterpart, a normal load of 5 N and a distance of 1000 m. The tribological measurements were carried out without lubricant at room temperature at a humidity of ~25%. The abrasive sliding behaviours were evaluated with a CSEM Calowear tester. The measurements were carried out at room temperature with an aqueous suspension of Al_2O_3 granulates with a particle size of approximately 4 µm. The calculation of the abrasive wear coefficient based on a ball – cratering geometry utilising a hard steel ball with a diameter of 25.4 mm was performed after [8]. The normal load was approximately 0.45 N and the total distance of the abrasive test was 50 m.

Results and discussion

XRD investigations of our combined HIPIMS and UBM sputtered films indicate a single CrN phase composition independent of the used cathode power at the UBM target. Also the individual HIPIMS and UBM sputtered films are single phase CrN, see Figure 1. The N/Cr composition of all coatings investigated is ~ 0.94 detected by EDX. With decreasing UBM sputtering power the XRD peak positions of CrN shift towards smaller diffraction angles compared to their standard position [9] indicating increasing compressive stresses, see Figure 1.

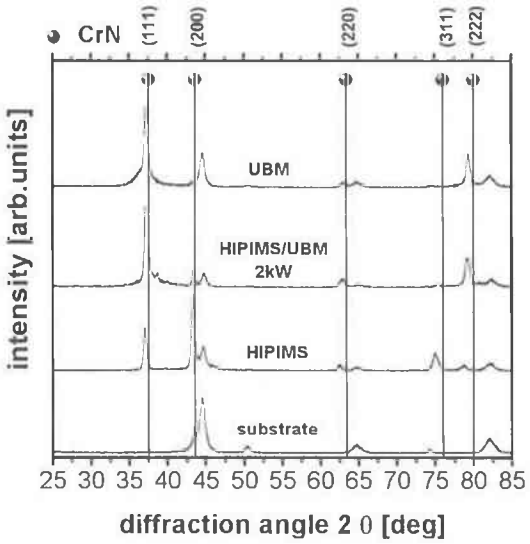

Fig. 1: XRD patterns of the substrate and the single HIPIMS and UBM sputtered films compared to simultaneous deposition of HIPIMS and UBM with a UBM cathode power of 2 kW. The standard positions for stress free cubic CrN are indicated.

This is attributed to the increased ionization rate, as the ratio between HIPIMS and UBM generated layers in our films increase with decreasing UBM sputtering power. Fracture cross sections of our coatings indicate that with increasing HIPIMS content the morphology changes from pronounced columnar for single UBM sputtering to dense fibrous for mixed HIPIMS/UBM sputtering to dense and almost equiaxed with single HIPIMS, see Figure 2 a, b and c, respectively.

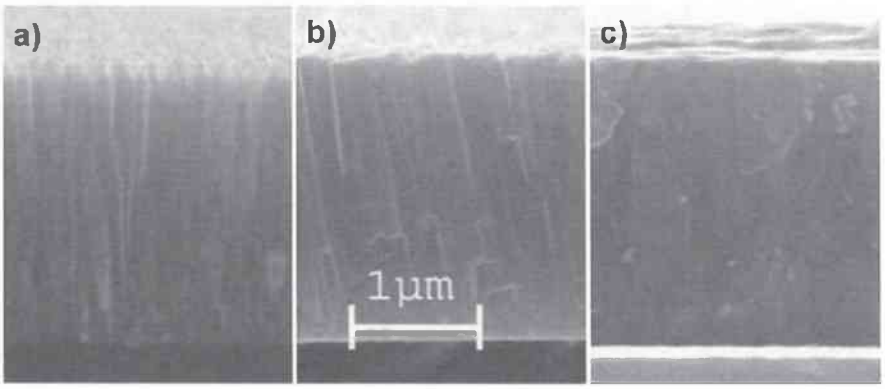

Fig. 2: Comparison of the SEM fracture cross sections for a) single HIPIMS deposition, b) HIPIMS/UBM deposition with a UBM cathode power of 2 kW and c) single UBM deposition.

The change in morphology is attributed to the increased ionization rate resulting in increased adatom mobility and re-nucleation sites with increasing HIPIMS content. In addition to the generation of the dense films with increasing HIPIMS content for the combined HIPIMS/UBM sputtering also the preferred orientation changes from almost (111) to pronounced (200), respectively. Hurkmans et al. [10] showed that the mechanical properties of sputtered CrN films can be increased if their orientation changes from (111) to (220). A further optimization of the mechanical properties can be obtained if the orientation changes to (200) [11]. Figure 3 shows the texture parameters for the (111) and (200) orientation as a function of the used UBM power for the combined HIPIMS/UBM generated films. The texture parameters are calculated after: $T_{(111)} = \frac{I_{(111)}}{I_{(111)} + I_{(200)}}$, $T_{(200)} = \frac{I_{(200)}}{I_{(111)} + I_{(200)}}$, where $_{(111)}$ and $_{(200)}$ are the intensities of the (111) and (200) XRD reflexes, see Figure 1. This two (111) and (200) orientations are chosen as they have the strongest intensities in the XRD plots. The $T_{(111)}$ quantifies the fraction of the (111) orientated crystals, the $T_{(200)}$ that of the (200) orientation.

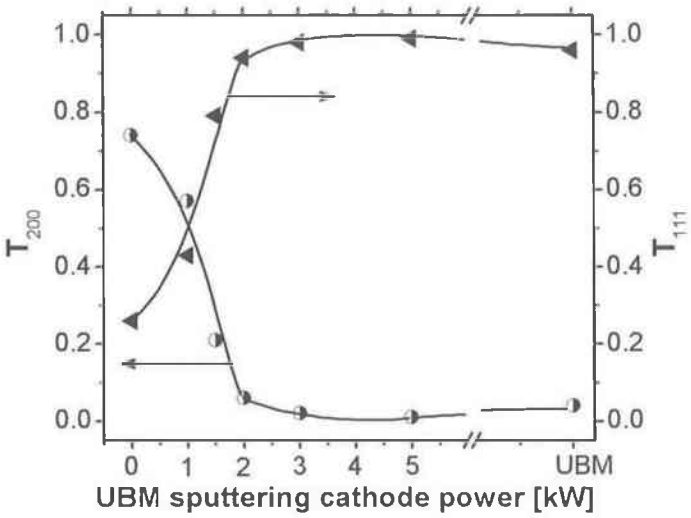

Fig. 3: Texture parameters as a function of the UBM cathode power from 0 to 5 kW for a combined HIPIMS/UBM deposition compared to single UBM deposition for the two main (111) and (200) reflexes in the XRD patterns.

With increasing HIPIMS content during the combined HIPIMS/UBM sputtering, i.e. with decreasing UBM cathode power, the orientation of our films changes from (111) to a pronounced (200). For powers ≥ 2 kW of the UBM cathode during the simultaneously HIPIMS/UBM process our films have a pronounced (111) orientation similar to that of single UBM generated films. Hardness measurements of our films indicate decreasing values from approximately 24 GPa for single HIPIMS generated films to approximately 7 GPa for combined HIPIMS/UBM sputtered films and a linear increase in deposition rate with increasing UBM sputtering cathode power from 0 to 5 kW, respectively, see Figure 4.

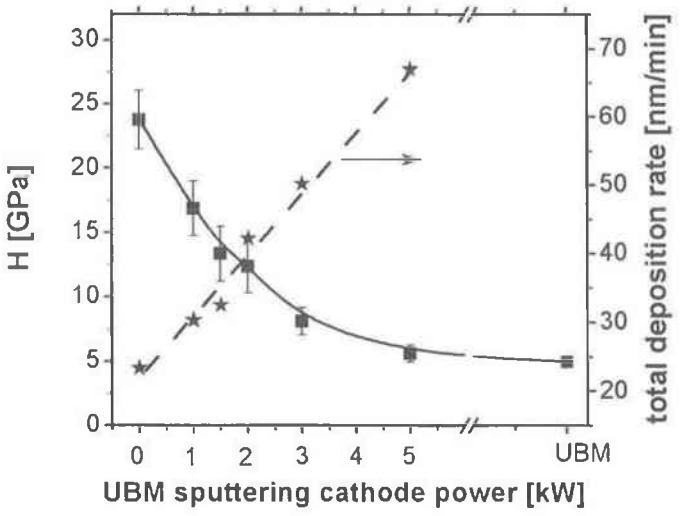

Fig. 4: Hardness values of our films and total deposition rates for the used UBM cathode power variation from 0 to 5 kW during combined HIPIMS/UBM deposition compared to single UBM sputtered films.

Due to the combination of HIPIMS and UBM the sputtering rate can be increased from 23 nm/min for single HIPIMS generated CrN to 65 nm/min for the combined HIPIMS/UBM technique, with 5.5 kW at the HIPIMS target and 5 kW at the UBM target. The hardness of the combined HIPIMS/UBM sputtered film with a UBM cathode power of 5 kW is comparable to single UBM sputtered films with hardness values of approximately 5 GPa. The decreasing hardness values with increasing UBM power are attributed to a decreasing (200) orientation, see Figure 3, and decreasing density with increasing columnar growth, see Figure 2, as consequently, the HIPIMS content decreases during the simultaneous HIPIMS/UBM sputtering. The open columnar structure of the single UBM generated films,

which results from a low adatom mobility due to low ionization rates and low substrate temperatures (below 150 °C), results in the extraordinary small hardness values of approximately 5 GPa. Due to different plasma and growth conditions during HIPIMS and UBM sputtering our films may have a nanoscale layered structure as they subsequently face the HIPIMS and UBM target during the rotation of the substrate holder with seven rounds per minute. The thereby generated layered variation in defect structure results in a concomitant layered variation in elastic moduli and hardness. Such nanoscale multilayers can build energy barriers for crack propagation and dislocation motion and glide which can improve the mechanical properties [12]. Generally, dense almost equiaxed structures, as generated during single HIPIMS (see Figure 2c), exhibit a better resistance against crack formation and crack growth as their open voided columnar counterparts while using single UBM sputtering (see Figure 2a). Consequently, also the wear resistance depends on the preparation technique as reported in [5].

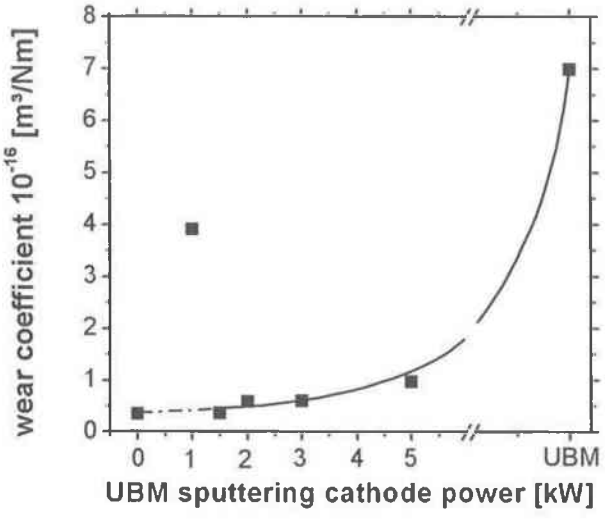

Fig. 5: Sliding (adhesive) wear coefficients of our films as a function of the used UBM cathode power variation from 0 to 5 kW during the combined HIPIMS/UBM deposition compared to single UBM sputtering deposition.

The wear coefficient of our films generally increases from approximately $0.4 \cdot 10^{-16}$ to $1.0 \cdot 10^{-16}$ m³/Nm for simultaneously HIPIMS/UBM sputtering with increasing UBM sputtering power from 1.5 to 5 kW, and hence decreasing HIPIMS content. The single HIPIMS generated CrN showed the lowest sliding wear coefficient of $\sim 3.5 \cdot 10^{-17}$ m³/Nm

and the single UBM generated CrN exhibited the highest wear coefficient of approximately $7 \cdot 10^{-16}$ m³/Nm of the coatings investigated, like indicated by [5]. The combined HIPIMS/UBM sputtered films with a UBM power of 1 kW shows a sliding wear coefficient of approximately $4 \cdot 10^{-16}$ m³/Nm which does not fit to the general trend of our films. This indicates that the low cathode power results in UBM sputtered layers with decreased mechanical and tribological properties which can act as crack propagation sites resulting in the observed lower wear resistance. For all other HIPIMS/UBM combinations wear rate values below $1 \cdot 10^{-16}$ m³/Nm are obtained. The abrasive wear coefficient measured with the CSM Calowear as a function of the used UBM cathode power during simultaneous HIPIMS/UBM sputtering is presented in Figure 6.

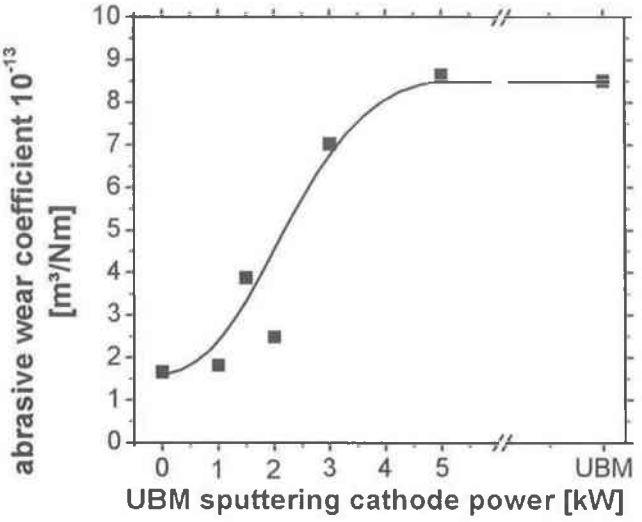

Fig. 6: Abrasive wear coefficient of our CrN films as a function of the used UBM cathode power during the combined HIPIMS/UBM deposition compared to single UBM sputtering deposition.

The general trend of an increased wear coefficient with increasing UBM sputtering power during simultaneous HIPIMS/UBM preparation is also obtained by this technique. Compared to the sliding wear coefficient (Figure 5) the abrasive wear coefficient shows a more pronounced dependence on the used UBM sputtering cathode power. With increasing UBM sputtering power from 0 to 5 kW the abrasive wear coefficient increases from approximately $1.6 \cdot 10^{-13}$ to $8.6 \cdot 10^{-13}$ m³/Nm, respectively. The latter is similar to the wear coefficient of the single UBM sputtered CrN film.

Conclusions

High power impulse magnetron sputtering (HIPIMS) has shown to be extremely effective in preparing dense coatings with excellent properties and adhesion due to the generated high rate of ionized particles. As the major drawback of HIPIMS is its low deposition rate (approximately one third of conventional unbalanced magnetron (UBM) sputtering). We investigated the effects of a combined HIPIMS/UBM sputtering process on microstructure, texture, mechanical and tribological properties, as well as deposition rate of single-phase CrN coatings. Increasing the UBM sputtering power from 0 to 5 kW while keeping the HIPIMS cathode power constant at 5.5 kW causes a change from a dense and almost equiaxed microstructure to an open columnar microstructure, and a transition from (200) pronounced orientation to a (111) dominated texture. Due to these changes the hardness decreases from 25±1 to 7±1 GPa, the sliding wear resistance increases from 0.35 to $1 \cdot 10^{-16}$ m^3/Nm and the abrasive wear resistance increases from 1.7 to $8.6 \cdot 10^{-13}$ m^3/Nm, respectively. An increase of the deposition rate from 23 to 65 nm/min with increasing UBM sputtering power from 0 to 5 kW during the combined HIPIMS/UBM process is obtained. Based on our results we can conclude that the simultaneous combination of HIPIMS and UBM sputtering is a powerful tool in developing hard coatings with tailored properties and deposition rates for individual applications.

References

[1] M. Lattemann, A.P. Ehiasarian, J. Bohlmark, P.Å.O. Persson, U. Helmersson, Surface and Coatings Technologies 200, pp. 6495-6499, 2006

[2] P. H. Mayrhofer, G. Tischler, C. Mitterer, Surf. and Coat. Techn. 142-144, pp. 78-84, 2001

[3] A. P. Ehiasarian, R. New, W.-D. Münz, L. Hultman, U. Helmersson, V. Kouznetsov, Vacuum 65, pp. 147-154, 2002

[4] V. Kouznetsov, K. Macák, J. M. Schneider, U. Helmersson, I Petrov, Surface and Coatings Technology, Volume 122, pp. 290-293, 1999

[5] A. P. Ehiasarian, P. Eh. Hovsepian, L. Hultman, U. Helmersson, Thin Solid Films, Volume 457, pp. 270-277, 2004

[6] W. D. Münz, M. Schenkel, S. Kunkel, K. Bewilogua, M. Keunecke, R. Wittorf: "Characterisation of HIPIMS deposited Cr_2N and CrN Coatings", 50th Annual Technical Conference Proceedings of the Society of Vacuum Coaters 2007

[7] G. M. P. W.C. Oliver, Journal of Materials Research 7, pp. 1564, 1992

[8] P. Berghofer: "Diploma Thesis at the Department of Physical Metallurgy and Materials Testing, University of Leoben, 2001

[9] PCPDFWIN v. 2.2, JCPDS-International Centre for Diffraction Data, Swarthmore, PA, 2001

[10] T. Hurkmans, D. B. Lewis, H. Paritong, J. S. Brooks, W. D. Münz, Surf. Coat. Technol. 114, pp.52-59, 1999

[11] C.-S. Shin, D. Gall, Y.-W. Kim, N. Hellgren, I. Petrov, J. E. Greene: "" J Appl Phys 92(9), pp. 5084, 2002

[12] B. M. Clemens, H. Kung, S. A. Barnett, MRS Bull. 24 (2) pp. 20, 1999

9 Paper II

Structure and properties of HIPIMS and DCMS CrN and TiN films deposited in an industrial scale unit

J. Paulitsch[a], M. Schenkel[b], P.H. Mayrhofer[c], W.-D Münz[d]

[a] Materials Center Leoben, A-8700 Leoben, Austria
[b] Systec SVS Vacuum Coating Technologies GmbH, D-97753 Karlstadt, Germany
[c] Department of Physical Metallurgy and Materials Testing, Montanuniversität Leoben, A-8700 Leoben, Austria
[d] Emeritus Sheffield Hallam University, A-8160 Weiz, Austria

Abstract

Deposition of complex shaped or round-symmetric samples require multi-fold substrate rotations during deposition or multiple cathode arrangements. The present paper investigates the influence of the high power impulse magnetron sputtering (HIPIMS) and dc magnetron sputtering (DCMS) process on the mechanical and triological properties as well as the resulting structure of CrN and TiN coatings using static (0-fold) and dynamic (1-, 2-, 3-fold) depositions in an industrial scale unit. Furthermore, to increase the deposition rate without loosing the high ion density in the plasma a hybrid HIPIMS/DCMS deposition technique is investigated. The results demonstrate the advantage of the HIPIMS technique when using multi-fold substrate rotation during deposition as it enables depositions of CrN_{HIPIMS} and TiN_{HIPIMS} coatings with hardness values around 23 and 35 GPa, respectively, compared with around 15 GPa for CrN_{DCMS} and TiN_{DCMS} coatings. Hardness values of 35 GPa for TiN_{DCMS} coatings prepared with substrate rotations could only be obtained when introducing an additional anode or using a multilayered CrN_{HIPIMS}/TiN_{DCMS} base-layer as a template.

Based on our results we can conclude that especially for up-scaling and multi-fold substrate rotations the HIPIMS process offers an improved performance as compared to DCMS.

Introduction

Chromium and titanium nitride (CrN, TiN) hard coatings are of great interest for automotive applications. Due to this, many investigations concentrate on the improvement of mechanical and tribological properties of these coatings by optimizing the growth morphology and resulting microstructure at the deposition process [1-4]. In general to avoid the formation of underdense coatings with high defect densities and hence decreased mechanical properties when prepared by dc magnetron sputtering (DCMS), which provides a low ionization rate of the metal species, an increase of the deposition temperature to values higher than 0.2 to 0.3 of the melting point of the coatings is necessary [5-10].

High power impulse magnetron sputtering (HIPIMS), which is characterised by high power dissipation at the target with peak electron densities up to 10^{19} m^{-3} [11,12], allows for a much higher ion to neutral ratio of the metal species as compared to conventional DCMS techniques [11,13,14]. The high ionization rate of the sputtered species (>40%), which are sometimes even two and three fold ionized, is the key-parameter to obtain dense coatings with optimized mechanical and tribological properties even when using low bias voltages and low deposition temperatures [11,13-17]. This high ion ratio is mostly utilized for substrate pre-treatment to increase the adhesion of the sputtered films, which has been shown in [14,18,19].

Here, we study the mechanical and tribological properties, crystallography and growth morphology of CrN and TiN coatings deposited in HIPIMS and DCMS mode as a function of the substrate rotation (zero-, one-, two- and three-fold substrate rotation). This is essential for up-scaling processes of laboratory scale obtained developments, where often static deposition conditions are used, to industrial sized units which require planetary rotation of the substrates to ensure uniform depositions. As shown in numerous publications, one of the main drawback during HIPIMS is the obtained low deposition rate when compared to conventional DCMS [20-22]. Therefore we study the deposition rate, microstructure, mechanical and tribological properties of coatings when prepared by a hybrid HIPIMS/DCMS deposition technique, which allows to combine the benefits of HIPIMS and DCMS [17].

Experimental details

The depositions were performed in a Z700HPM PVD coating plant manufactured by the Systec SVS Vacuum Coating Technologies GmbH Karlstadt, Germany, in an Ar and N2 gas mixture on steel disks (diameter 3.5 mm, 0.5 mm height) and Si (001) striped substrates (rectangular shape of 15x30mm), which were mounted at a minimum distance of 8 cm to the target. The gas flow of Argon and Nitrogen was varied for HIPIMS and DCMS deposition to achieve stoichiometric coatings. The samples (steel and silicon substrates) are mounted on substrate holders, which allow planetary rotation during deposition. Four kinds of substrate rotation modes are used: static deposition, where the substrates are always facing the target material and depositions with one-, two- and three-fold substrate rotation. The used parameters for all depositions, static and up to three-fold substrate rotation, were kept constant, to investigate the difference between the HIPIMS and the DCMS technique when changing from zero to multiple substrate rotation.

Prior to all depositions the samples are thermally cleaned at 450 °C (Cr depositions) and 600 °C (Ti depositions) within the vacuum chamber for 30 and 60 min respectively, at a base pressure below 1 mPa. To maximize the difference between HIPIMS and DCMS conditions and their effects on microstructure and resulting properties of the CrN coatings no external heating was used, which results in substrate temperatures below 150 °C [23]. For the TiN and CrN/TiN multilayer coatings additional heating to 450 °C during deposition was necessary to obtain dense coatings even during DCMS [17].

To improve the adhesion of the coatings, all substrates are metal ion etched, using a Cr target in HIPIMS mode and a bias voltage applied to the substrate of -1000 V, resulting in Cr implantation into surface near regions [7]. The powering of the cathodes during deposition of CrN or TiN were set to 5.5 kW for Cr or 4 kW for Ti when using HIPIMS, and 2 kW for Cr or 4 kW for Ti when using DCMS respectively. During the hybrid HIPIMS/DCMS deposition of CrN_{HIPIMS}/CrN_{DCMS} and CrN_{HIPIMS}/TiN_{DCMS} coatings, the power applied to the Cr_{HIPIMS} cathode was 5.5 kW and the power applied to the DCMS cathode was varied from 1 to 5 kW when equipped with Cr, and from 4 to 7 kW when equipped with Ti, respectively. To obtain comparable film thickness of approximately 2 µm for all

deposition conditions investigated the individual deposition times were adjusted accordingly.

Scanning electron microscopy (SEM) investigations of fracture cross-sections of coated Si (001) stripes were carried out with a Zeiss EVO 50 type. Detailed studies on morphology and structure of the coated materials are carried out using a Phillips CM 12 transmission electron microscopy (TEM). Structural and phase analyses by X-ray diffraction (XRD) in the Bragg-Brentano mode using a Siemens D500 equipped with a CuK radiation source are conducted on coated steel substrates. The hardness (H) and modulus of indentation (E) of our coatings (evaluated on steel substrates) are obtained by nanoindentation with a Berkovich indenter using an ultra micro indentation system (UMIS). The maximum loads are ranging from 10 to 35 mN to keep the indentation depth below 10% of the film thickness. The values for H and E were obtained from analysing the loading and unloading segments of the indentation curves after the Oliver-Pharr method [24]. The sliding wear behaviour of our coatings was calculated by profilometrical evaluation (Wyko NT1000, white-light profilometer) of the wear track after dry ball on disk (BOD) tests at RT employing a CSM tribometer equipped with an alumina ball (diameter of 6 mm) as counterpart. A normal load of 5 N and distances up to 2000 m were used. Biaxial residual stresses in our coatings on the Si substrates were evaluated by the cantilever beam method, using the modified Stoney equations [25,26].

Results and discussion

Figure 1 shows schematic cross sections of the Systec SVS Z700 coating plant with indicated deposition arrangement and substrate rotations (0-, 1-, 2-, 3-fold) used during DCMS (Fig. 1a) and HIPIMS (Fig. 1b) as well as during simultaneous HIPIMS/DCMS deposition with 1-fold substrate rotation between the two facing cathodes. The red and blue areas in front of the targets indicate the generated plasmas. During 0-fold substrate rotation the samples are always facing the respective target material. The 1-fold rotation describes the arrangement where the samples rotate on the second largest diameter in front of the target used. During 2-fold rotation the samples rotate additionally around the largest diameter, and during 3-fold rotation the substrate rotates additionally around the

smallest diameter (almost around their own sample axis). Hence, except for the 0-fold substrate rotation the samples periodically leave and enter the plasma region between the cathodes 3 and 4.

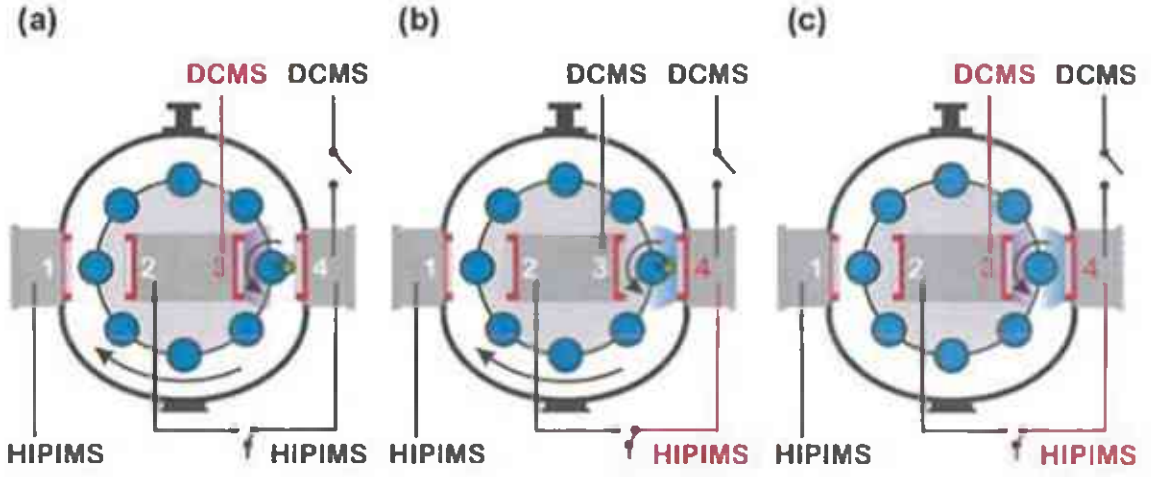

Fig. 1: Top view cross section of the Z700 coating plant. Images (a) and (b) indicate monolithic DCMS and HIPIMS deposition, respectively, with multifold substrate rotation. Image (c) shows the arrangement during the hybrid HIPIMS/DCMS deposition using 1-fold substrate rotation in-between the two facing cathodes.

XRD patterns of the monolithic HIPIMS CrN (CrN_{HIPIMS}) and DCMS CrN (CrN_{DCMS}) coatings for different substrate rotations used are given in Figs. 2a and b, respectively. For CrN_{HIPIMS} coatings the preferred (200) orientation, obtained with a 0-fold substrate rotation, changes to a mixed (111)-(200) orientation with increased (111) content when changing to 1-, 2- and 3-fold rotation, respectively. In contrast to these findings, the CrN_{HIPIMS} coatings indicate a preferred (200) orientation, almost independent of the substrate rotation used. This is an agreement to earlier studies with preferred (200) orientations for increased ion density [15]. In addition to a pronounced (200) orientation also denser films are prepared as compared to their DCMS counterparts.

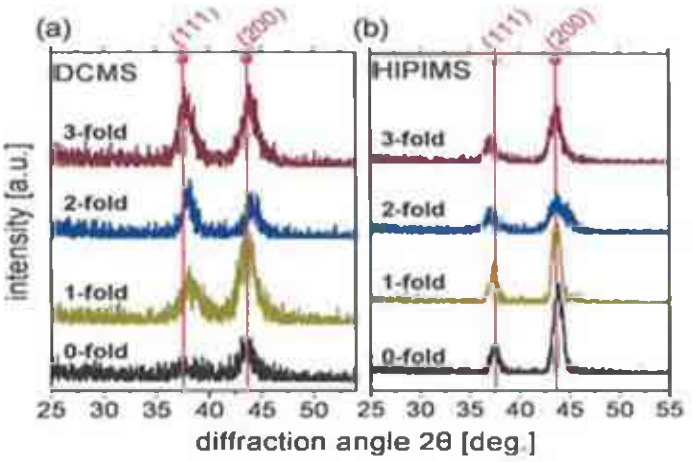

Fig. 2: XRD pattern of monolithic CrN_{DCMS} (a) and CrN_{HIPIMS} (b) coatings deposited at temperatures around 150°C using 0-, 1-, 2-, and 3- fold substrate rotation.

Figure 3 shows that the hardness (H) for HIPIMS CrN coatings stays almost constant at 22 ± 1 GPa for the different substrate rotations used, whereas the hardness for CrN_{DCMS} decreases from ~23 GPa to 15 GPa when increasing the substrate rotations from 0- to 2-fold and than stays at ~15 GPa when further increasing the substrate rotation to 3-fold. The obtained hardness dependence on the substrate rotations are in agreement to the results obtained by XRD investigations indicating a pronounced (200) orientation for CrN_{HIPIMS} independent of the substrate rotation but a decreasing (200) orientation for CrN_{DCMS} when increasing the substrate rotation.

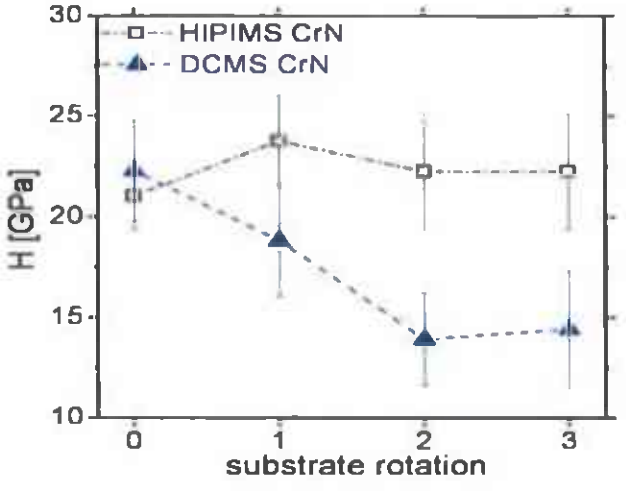

Fig. 3: Hardness (H) values of monolithic CrN_{HIPIMS} and CrN_{DCMS} coatings deposited at ~150 °C using 0-, 1-, 2-, and 3- fold substrate rotation.

Hurkmans et al. [27] showed that the mechanical properties of sputtered CrN films can be increased if their orientation changes from a pronounced (111) to a preferred (220), and Shin et al. [28] showed that a further optimization is obtained for preferred (200) oriented CrN.

Figure 4 shows, that the deposition rate (r) of HIPIMS and DCMS sputtered CrN coatings when powering the cathodes with 5.5 kW and 2 kW decreases comparably from ~80 to 5 nm/min and from ~90 to 7 nm/min with increasing the substrate rotation from 0- to 3-fold rotation, respectively.

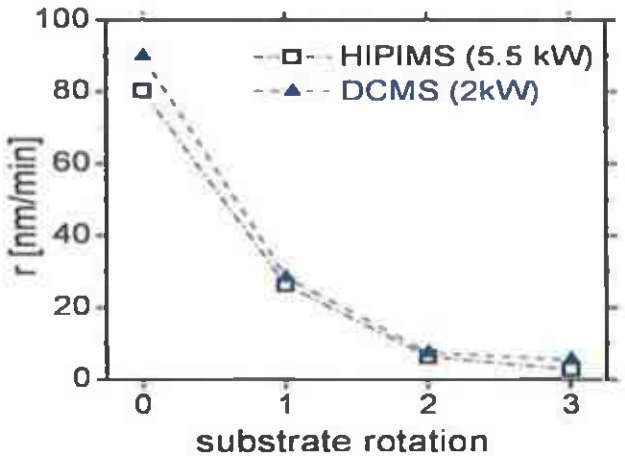

Fig. 4: Deposition rate of monolithic CrN_{HIPIMS} and CrN_{DCMS} coatings (2 and 5.5 kW powering of the DCMS and HIPIMS cathode, respectively) deposited at ~150 °C using 0-, 1-, 2-, and 3- fold substrate rotation.

Consequently, when correlated with the power-input, the DCMS coatings exhibit a three-times higher specific deposition rate than the HIPIMS coatings. To combine the advantages of both techniques (denser morphology and excellent mechanical properties with higher deposition rates) the effect of a simultaneous operation of two facing targets in HIPIMS and DCMS mode on the properties of CrN coatings is investigated for a 7 rpm 1-fold substrate rotation, see Fig. 1c. This arrangement results in the deposition of bilayered CrN coatings with alternating HIPIMS and DCMS CrN layers. Due to the different plasma and growth conditions the films have a nanoscale layered structure. Such nanoscale multilayer films can build energy barriers for crack propagation and dislocation motion and glide which can improve the mechanical properties [29].

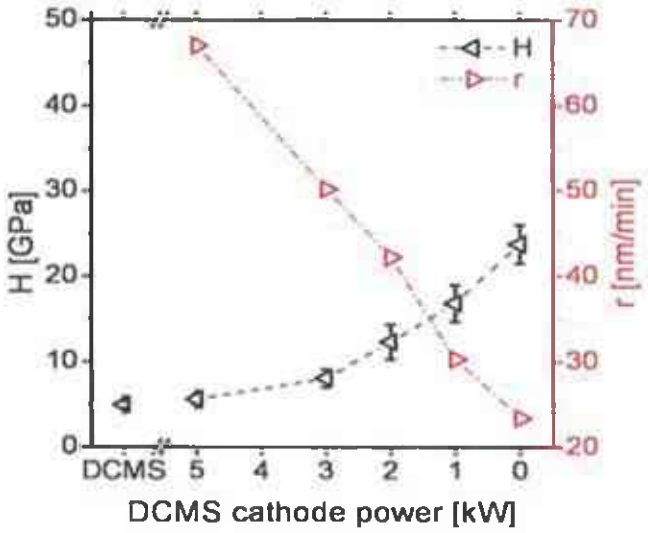

Fig. 5: Hardness (H) and deposition rate (r) of multilayered CrN_{HIPIMS}/CrN_{DCMS} as a function of the dc power applied to the Cr cathode (i.e. CrN_{DCMS} layer thickness) while keeping the CrN_{HIPIMS} layer thickness constant (5.5 kW powering).

Figure 5 shows that with increasing the DCMS cathode powering from 1 to 5 kW, while powering the HIPIMS cathode with 5.5 kW, the deposition rate increases linearly from 22 to 68 nm/min and the hardness decreases from 23 to 5 GPa, respectively, a value which is similar to the monolithic CrN_{DCMS} coating. We need to mention that for this experiment no substrate heating other than plasma-heating was used, hence substrate temperature is ~150 °C. SEM fracture cross-sections of the films show that the CrN_{DCMS} exhibit an open columnar structure (Fig. 6a), whereas the multilayered CrN_{HIPIMS}/CrN_{DCMS} coating (Fig. 6b) prepared with a power-input to the HIPIMS and DCMS cathode of 5.5 and 2 kW, respectively, exhibits a fibrous morphology. The monoloithic CrN_{HIPIMS} coatings are characterized by an extremely dense morphology, see Fig. 6c, giving rise to their extraordinary hardness values of 23 GPa even when deposited at ~150 °C. Furthermore, Fig. 6 shows that the CrN_{DCMS} coating exhibits a much rougher surface than the hybrid CrN_{HIPIMS}/CrN_{DCMS} coatings (Fig. 6b) and (Fig. 6a) the CrN_{HIPIMS}.

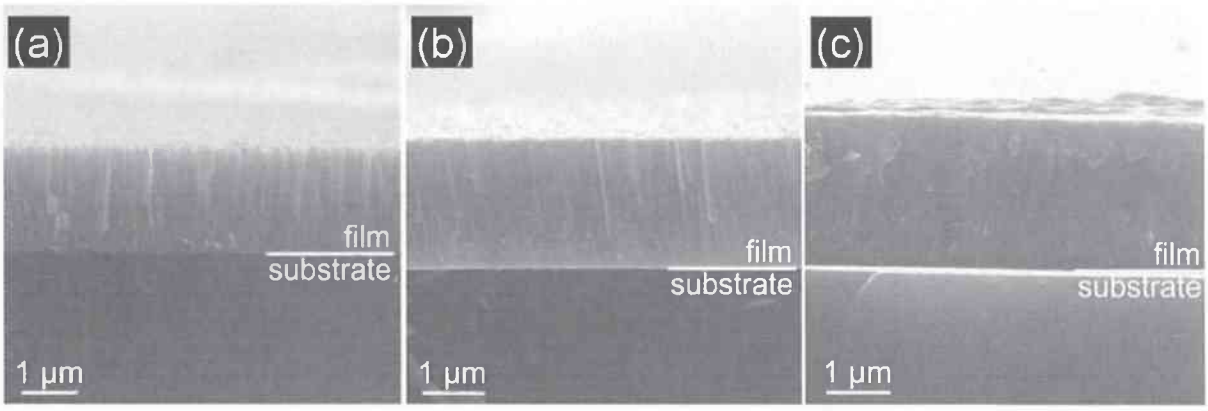

Fig. 6: SEM fracture cross-section images of monolithic CrN_{DCMS} (a), multilayered CrN_{HIPIMS}/CrN_{DCMS} (b) and monolithic CrN_{HIPIMS} (c) coatings deposited at temperatures around 150 °C and using 1-fold substrate rotation.

As measured by white-light profilometer the mean roughness values Ra are 13.5 nm for CrN_{DCMS} and 8 and 9 nm for the CrN_{HIPIMS} and the multilayered CrN_{HIPIMS}/CrN_{DCMS}, respectively. The higher surface roughness for the CrN_{DCMS} coatings is the result of the open columnar structure and the preferred (111) oriented growth resulting in pyramidal column tips, see Fig. 6a.

Figure 7 presents the dependence of the (200) and (111) texture coefficient calculated after: $T_{(111)} = \frac{I_{(111)}}{I_{(111)} + I_{(200)}}$, $T_{(200)} = \frac{I_{(200)}}{I_{(111)} + I_{(200)}}$, where (111) and (200) are the intensities of the (111) and (200) XRD reflexes, of the CrN_{HIPIMS}/CrN_{DCMS} multilayer coatings on the used power-input to the DCMS cathode. The HIPIMS cathode was supplied constantly with 5.5 kW. For power-inputs to the DCMS cathode above 2 kW the coatings exhibit a pronounced (111) orientation similar to that of monolithic DCMS coatings when prepared with a 1-fold substrate rotation. By decreasing the powering of the DCMS cathode to values below 2 kW, the orientation changes to preferred (200) and approaches that of monolithic HIPIMS CrN coatings, see Fig. 7. As shown before, see Fig. 4, the deposition rates of HIPIMS and DCMS CrN are comparable when fed with 5.5 and 2 kW, respectively. Hence, a multilayer CrN_{HIPIMS}/CrN_{DCMS} prepared with these settings is composed of similar fraction of HIPIMS and DCMS content. Consequently, when the power-input to the DCMS cathode increases above 2 kW the microstructural characteristics of DCMS coatings are

approached and when decreasing the power-input to the DCMS cathode below 2 kW the microstructural characteristics of HIPIMS coatings are approached.

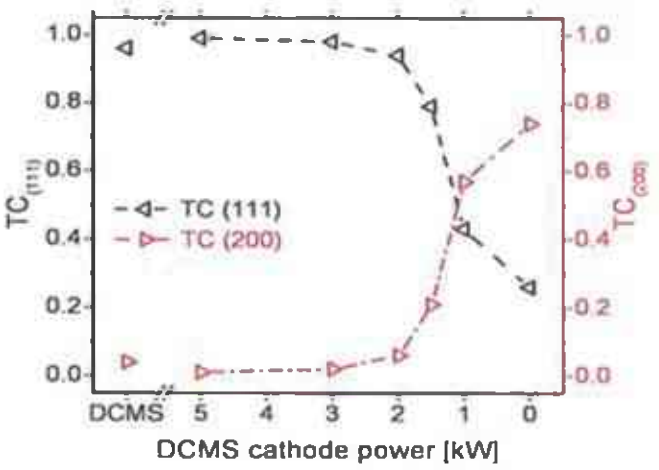

Fig. 7: Texture coefficient (TC) of multilayered CrN_{HIPIMS}/CrN_{DCMS} as a function of the dc power applied to the Cr cathode (i.e. CrN_{DCMS} layer thickness) while keeping the CrN_{HIPIMS} layer thickness constant (5.5 kW powering). For comparison the values for monolithic CrN_{DCMS} are added. The coatings are prepared at ~150 °C and using 1-fold substrate rotation.

Contrary to these findings the wear coefficient of the CrN_{HIPIMS}/CrN_{DCMS} coatings is by almost two-order of magnitude smaller than that of CrN_{DCMS} coatings. With increasing power-input to the DCMS cathode up to 5 kW, hence decreasing HIPIMS content of the coating, the wear coefficient increases from approximately $0.4 \cdot 10^{-16}$ to $1.0 \cdot 10^{-16}$ m³/Nm, see Fig. 8. The monolithic CrN_{HIPIMS} coating exhibits the lowest sliding wear coefficient of $\sim 0.35 \cdot 10^{-16}$ and the monolithic CrN_{DCMS} exhibits the highest wear coefficient with approximately $30 \cdot 10^{-16}$ m³/Nm of the coatings investigated. Hence the multilayer CrN_{HIPIMS}/CrN_{DCMS} are always much closer to the HIPIMS prepared coatings as to the DCMS prepared coating, and strongly deviated from linear interpolation. The small insert in Fig. 8 shows the wear track profiles after BOD testing with a normal load of 5 N for the monolithic HIPIMS and DCMS CrN coatings as well as for the multilayer CrN_{HIPIMS}/CrN_{DCMS} coating prepared with a 5.5 and 2 kW power-input to the HIPIMS and DCMS power supply, respectively.

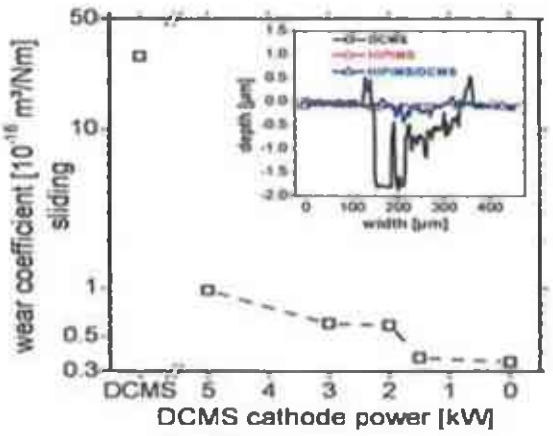

Fig. 8: Wear coefficient of multilayered CrN_{HIPIMS}/CrN_{DCMS} as a function of the dc power applied to the Cr cathode (i.e. CrN_{DCMS} layer thickness) while keeping the CrN_{HIPIMS} layer thickness constant (5.5 kW powering). For comparison the values for monolithic CrN_{DCMS} are added. The coatings are prepared at ~150 °C and using 1-fold substrate rotation. The 2D wear inset shows profiles of monolithic CrN_{HIPIMS} and CrN_{DCMS} coatings (2 and 5.5 kW powering of the DCMS and HIPIMS cathode, respectively) compared with multilayered CrN_{HIPIMS}/CrN_{DCMS} coating (hybrid deposition with 2 and 5.5 kW powering of the DCMS and HIPIMS cathode, respectively).

According to the wear coefficients, the CrN_{HIPIMS} and the multilayered CrN_{HIPIMS}/CrN_{DCMS} coatings exhibit the smallest wear depths of 100 to 200 nm, whereas the CrN_{DCMS} coatings are almost totally worn through, indicated by a wear depth maximum of 1.8 µm. The total film thickness was approximately 2 µm. The high wear rates for the DCMS coatings are due to their open columnar structure.

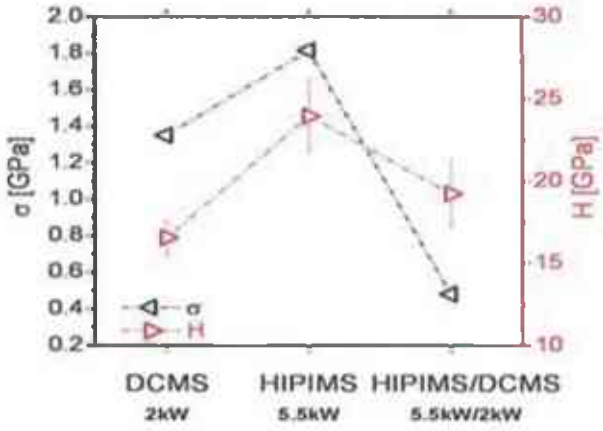

Fig. 9: Residual stress ( ) and hardness (H) values of monolithic CrN_{HIPIMS} and CrN_{DCMS} coatings (2 and 5.5 kW powering of the DCMS and HIPIMS cathode, respectively) and multilayered CrN_{HIPIMS}/CrN_{DCMS} coating (hybrid deposition with 2 and 5.5 kW powering of the DCMS and HIPIMS cathode, respectively) deposited at ~150 °C and using 1-fold substrate rotation.

Figure 9 shows the residual stresses and the hardness H for monolithic CrN_{DCMS} and CrN_{HIPIMS} and the multilayered CrN_{HIPIMS}/CrN_{DCMS} coatings with a powering of 5.5 and 2 kW of the HIPIMS and the DCMS cathode, respectively. The evaluated residual stresses are in the range of 1.3 and 1.9 GPa for the monolithic CrN_{DCMS} and CrN_{HIPIMS} coatings. By combining both deposition techniques for the hybrid HIPIMS/DCMS deposition the residual stresses decrease to values around 0.5 GPa. These results in combination with the increased deposition rates and the only minor reduction of the excellent mechanical and tribological properties of HIPIMS CrN, when simultaneously adding DCMS to HIPIMS, demonstrate the enormous advantage of the hybrid HIPIMS/DCMS deposition technique. By the variation of the HIPIMS and DCMS ratio during deposition, the properties of the coatings prepared can individually steered to meet the requirements.

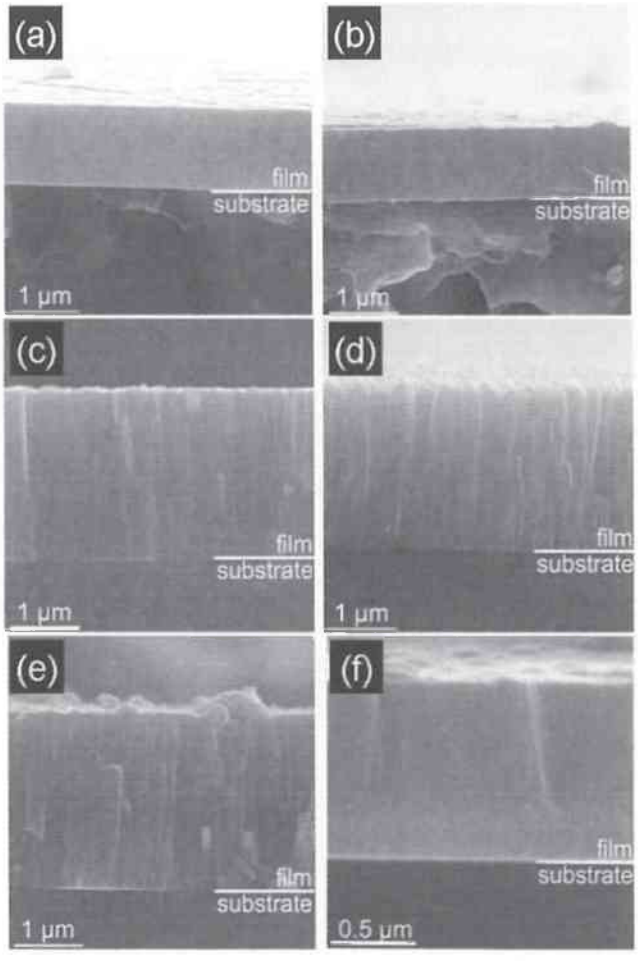

Fig. 10: SEM fracture cross-sections of monolithic TiN_{HIPIMS} coatings deposited at ~150 °C using 0-fold (a) and 1-fold substrate rotation (b), monolithic TiN_{DCMS} coatings deposited at ~150 °C using 0-fold (c) and at ~400 °C using 1-fold substrate rotation (d) and TiN_{DCMS} coatings prepared with an additional anode and 1-fold substrate rotation with Ts ~150 °C (e) and Ts ~400 °C (f).

The effect of changing from static (0-fold) to 1-fold substrate rotation during deposition at ~150 °C on the hardness of TiN sputtered coatings is reported in [17]. Here we add new findings to these results and present the investigations of multilayered CrN_{HIPIMS}/TiN_{DCMS} coatings. Figures 10a and b show SEM fracture cross-sections of TiN_{HIPIMS} coatings deposited at low (~150 °C) substrate temperatures with 0- and 1-fold substrate rotation, respectively, exhibiting dense morphology with smooth surfaces. The comparable TiN_{DCMS} coatings exhibit a dense columnar morphology with surface roughness values R_a ~11 nm for 0-fold substrate rotation and Ts ~150 °C, see Fig. 10c. As reported in [17] the coatings' morphology changes dramatically when a 1-fold substrate rotation is used instead of the static deposition, while keeping Ts at 150 °C and the other deposition conditions unchanged. Even by increasing the substrate temperatures to values around 400 °C the coatings still exhibit an open columnar growth-structure when a 1-fold rotation is used, see Fig. 10d. By adding an anode during the deposition with Ts ~150 °C to increase the growth kinetics, a dense morphology with smooth surfaces is obtained for 0- and 1-fold substrate rotation, see Fig. 10e and f, respectively. The anode was placed at cathode position number three (see Fig. 1) to ensure a closed plasma condition during 1-fold substrate rotation.

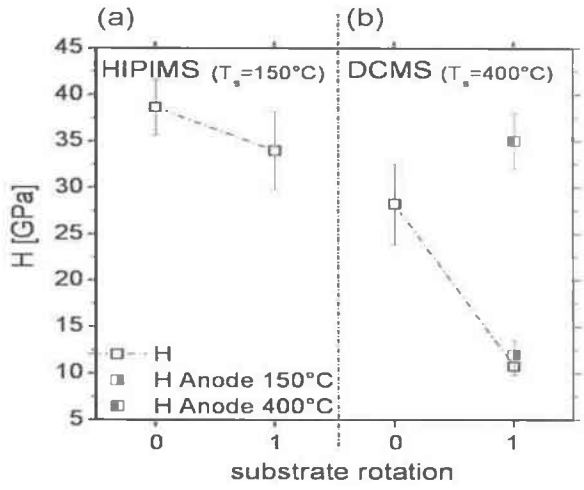

Fig. 11: Hardness (H) values of monolithic TiN_{HIPIMS} (a) coatings deposited at ~150 °C using 0- and 1-fold substrate rotation and monolithic TiN_{DCMS} (b) coatings deposited at ~400 °C using 0- and 1-fold substrate rotation and depositions with an additional anode using 1-fold rotation and temperatures around 150 and 400 °C.

Corresponding to the morphology change due to changed deposition conditions, also the respective hardness values change. The hardness of the monolithic TiN_{HIPIMS} coatings only slightly decrease from ~38 to 35 GPa when changing from static to 1-fold substrate rotation, see Fig. 11a, whereas the modulus of indentation is nearly unaffected at ~400 GPa. For monolithic DCMS TiN coatings the hardness strongly depends on the used deposition conditions as well as the coatings' morphology. When changing from static to dynamic depositions with a 1-fold substrate rotation, the hardness decreases drastically from ~29 GPa to immeasurable values, as the morphology is underdense when Ts ~150 °C, see [17]. When the temperature is increasing to 400 °C hardness values of ~19 GPa for 1-fold rotation are obtained, see Fig. 11b. By adding an anode during the deposition, the hardness can be increased to ~35 GPa for 1-fold substrate rotation and Ts ~400°C. The hardness for the TiN_{DCMS} coatings prepared with an additional anode, 1-fold rotation and without substrate heating (Ts ~150 °C) is about H ~12 GPa, comparable to those for TiN_{DCMS} coatings prepared without anode but with additional substrate heating to Ts ~400 °C. As the properties of the multilayered CrN_{HIPIMS}/TiN_{DCMS} coatings do not follow a linear interpolation between the respective monolithic CrN_{HIPIMS} and TiN_{DCMS} coatings we investigated the template effect of such arrangement on the TiN growth using DCMS.

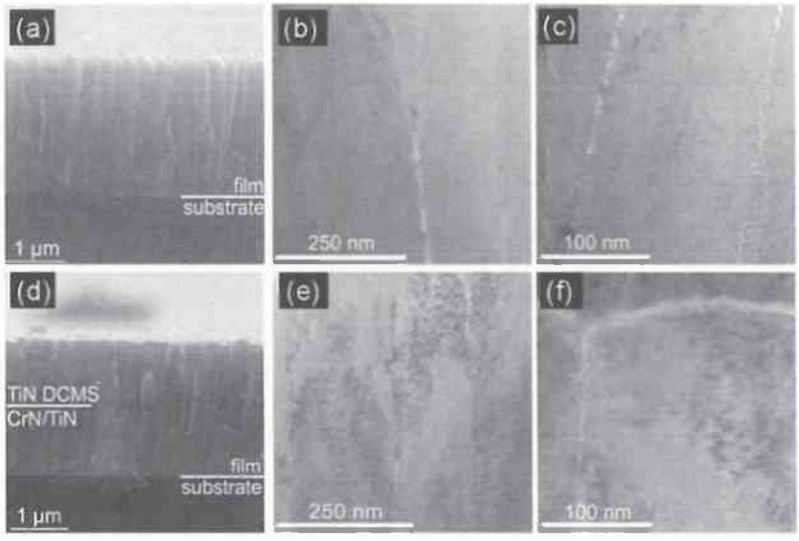

Fig. 12: SEM (a) and TEM (b) and (c) cross-sections of a monolithic TiN_{DCMS} coating prepared at Ts ~400 °C using a 1-fold substrate rotation. The images (d), (e) and (f) show the corresponding cross-sections when using a multilayered CrN_{HIPIMS}/TiN_{DCMS} base-layer (Ts ~400 °C, 1-fold substrate rotation) as a template for the TiN_{DCMS} coating.

Figure 12 shows SEM fracture cross-sections and TEM cross-sections of TiN_{DCMS} coatings grown without a base layer (Figs. 12a, b and c), and of TiN_{DCMS} grown on top of a multilayered CrN_{HIPIMS}/TiN_{DCMS} base film (Figs. 12d, e and f). All of these coatings were deposited with a 1-fold substrate rotation and at Ts ~400 °C. The TEM images clearly show the difference between the two TiN_{DCMS} coatings. Without the CrN_{HIPIMS}/TiN_{DCMS} base layer (which itself exhibits a dense morphology), the TiN_{DCMS} coating exhibits an open structured columnar morphology (see Fig. 10a). This can clearly be seen by the bright areas separating the columns in the TEM images shown in Figs. 12b and c. On the other hand, the TiN_{DCMS} coating on top of the multilayered CrN_{HIPIMS}/TiN_{DCMS} base layer, exhibits a dense columnar morphology and a smooth surface (see Figs. 10d, e and f). These results clearly indicate a template effect of the CrN_{HIPIMS}/TiN_{DCMS} base layer on the TiN_{DCMS} coatings, resulting in a dense morphology and increasing hardness values from ~12 to ~27 GPa for the TiN_{DCMS} coatings.

Conclusions

High power impulse magnetron sputtering (HIPIMS) has shown to be extremely effective in preparing dense coatings with excellent properties. The advantage of a high ion density of the HIPIMS process, compared to DCMS, is even more pronounced when changing the deposition conditions from simple static deposition to multifold substrate rotation and decreasing the substrate temperature.

Investigations on monolithic CrN coatings deposited in HIPIMS and DCMS mode using 0-, 1-, 2- and 3-fold substrate rotation indicate, that HIPIMS allows for denser coatings with superior mechanical and tribological properties as compared with DCMS. Nevertheless, to combine the benefits of HIPIMS and DCMS (especially the higher deposition rate) investigations of hybrid CrN_{HIPIMS}/CrN_{DCMS} coatings were conducted as a function of the CrN_{DCMS} content. With increasing CrN_{DCMS} content (increasing the dc power at the Cr target from 2 to 5 kW while keeping the power for the HIPIMS cathode constant at 5.5 kW) the deposition rate increases linearly from ~23 to 65 nm/min while the hardness decreases from ~25 to 7 GPa, respectively, for coatings prepared with 1-fold substrate rotation and Ts ~150 °C. On the other hand, the wear coefficients of all the CrN_{HIPIMS}/CrN_{DCMS} coatings

investigated are with values around $1 \cdot 10^{-16}$ m^3/Nm at least two orders of magnitude lower than their monolithic CrN_{DCMS} counterparts.

Comparable results are obtained for HIPIMS and DCMS prepared TiN coatings. The hardness values for TiN_{DCMS} coatings decrease from ~30 to 10 GPa when using a substrate temperature of 400 °C and changing from static to dynamic deposition, respectively. Introducing an additional anode to the DCMS deposition (with 1-fold substrate rotation) allows for hardness values ~10 and 35 GPa when using a substrate temperature of ~150 and 400 °C, respectively. Contrary to these findings, hardness values of ~35 GPa for 0- and 1-fold substrate rotation are obtained for HIPIMS prepared TiN_{HIPIMS} coatings even when using a low substrate temperature of ~150 °C.

Based on our results we can conclude that HIPIMS offers a higher versatility (by providing uniform and dense coatings) than DCMS when thermally sensitive materials need to be deposited and/or the deposition process needs to be up-scaled or substrate-rotations need to be changed for complex shaped specimens. Our results furthermore show, that the deposition rate of hybrid HIPIMS/DCMS deposited coatings linearly increase with the DCMS content while keeping the beneficial properties of HIPIMS coatings.

Acknowledgement

Financial support by the Austrian Federal Government and the Styrian Provincial Government, represented by Österreichische Forschungsförderungsgesellschaft mbH and Steirische Wirtschaftsförderungsgesellschaft mbH, within the research activities of the K2 Competence Centre on "Integrated Research in Materials, Processing and Product Engineering", operated by the Materials Center Leoben Forschung GmbH under the frame of the Austrian COMET Competence Centre Program, is gratefully acknowledged.

References

[1] J.-E. Sundgren, Thin Solid Films 128 (1985) 21

[2] I. Petrov, L. Hultman, J.-E. Sundgren, J. E. Greene, Journal of Vacuum Science and Technology A 10 (2) (1992) 265

[3] L. Hultmann, J.-E. Sundgren, L.C. Markert, J.E. Greene, Journal of Vacuum Science and Technology A 7 (3) (1989) 1187

[4] J. Musil, S. Kadlec, J. Vyskocil, V. Valvoda, Thin Solid Films 167 (1988) 107

[5] M. Lattemann, A. P. Ehiasarian, J. Bohlmark, P. Å. O. Persson, U. Helmersson, Surface and Coatings Technology 200 (2006) 6495

[6] P. H. Mayrhofer, G. Tischler, C. Mitterer, Surface and Coatings Technology 142-144 (2001) 78

[7] A. P. Ehiasarian, W.-D. Münz, L. Hultman, U. Helmersson, I. Petrov, Surface and Coatings Technology 163-164 (2003) 267

[8] J. E. Greene, S. A. Barnett, Journal of Vacuum Science and Technology 21(2) (1982) 285

[9] I. Petrov, L. Hultman, U. Helmersson, J. E. Sundgren, J. E. Greene, Thin Solid Films 169(2) (1989) 299

[10] L. Hultman, W.-D. Münz, J. Musil, S. Kadlec, I. Petrov, J. E. Greene, Journal of Vacuum Science and Technology A 9(3) (1991) 434

[11] V. Kouznetsov, K. Macák, J. M. Schneider, U. Helmersson, I. Petrov, Surface and Coatings Technology 122 (1999) 290

[12] J. Alami, J. T. Gudmundsson, J. Bohlmark, J. Birch, U. Helmersson, PSST 14 (2005) 525

[13] A. P. Ehiasarian, R. New, W.-D. Münz, L. Hultman, U. Helmersson, V. Kouznetsov, Vacuum 65 (2002) 147

[14] A. P. Ehiasarian, P. Eh. Hovsepian, L. Hultman, U. Helmersson, Thin Solid Films 457 (2004) 270

[15] I. Petrov, P. B. Barna, L. Hultman, J. E. Greene, Journal of Vacuum Science and Technology A 21(5) (2003) 117

[16] P. H. Mayrhofer, F. Kunc, J. Musil, C. Mitterer, Thin Solid Films 415 (2002) 151

[17] J. Paulitsch, P. H. Mayrhofer, W.-D. Münz, M. Schenkel, Thin Solid Films 517 (2008) 1239

[18] C. Schönjahn, L. Donohue, D. B. Lewis, W.-D. Münz, I. Petrov, J, Journal of Vacuum Science and Technology A 18(4) (2000) 1718

[19] G. Hakansson, L. Hultman, J.-E. Sundgren, J. E. Greene, W.-D. Münz, Surface and Coatings Technology 48 (1991) 51

[20] U. Helmesson, M. Lattemann, J. Bohlmark, A. P. Ehiasarian, J. T. Gudmundsson, Thin Solid Films 513 (2006) 1

[21] W. D. Sproul, D. J. Christie, M. Geisler, 47th Annual Technical Conference Proceedings of the Society of Vacuum Coaters (2004) 215

[22] B. M. DeKoven, P. R. Ward, R. E. Weiss, D. J. Christie, R. A. Scholl, W. D. Sproul, F. Tomasel, A. Anders, 46th Annual Technical Conference Proceedings of the Society of Vacuum Coaters (2003) 158

[23] W.-D. Münz, M. Schenkel, S. Kunkel, K. Bewilogua, M. Keunecke, R. Wittorf, 50th Annual Technical Conference Proceedings of the Society of Vacuum Coaters (2007) 155

[24] G. M. P. W.C. Oliver, Journal of Materials Research 7 (1992) 1564

[25] J. D. Wilcock, D. S. Campbell, Thin Solid Films 3 (1969) 3

[26] P. H. Mayrhofer, C. Mitterer, Surface and Coatings Technology 133-134 (2000) 131

[27] T. Hurkmans, D. B. Lewis, H. Paritong, J.S. Brooks, W.-D. Münz, Surface and Coatings Technology 114 (1999) 52

[28] C.-S. Shin, D. Gall, Y.-W. Kim, N. Hellgren, I. Petrov, J. E. Greene, Journal of Applied Physics 92 (2002) 5084

[29] B. M. Clemens, H. Kung, S. A. Barnett, MRS Bull. 24 (1999) 20

10 Paper III

Structure and mechanical properties of CrN/TiN multilayer coatings prepared by a combined HIPIMS/UBMS deposition technique

J. Paulitsch[1,*], P.H. Mayrhofer[2], W.-D. Münz[3], M. Schenkel[3]

[1] Materials Center Leoben Forschung GmbH, 8700 Leoben, Austria
[2] Department of Physical Metallurgy and Materials Testing, Montanuniversität Leoben, 8700 Leoben, Austria
[3] Systec SVS Vacuum Coating Technologies, 97753 Karlstadt, Germany

Abstract

CrN and TiN coatings are known for their high hardness and good wear resistance. The structure and the mechanical properties of such coatings can be improved by increasing the ion bombardment during film growth. As high power impulse magnetron sputtering (HIPIMS) is known to allow high ion densities in the plasma, with a small deposition rate, we study the structure and mechanical properties of CrN/TiN multilayer coatings deposited by combining HIPIMS with conventional unbalanced magnetron sputtering (UBMS).

Our results demonstrate that the microstructure of TiN coatings prepared by UBMS changes from dense columnar to open voided if a one fold substrate rotation is used where the films periodically leave and enter the plasma region in front of the target. Hence, also the hardness decreases from ~28 to 12 GPa if a one fold substrate rotation is used. This drawback can be overcome if the coatings are prepared by HIPIMS, resulting in hardness values of ~39 and 34 GPa without and with a one fold substrate rotation, respectively. Recently, we reported a corresponding behaviour of CrN coatings. In a multilayer arrangement of TiN and CrN, where the TiN layers are prepared by UBMS and the CrN layers are prepared by HIPIMS the hardness with around 26 GPa is also much higher as compared to 11 GPa of the TiN single layer deposited by UBMS. Hence, HIPIMS also influences the plasma conditions in front of the cathode operated by UBMS.

Introduction

Chromium and titanium nitride (CrN, TiN) thin films are well known for their unique properties like high hardness and good wear resistance. Therefore, great attention has been paid on the interrelation between microstructure, morphology and resulting mechanical properties of CrN and TiN [1-4]. In general, the coating's microstructure and morphology can be improved by applying substrate temperatures as high as 700 °C. This limits the deposition to thermally stable substrates such as cemented carbides. If high bias potentials are applied to the substrates their microstructure can also be improved. Former investigations on TiN showed, that with increased bias voltage the ion energy increases and causes a change of preferred (111) orientation into a pronounced (002) orientation. The drawback of using high ion energy by increasing the bias voltage is the generation of high residual stresses and high defect densities [5]. Detailed studies on the microstructure evolution during film growth yield optimized properties by using a low energy but intense ion bombardment during deposition [5,6]. Conventional unbalanced magnetron sputtering (UBMS), which is well established for physical vapour deposition (PVD) techniques, has the drawback of a low density and degree of ionized sputtered species. This often results in the formation of porous and underdense films with a high defect density if the deposition temperature is below 0.2–0.3 of the melting point of the generated film [7-12]. High power impulse magnetron sputtering (HIPIMS), being a novel PVD technique, allows a much higher ion to neutral ratio of the sputtered species due to the high power dissipation at the target. Ionization rates above 40% with also multiple ionized sputtered species are reported for HIPIMS [13,14,15]. In general HIPIMS is used only for the substrate pre-treatment, as it provides the advantage of improved adhesion due to implantation of metal species into the near substrate regions without generating droplets, as it is the case for cathodic arc pre-treatment [15,16,17].

Nevertheless, the high ion to neutral ratio of the HIPIMS process results also in a densification of the growing film due to increased adatom mobility. Recently we showed that the combination of HIPIMS and UBMS during deposition of CrN results in excellent mechanical and tribological properties [18]. Here we study the microstructure, mechanical properties and the resistance to adhesive and abrasive wear of TiN coatings prepared by

HIPIMS and UBMS without and with a one fold substrate rotation. Furthermore, the effect of HIPIMS on structure, mechanical properties, and wear resistance of CrN/TiN multilayer coatings is studied, by using a multilayer arrangement of TiN and CrN, where the CrN layers are prepared by HIPIMS and the TiN layers are prepared by UBMS.

Experimental

The depositions were performed in a Z700HPM PVD coating plant, manufactured by SVS Vacuum Coating Technology Karlstadt, Germany. All substrates are mounted on substrate holders which also allow planetary rotation. Depositions are conducted at a substrate temperature of 450 °C in a mixed Ar+N_2 (gas flow rates 1/1) glow discharge using one fold substrate rotation between two facing magnetron cathodes (one operating in HIPIMS the other in UBMS mode). The substrate holder allows a direct interaction of the HIPIMS and the UBMS plasma. The area of the magnetron sources are about 440 cm² each. For the preparation of multilayer, the UBMS cathode is equipped with a titanium target and the HIPIMS cathode is equipped with a chromium target. Prior to deposition, the substrates are thermally cleaned within the vacuum chamber at 650 °C for 30 minutes at a base pressure below 1 mPa [19], and both targets are sputter-cleaned with Ar ions for ten minutes.

For improved adhesion of the coatings, the substrates are ion etched using a Cr target sputtered by HIPIMS, whereas the HIPIMS supply is powered with 1 kW DC, in Ar atmosphere and applying a substrate bias potential of -1200 V. The repeat frequency in HIPIMS mode is 75 Hz with pulse duration of 150 µs. Thereby, surface near regions of the substrate are also implanting species generated during this HIPIMS pre-treatment step. The 100Cr6 steel disk (diameter 3.5 mm, 0.5 mm height) and Si (100) waver substrates are positioned at a distance of approximately 5 cm to the target while facing it. The maximum distance to the target at a one fold rotation is approximately 15 cm. The substrate holder rotates with seven rounds per minute during the HIPIMS etching and implantation process, as well as during deposition.

Recently we showed that the deposition of stoichiometric CrN films by HIPIMS requires a N_2 gas flow rate of 100 sccm [18]. Stoichiometric TiN films can be prepared by UBMS

using a gas flow rate of 30 sccm. Consequently, to meet the requirements of stoichiometric CrN and TiN layers in our CrN/TiN multilayer nitrogen and argon gas flow rates of 100 sccm each are used.

For the preparation of different CrN/TiN multilayer the cathode for the HIPIMS Cr target was set constant at 5.5 kW DC (DC power which fed the HIPIMS supply), whereas the UBMS Ti cathode power was individually varied between 4 and 7 kW. A substrate bias of -80 V was used for all deposition runs and the cathode frequency and pulse duration for the HIPIMS source was 75 Hz and 150 µs, respectively. The deposition time was varied between 45 and 60 minutes to obtain a film thickness of 2 µm for the combined HIPIMS/UBMS deposition. For comparison also single layers of TiN and CrN are prepared by UBMS and HIPIMS, respectively, without additional substrate heating and using a substrate temperature of 450 °C.

Scanning electron microscopy (SEM) investigations of coated Si (100) waver fracture cross-sections were carried out with a Zeiss EVO 50 type. Structural and phase analyses of coated steel substrates are conducted by X-ray diffraction (XRD) in the Bragg-Brentano mode using a Siemens D500 equipped with a CuK radiation source. The hardness (*H*) and modulus of indentation (*E*) of our coatings (on steel substrates) are obtained by nanoindentation with a Berkovich indenter using an ultra micro indentation system (UMIS). The maximum loads are ranging from 10 to 35 mN to keep the indentation depth below 10% of the film thickness. The values for *H* and *E* were obtained from analysing the loading and unloading segments of the indentation curves after the Oliver-Pharr method [20].

The sliding wear behaviour of the CrN/TiN multilayer were evaluated with an optical profilometer (Wyko NT1000) after ball on disk tests using a CSM tribometer equipped with an alumina ball (diameter of 6 mm) as counterpart, a normal load of 5 N and a distance of 1000 m. For coatings with decreased tribological properties the normal load and the distance have to be varied to achieve a valuable wear track. The tribological measurements were carried out without lubricant at room temperature (RT) at a humidity of ~25%. The abrasive sliding behaviours were evaluated with a CSM Calowear tester. The measurements were carried out at RT with an aqueous suspension of Al_2O_3 granulates

with a particle size of approximately 4 µm. The calculation of the abrasive wear coefficient, based on a ball-cratering geometry utilising a hard steel ball, was performed after [21]. The normal load was approximately 0.45 N for a ball with a diameter of 25.4 mm and approximately 0.8 N for the 30 mm hard steel ball. The total distance of the abrasive test was at minimum 50 m.

Results and discussion

Figure 1 indicates a preferred (200) orientation for the single layer TiN prepared by HIPIMS without substrate heating, whereas the films prepared by UBMS exhibit a pronounced (111) orientation (deposition of both films (HIPIMS and UBMS) with a one fold rotation). Generally the preferred orientation of TiN films changes from (200) to (111) with increased film thickness [22,23]. The (200) orientation can be stabilized by a high ion to neutral ratio during deposition [2,18]. Corresponding results are obtained here for the coatings prepared by HIPIMS due to the high ion density provided. Investigations for single layer CrN films exhibit increased mechanical and tribological properties by applying HIPIMS instead of UBMS [18], as thereby the (200) orientation can be stabilized, see Fig. 1. The (200) orientation peak of the HIPIMS deposited CrN film is overlapping with the substrate peak, which results in a peak broadening and decreases the resolution of the (200) peak (Figs. 1 and 4).

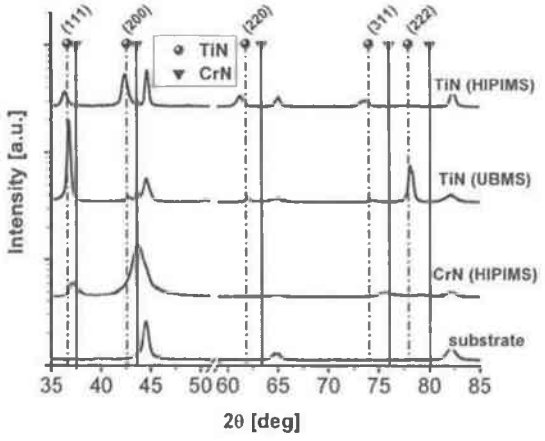

Fig. 1: XRD patterns of single layer TiN and CrN coatings prepared without substrate heating with HIPIMS and UBMS.

The XRD patterns of CrN and TiN coatings prepared by HIPIMS or UBMS without substrate rotation (static, where the substrate always faces the target) are comparable to those prepared with a one fold substrate rotation (dynamic). Nevertheless, the morphology of the coatings is strongly influenced if the deposition is conducted in the static or dynamic mode. Figures 2a and b show SEM fracture cross sections of our TiN coatings prepared by UBMS without and with substrate rotation, respectively. For the static deposition a dense microstructure with a smooth surface is obtained, whereas the dynamic deposition exhibits an underdense open voided microstructure with a rough surface, see Fig. 2b.

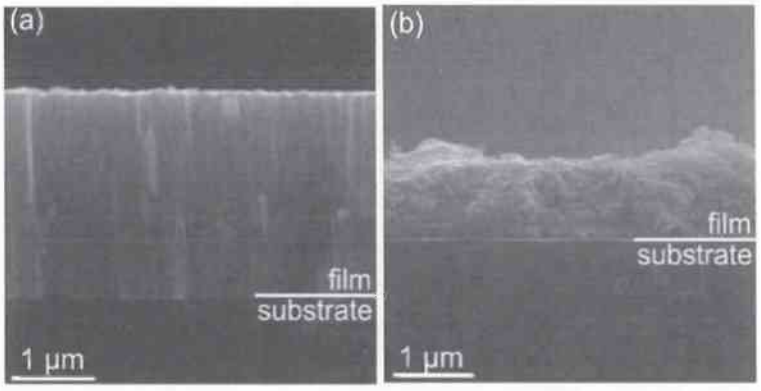

Fig. 2: SEM fracture cross sections of single layer TiN deposited by UBMS without substrate heating using no substrate rotation (a) and using a one fold substrate rotation (b).

By applying HIPIMS instead of UBMS this drastic change in morphology by changing from static to dynamic deposition can be avoided. Therefore, also the hardness and elastic modulus for TiN prepared by HIPIMS with and without substrate rotation are comparable, Fig. 3. For the static and dynamic depositions the same deposition parameters were used. The change in morphology from dense to open porous when changing from static to dynamic deposition results in an enormous reduction of the mechanical properties of TiN coatings prepared by UBMS, see Fig. 3. The hardness decreases from approximately 28 to 10 GPa and the modulus of indentation decreases from approximately 470 to 275 GPa, for changing from static to dynamic deposition, respectively. By applying HIPIMS for our TiN films H only decreases from ~38 to 34 GPa, and E only decreases from ~405 to 398 GPa, by changing from static to dynamic deposition, respectively. The hardness of the films prepared by HIPIMS is always higher than the films prepared by UBMS. This is

attributed to the better morphology and microstructure of films prepared by HIPIMS as compared to UBMS (see Figs. 1 and 2). The difference is even more pronounced when a substrate rotation is used during deposition. It has to be mentioned, that our dynamic depositions demonstrate extreme conditions as the substrates periodically leave and enter the plasma region in front of the target. Nevertheless, as the same is valid for UBMS and HIPIMS, the comparison demonstrates clearly the enormous advantage of HIPIMS over UBMS.

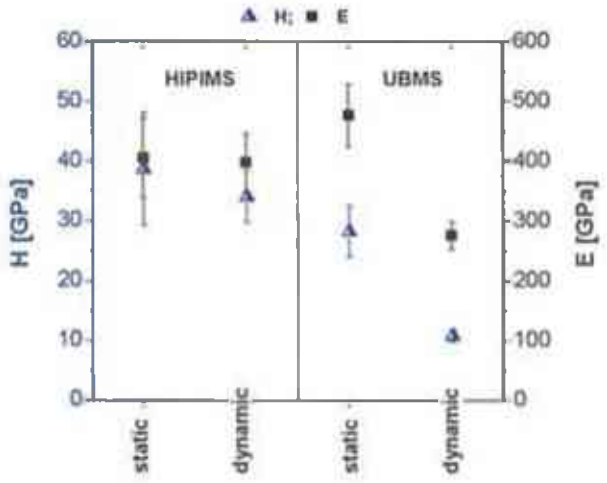

Fig. 3: Hardness and modulus of indentation of single layer TiN prepared without substrate heating by HIPIMS and UBMS without and with a one fold substrate rotation.

Residual compressive stresses of our coatings, measured with the cantilever beam technique [24], are in the range of 1 to 2 GPa.

For depositing a CrN/TiN multilayer, with optimized mechanical and tribological properties, the gas flow has to be adjusted to fulfil the requirements of both target materials and both cathodes, operating in UBMS and HIPIMS mode. The deposition of optimized TiN using HIPIMS requires a nitrogen gas flow between 8 and 10 sccm. Hence a combination with CrN prepared by HIPIMS or UBMS which requires a nitrogen gas flow of above 30 sccm is difficult. Furthermore, as the deposition rate is smaller for TiN compared to CrN, and HIPIMS exhibits smaller deposition rates as UBMS, our CrN/TiN multilayer films are deposited applying HIPIMS to the chromium cathode and UBMS to the titanium cathode with a gas flow rate of argon and nitrogen of 100 sccm each. The influence of various thickness ratios between the alternating TiN and CrN layers on the mechanical and

wear properties of our TiN/CrN multilayer coatings is investigated by applying different UBMS powers to the Ti cathode.

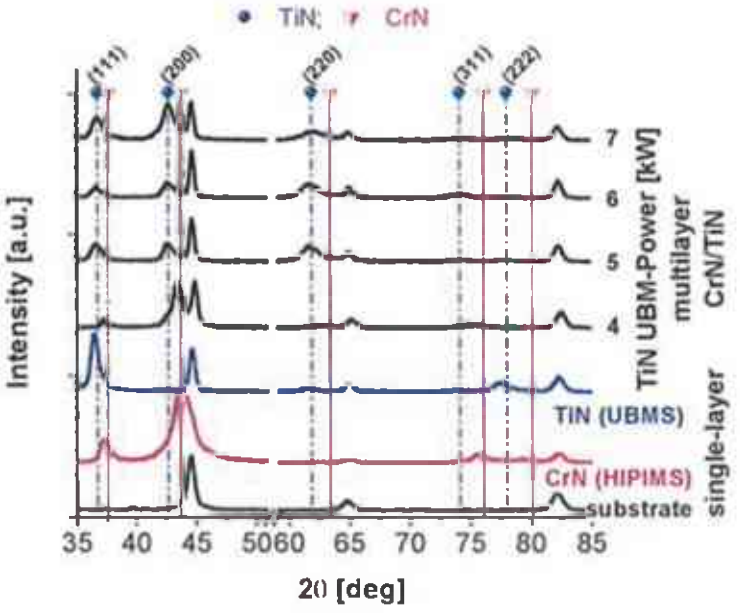

Fig. 4: XRD patterns of our multilayer CrN/TiN coatings prepared with different UBMS power at the Ti cathode using a substrate temperature of 450 °C. The XRD patterns of the single layer CrN and TiN prepared by HIPIMS and UBMS (4 kW) are added for comparison.

XRD investigations of our multilayer composed of CrN (HIPIMS) and TiN (UBMS) layers indicate the presence of TiN and CrN phases, see Fig. 4. With increasing power from 4 to 7 kW during UBM sputtering of the Ti cathode the intensities for the TiN reflections increase, indicating increasing thickness of the TiN layers of our CrN/TiN multilayer. According to deposition rate calculations the TiN layer thicknesses are 2.5 nm at 4 kW, 3.3 nm at 5 kW, 3.9 nm at 6 kW and 4.9 nm for 7 kW UBMS power. For the HIPIMS deposited CrN layers (with 5.5 kW set at the power supply) the calculations show a layer thickness of approximately 3.5 nm. With the highest UBMS power at the Ti cathode of 7 kW the coating still exhibits a (200) orientation, although a TiN single layer deposited by UBMS exhibits a preferred (111) orientation. This indicates that the CrN layer prepared by HIPIMS, which has a preferred (200) orientation (see Fig. 4), has a template effect for the TiN layer. Furthermore, the HIPIMS plasma can influence the plasma generated by UBMS and result in increasing deposition kinetics also for the TiN layer (which is prepared by UBMS).

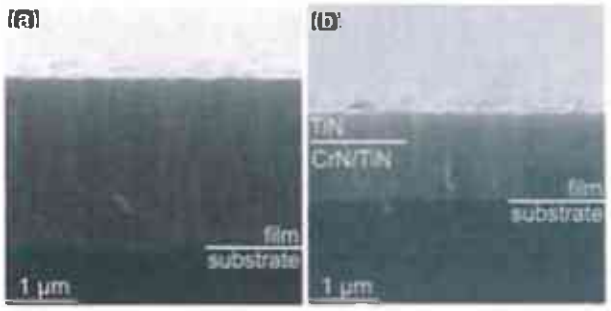

Fig. 5: SEM fracture cross sections of the multilayer CrN/TiN coating prepared with one fold rotation at a substrate temperature of 450 °C using a UBMS power at the Ti cathode of 4 kW (a) and adding a TiN top layer prepared by UBMS with 4 kW (b).

Figure 5a shows a SEM fracture cross section for our CrN/TiN multilayer prepared with a UBMS power at the Ti target of 4 kW. The coating exhibits a dense microstructure where the individual CrN and TiN layers can not be separated with the resolution of the used SEM equipment. Figure 5b illustrates a CrN/TiN multilayer with an approximately 0.5 µm thick TiN top layer prepared by UBMS. This top layer shows no difference in morphology and microstructure compared to the CrN/TiN multilayer underneath, which further emphasizes the above mentioned template effect of the CrN layer. Thereby, a dense TiN layer can be prepared by UBMS even during one fold substrate rotation.

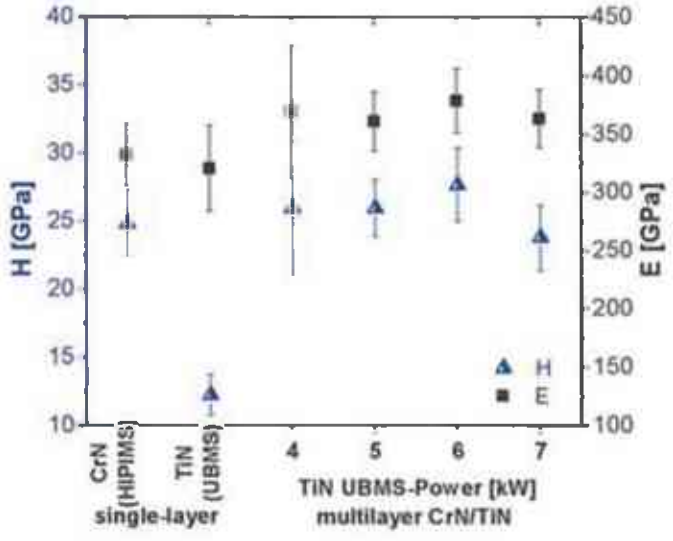

Fig. 6: Hardness and modulus of indentation of our multilayer CrN/TiN coatings prepared with different UBMS power at the Ti cathode using a substrate temperature of 450 °C. The values for H and E of the single layer CrN and TiN prepared by HIPIMS and UBMS (4 kW) are added for comparison.

Due to the dense microstructure the hardnesses and moduli of indentation are 26 ± 2.5 GPa and 369 ± 25 GPa for all CrN/TiN multilayers independent of the TiN layer thickness (i.e. UBMS power), see Fig. 6. The *H* and *E* values for our CrN/TiN multilayer are higher as compared to the single layer CrN prepared by HIPIMS and the single layer TiN prepared by UBMS with a one fold substrate rotation at 450 °C. The latter exhibits again a very low hardness value of ~12 GPa, which is comparable to the TiN film deposited without substrate heating. As already shown in Fig. 2, dynamic deposition with a one fold substrate rotation leads to an open porous structure of TiN with a loss in mechanical properties. This indicates that an increase in deposition temperature to ~450 °C, which is only ~0.2 of the melting (or dissociation) temperature of TiN, can not overcome the shortage of decreased growth kinetics if the substrates leave the plasma region during dynamic deposition.

Dense coating structures, as generated by HIPIMS or combined HIPIMS/UBMS, see Fig.6, generally provide a better resistance against crack formation and crack growth compared to the open porous structures of coatings prepared by UBMS with substrate rotation (see Fig.2b). Consequently, the wear resistance of coatings strongly depends on the preparation technique as also reported in [15].

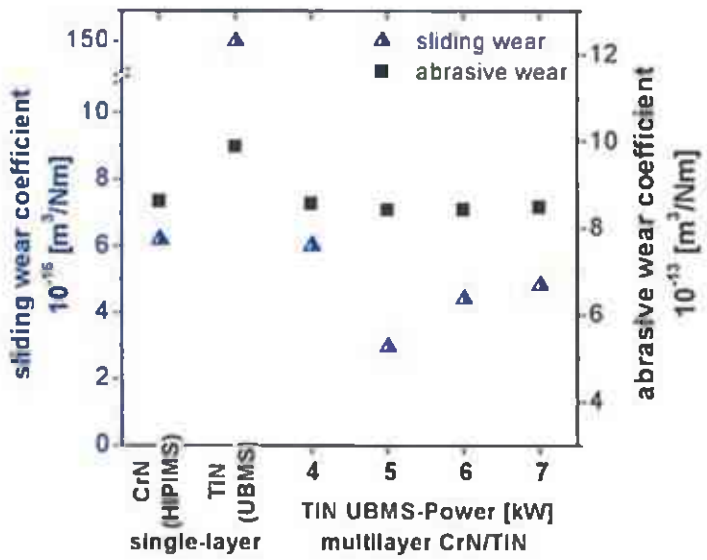

Fig. 7: Sliding and abrasive wear coefficients of our multilayer CrN/TiN coatings prepared with different UBMS power at the Ti cathode using a substrate temperature of 450 °C. The values for the single layer CrN and TiN prepared by HIPIMS and UBMS (4 kW) are added for comparison.

Figure 7 shows that the sliding wear coefficient of our multilayer coatings is in the range $3–6 \cdot 10^{-16}$ m³/Nm. The minimum value of approximately $3 \cdot 10^{-16}$ m³/Nm exhibits the coating where the Ti target is operated with 5kW UBMS power. The sliding wear coefficients for the CrN/TiN multilayer coatings are always below the values of $6.2 \cdot 10^{-16}$ m³/Nm and $150 \cdot 10^{-16}$ m³/Nm for the respective single layer coatings CrN (HIPIMS) and TiN (UBMS), respectively. The extremely high sliding wear coefficient for the single layer TiN is due to its very low hardness and open porous structure if prepared by UBMS with substrate rotation, compare Fig. 2b. The abrasive wear coefficients of the CrN/TiN multilayer coatings, measured with a CSM Calowear, are around $8.5 \cdot 10^{-13}$ m³/Nm independent of the used UBMS power at the Ti cathode. These values are slightly below the abrasive wear coefficients of $\sim 8.6 \cdot 10^{-13}$ m³/Nm and $9.9 \cdot 10^{-13}$ m³/Nm obtained for the respective single layer coatings CrN (HIPIMS) and TiN (UBMS). These results indicate that especially the sliding wear resistance is strongly influenced by the microstructure of the coatings.

Conclusion

Based on our results we can conclude that high power impulse magnetron sputtering (HIPIMS) is extremely effective in preparing dense single layer CrN and TiN coatings with excellent properties. Especially if a substrate rotation is used where the films leave and enter the plasma region in front of a target, HIPIMS exhibits a pronounced advantage of over UBMS. The microstructure of TiN coatings prepared by UBMS changes from dense columnar to open voided if a one fold substrate rotation is used, thereby also the hardness decreases from ~28 to 11 GPa, respectively. This drawback can be overcome if the coatings are prepared by HIPIMS, resulting in hardness values of ~39 and 34 GPa without and with a one fold substrate rotation, respectively. Corresponding results are obtained for CrN coatings. In a multilayer arrangement of TiN and CrN, where the TiN layers are prepared by UBMS and the CrN layers are prepared by HIPIMS the hardness with around 26 GPa is also much higher as compared to 12 GPa of the TiN single layer deposited by UBMS. This indicates that HIPIMS also influences the plasma conditions in front of the cathode operated by UBMS. Single layer TiN coatings deposited by UBMS

yield a pronounced (111) orientation. Contrary, the CrN/TiN multilayer coatings exhibit a strong (200) orientation, even for increased TiN layer thicknesses, which are obtained by increasing the UBMS power from 4 to 7 kW while keeping the HIPIMS power at 5.5 kW DC (DC power which fed the HIPIMS supply). Due to their dense microstructure our multilayers have hardness values of around 26 GPa, independent of the individual TiN layer thicknesses. The sliding wear coefficients of our multilayer TiN/CrN coatings are in the range of $3.5\text{-}6 \cdot 10^{-16}$ m³/Nm and hence much smaller as compared to $150 \cdot 10^{-16}$ m³/Nm obtained for the single layer TiN deposited by UBMS with a one fold substrate rotation.
Our results demonstrate that HIPIMS is an innovative process in influencing the microstructure and hence mechanical and tribological properties of hard coatings. The combination of HIPIMS and UBMS allows the preparation of dense coatings with excellent properties with increased deposition rates compared to single HIPIMS deposition.

Acknowledgement

Financial support by the Austrian Federal Government and the Styrian Provincial Government, represented by Österreichische Forschungsförderungsgesellschaft mbH and Steirische Wirtschaftsförderungsgesellschaft mbH, within the research activities of the K2 Competence Centre on "Integrated Research in Materials, Processing and Product Engineering", operated by the Materials Center Leoben Forschung GmbH under the frame of the Austrian COMET Competence Centre Program, is gratefully acknowledged.

References

[1] J.-E. Sundgren, Thin Solid Films 128 (1985) 21

[2] I. Petrov, L. Hultman, J.-E. Sundgren, J. E. Greene, Journal of Vacuum Science and Technology A 10 (2) (1992) 265

[3] L. Hultmann, J.-E. Sundgren, L.C. Markert, J.E. Greene, Journal of Vacuum Science and Technology A 7 (3) (1989) 1187

[4] J. Musil, S. Kadlec, J. Vyskocil, V. Valvoda, Thin Solid Films 167 (1988) 107

[5] I. Petrov, P. B. Barna, L. Hultman, J. E. Greene, Journal of Vacuum Science and Technology A 21(5) (2003) 117

[6] P. H. Mayrhofer, F. Kunc, J. Musil, C. Mitterer, Thin Solid Films 415 (2002) 151

[7] M. Lattemann, A. P. Ehiasarian, J. Bohlmark, P. Å. O. Persson, U. Helmersson, Surface and Coatings Technology 200 (2006) 6495

[8] P. H. Mayrhofer, G. Tischler, C. Mitterer, Surface and Coatings Technology 142-144 (2001) 78

[9] A. P. Ehiasarian, W.-D. Münz, L. Hultman, U. Helmersson, I. Petrov, Surface and Coatings Technology 163-164 (2003) 267

[10] J. E. Greene, S. A. Barnett, Journal of Vacuum Science and Technology 21(2) (1982) 285

[11] I. Petrov, L. Hultman, U. Helmersson, J. E. Sundgren, J. E. Greene, Thin Solid Films 169(2) (1989) 299

[12] L. Hultman, W.-D. Münz, J. Musil, S. Kadlec, I. Petrov, J. E.Greene, Journal of Vacuum Science and Technology A 9(3) (1991) 434

[13] A. P. Ehiasarian, R. New, W.-D. Münz, L. Hultman, U. Helmersson, V. Kouznetsov, Vacuum 65 (2002) 147

[14] V. Kouznetsov, K. Macák, J. M. Schneider, U. Helmersson, I Petrov, Surface and Coatings Technology, Volume 122 (1999) 290

[15] A. P. Ehiasarian, P. Eh. Hovsepian, L. Hultman, U. Helmersson, Thin Solid Films 457 (2004) 270

[16] C. Schönjahn, L. Donohue, D.B. Lewis, W.-D. Münz, I. Petrov, J, Journal of Vacuum Science and Technology A 18(4) (2000) 1718

[17] G. Hakansson, L. Hultman, J.-E. Sundgren, J.E. Greene, W.-D. Münz, Surface and Coatings Technology 48 (1991) 51

[18] J. Paulitsch, P. Mayrhofer, W.-D. Münz, M. Schenkel, Annual Technical Conference Proceedings of the Society of Vacuum Coaters (2007) 150

[19] W.-D. Münz, M. Schenkel, S. Kunkel, K. Bewilogua, M. Keunecke, R. Wittorf, 50th Annual Technical Conference Proceedings of the Society of Vacuum Coaters (2007) 155

[20] G. M. P. W.C. Oliver, Journal of Materials Research 7 (1992) 1564

[21] P. Berghofer, Diploma Thesis, University of Leoben, (2001)

[22] D. S. Rickerby, A. M. Jones, B. A. Bellamy, Surface and Coating Technology 37 (1989) 4375

[23] N. Schell, W. Matz, J. Bottinger, J. Chevallier, P. Kringhoj, Journal of Applied Physics 81 (1997) 6126

[24] P.H. Mayrhofer, C. Mitterer, Surface and Coatings Technology 133-134 (2000) 131

11 Paper IV

Low friction CrN/TiN multilayer coatings prepared by a hybrid HIPIMS/DCMS deposition technique

J. Paulitsch[1]*, M. Schenkel[2], A. Schintlmeister[3], H. Hutter[3], P.H. Mayrhofer[4]

[1)] Materials Center Leoben Forschung GmbH, 8700 Leoben, Austria
[2)] Systec SVS Vacuum Coating Technologies, 97753 Karlstadt, Germany
[3)] Institute of Chemical Technology and Analytics, Vienna University of Technology, 1060 Vienna, Austria
[4)] Department of Physical Metallurgy and Materials Testing, Montanuniversität Leoben, 8700 Leoben, Austria

Acknowledgement

CrN and TiN coatings, known for their high hardness and good wear resistance, are the topic of many research activities which concentrate on the correlation between plasma conditions, microstructure and resulting properties. By increasing the plasma density and the ion energy, the coating microstructure and their mechanical properties can be improved significantly. High power impulse magnetron sputtering (HIPIMS) has gained increasing scientific and industrial attention as it allows high plasma densities without the drawback of droplet formation. Recently, we showed that by a combination of HIPIMS with dc magnetron sputtering (DCMS) the properties of the coatings are comparable to those prepared solely with HIPIMS, but with the advantage of increased deposition rate.

Here, we show that for CrN_{HIPIMS}/TiN_{DCMS} multilayered coatings the friction coefficient decreases from 0.7 to 0.35 (with an almost constant hardness H around 25 GPa, and modulus of indentation around 375 GPa) when decreasing the bilayer period from 7.8 to 6.4 nm, while keeping the CrN_{HIPIMS} layer thickness constant at 3.2 nm. A further reduction of the friction coefficient at RT dry-sliding testing to ~0.25 or 0.05 is obtained when an additional HIPIMS cathode equipped with a Cr or Ti target material, respectively, is added to the process. These results were achieved with two and three fold substrate rotation, which meet the industrial requirements of uniform deposition on complex shaped specimens.

Introduction

Chromium and titanium nitride (CrN, TiN) thin films are well known for their excellent properties like high hardness and good wear resistance. Therefore, great attention has been paid on the interrelation between their microstructure, morphology and resulting mechanical properties [1-4]. In general, the coating's microstructure and morphology can be improved by applying substrate temperatures as high as 700 °C. The drawback by using high temperatures during deposition is the limited number of suitable substrate materials, which need to be thermally stable in the used temperature range. Reports for TiN films show that with increased bias voltage the energy of the ions, impinging at the substrate and growing film, increases and cause a densification and often a preferred (111) orientation [5]. The thereby obtained densification is generally connected with high defect densities and high residual stresses [5,6]. Detailed studies on TiN microstructure evolution during film growth yield optimized properties when using an ion bombardment of the growing film with a high ion/neutral ratio and low energy [7,8]. DC unbalanced magnetron sputtering (DCMS), which is a well established physical vapour deposition (PVD) technique, is generally characterized by a low ionization degree of sputtered species. This often results in formation of porous and underdense films with a high defect density if the deposition temperature is below 0.2–0.3 of the melting point of the films [8-13]. High power impulse magnetron sputtering (HIPIMS) allows a much higher ion to neutral ratio of the sputtered species due to the high power dissipation at the target. Ionization rates above 40%, where also multiple ionized sputtered species can occur, are reported for various target materials [14-16]. Due to the ability of implanting metal species into surface-near substrate regions by applying a high bias voltage during HIPIMS etching, the adhesion between coating and substrate can be optimized. Compared to a corresponding cathodic arc pre-treatment, the HIPIMS pre-treatment has the advantage of an essentially zero-droplet-rate and therefore an even further improved adhesion [16-18].

Furthermore, the high metal-ion and plasma density of the HIPIMS process is extremely beneficial for the coating morphology and structure itself. Recently, we showed that CrN and TiN coatings prepared by HIPIMS have a much higher density than their

corresponding DCMS counterparts [19]. Consequently, also the mechanical and tribological properties are increased for HIPIMS coatings compared to DCMS coatings. By a controlled combination of HIPIMS cathodes with DCMS cathodes the advantage of both processes can be combined, resulting in e.g., depositions with dense coating microstructure and high growth rates [20].

Here we show that for CrN_{HIPIMS}/TiN_{DCMS} multilayered coatings the friction coefficient decreases from 0.7 to 0.35 when decreasing the bilayer period from 7.8 to 6.4 nm, while keeping the CrN_{HIPIMS} layer thickness constant at 3.2 nm. A further reduction of the friction coefficient to ~0.25 or 0.05 at RT dry-sliding testing is obtained when an additional HIPIMS cathode equipped with a Cr or Ti target material, respectively, is added to the process. These results were achieved with two and three fold substrate rotation.

Experimental

The depositions were performed in a Z700HPM PVD coating plant, manufactured by Systec SVS Vacuum Coating Technology Karlstadt, Germany. The substrates, steel disks and Si (001) strips, are mounted on substrate holders which allow planetary rotation and face the targets at a minimum distance of 8 cm. All depositions are performed in a mixed Ar+N2 glow discharge with additional heating which results in a substrate temperature of approximately 400°C. Four different CrN/TiN multilayer coatings have been developed by varying the power at the DCMS Ti cathode between 4 and 7 kW while the HIPIMS Cr cathode was fed with 5.5 kW, using a one fold substrate rotation between these two facing cathodes. Two further variations are obtained by introducing a third cathode operating in HIPIMS mode, either equipped with a Cr or Ti target, using two and three fold substrate rotation. For convenience and easier identification these multilayer coatings are abbreviated with CrN/TiN/CrN and CrN/TiN/TiN, respectively. The deposition time was adjusted to achieve a film thickness of approximately 2 µm. More details on the deposition parameters used are reported in [19].

Prior to all depositions, the substrates are thermally cleaned within the vacuum chamber at a base pressure below 1 mPa [21], and both targets are sputter-cleaned with Ar ions. The substrates are ion etched in an Ar atmosphere using the Cr target in HIPIMS mode

and applying a substrate bias potential of -1000 V. To avoid cross-contaminations during this process, a constant sputtering potential of 180 V is applied to the Cr facing Ti target. Fracture cross-section scanning electron microscopy (SEM) investigations of coated Si (001) substrates were conducted in a Zeiss EVO 50 microscope. Detailed studies on morphology and film structure are evaluated using a Phillips CM 12 transmission electron microscope (TEM). Structure and phase analyses of coated steel substrates are conducted by X-ray diffraction (XRD) in the Bragg-Brentano mode using a Siemens D500 equipped with a CuK radiation source. Hardness (H) and modulus of indentation (E) of our coatings (evaluated on steel substrates) are obtained by nanoindentation with a Berkovich indenter using an ultra micro indentation system (UMIS). The maximum loads are ranging from 10 to 35 mN to keep the indentation depth below 10% of the film thickness. The values for H and E were obtained from analysing the loading and unloading segments of the indentation curves after the Oliver-Pharr method. The time-of-flight secondary ion mass spectrometry (ToF-SIMS) measurements were performed on a TOF.SIMS V instrument from IONTOF GmbH Muenster, Germany. The mass spectra were recorded by detection of positive secondary ions, generated by sample surface bombardment with 25 keV Bi+ ions in high current bunched mode. Depth profiles were acquired by sequential sputtering with 2 keV O_2+ ions in interlaced mode. In order to avoid crater edge effects, the Bi+ and O_2+ ion beams were scanned over 500 µm x 500 µm and 900 µm x 900 µm, respectively.
Dry sliding tribological investigations are conducted at RT using a CSM ball on disk (BOD) tribometer equipped with an alumina ball (diameter of 6 mm) as counterpart. A normal load of 1 N and sliding distances from 500 to 3500 m were used. Experiments are performed in ambient atmosphere (relative humidity ~25%), dry nitrogen, argon and synthetic air atmospheres (relative humidity ~1%), and in distilled water. The relative humidity was measured by a Testo 608-H2 hygrometer with an absolute error of 2% [23]. The sliding wear coefficients, of our multilayered coatings, are calculated after evaluating the wear track with a Wyko NT1000 optical profilometer.

Results and discussion

Figure 1 shows the intensity for Fe, Mn, Cr, and Ti species versus the implantation depth of HIPIMS ion etched steel samples (see experimental section), without depositing the CrN/TiN multilayer films, obtained by ToF-SIMS measurements. The Cr HIPIMS etching of the steel substrates at -1000V substrate bias resulted in an increased adhesion of our multilayer coatings, yielding a HF 1 value according to Rockwell adhesion testing [24]. The approximately 20 nm extension of the Cr signal within the region of Fe indicates that Cr was incorporated into the substrate, likely originating from implantation and surface near diffusion during the etching process.

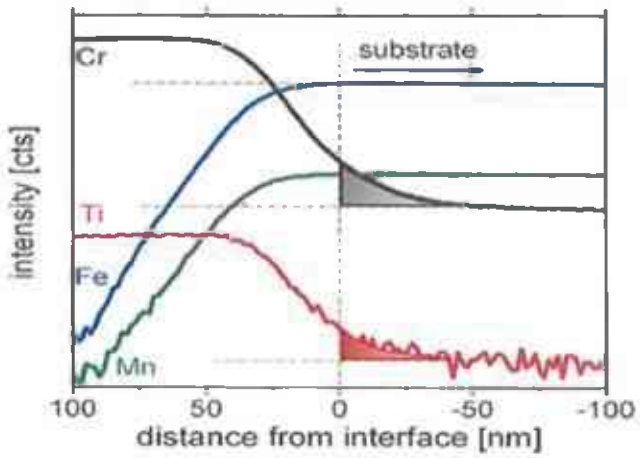

Fig. 1: SIMS analyses of the steel substrate surface near region after Cr HIPIMS etching.

Cr incorporation in stainless steel substrates by HIPIMS etching at −1200V substrate bias has already been reported by [10], who found an incorporation depth of approx. 40 nm by XTEM-EDS analysis. Schönjahn et al. observed deposition of a 10 nm thick Cr coating at - 600V substrate bias in a cathodic arc plasma, however at - 1200V their XTEM-EDS profiles suggest selective Cr incorporation within a depth of approx. 10 nm [17]. With respect to the thickness of the Cr layer and the depth of the Cr incorporation zone it has to be stated that our values represent estimations based on comparison of the total O_2+ sputter time with the depth of the sputter-craters as determined by white-light profilometry (Wyko NT1000 optical profilometer, see experimental section). Such a one-

to-one conversion of sputter time and erosion depth can lead to significant deviations in thickness/depth for materials with differing erosion rates. The profile also reveals a Cr and Ti film deposition of around 20 nm during the etching process. It is expected that this deposited layer is thinner when immediately after the etching process the deposition of the nitride layers start. The plot would also suggest diffusion of Fe and Mn into the Cr and Ti layer, but this effect is an artefact and mainly due to the high surface roughness of the HIPIMS etched steel substrate (R_a around 25 nm).

With decreasing the DCMS power at the Ti cathode from 7 to 4 kW at constant HIPIMS power of 5.5 kW at the Cr cathode the bilayer period decreases from 7.8 to 6.4 nm with a constant CrN layer thickness of 3.4 nm. These values are obtained after a simple estimation from the total coating thickness after single HIPIMS CrN and single DCMS TiN deposition including the one fold rotation frequency.

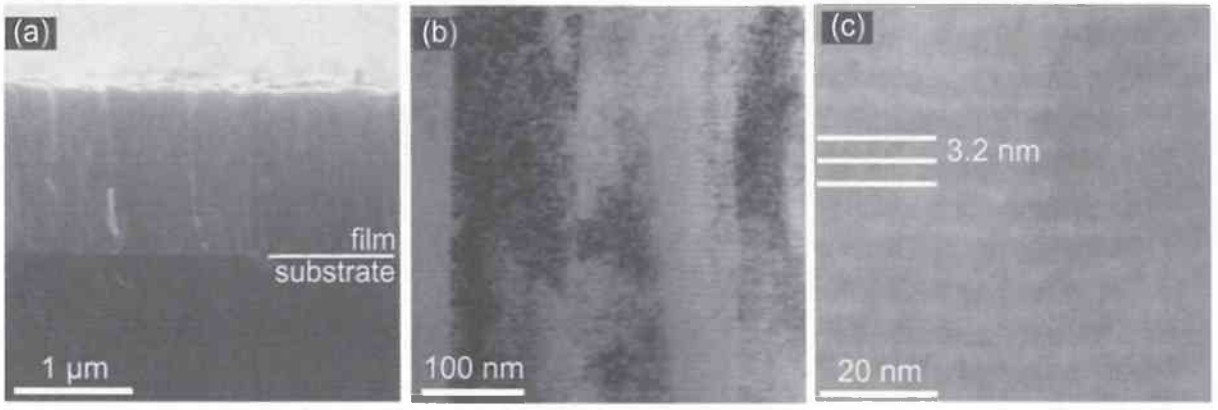

Fig. 2: SEM (a) and TEM (b, c) micrograph of multilayered CrN_{HIPIMS}/TiN_{DCMS} coating with bilayer period = 6.4 nm.

Figure 2a shows a SEM fracture cross section of the multilayered CrN/TiN coating prepared with a 5.5 kW supplied HIPIMS Cr cathode and a 4 kW powered DCMS Ti cathode. The film is characterized by a dense microstructure with a smooth surface. Figures 2b and 2c are cross-sectional TEM images of this CrN/TiN multilayer, showing the individual layers with a similar thickness of approximately 3.2 nm each. This result is in excellent agreement with the 3.4 nm estimated from the substrate rotation frequency and total film thickness of single HIPIMS and single DCMS nitrides.

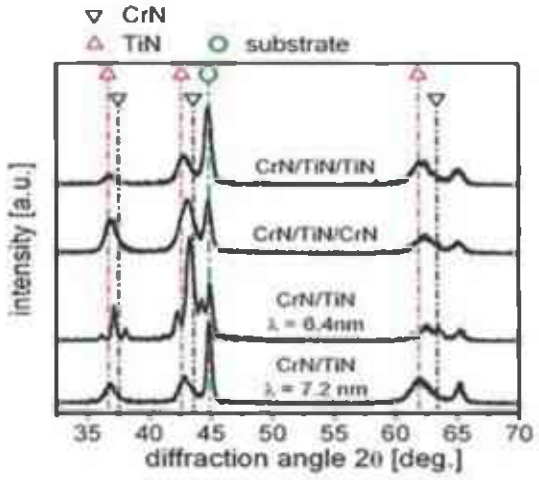

Fig. 3: XRD analyses of CrN_{HIPIMS}/TiN_{DCMS} coatings with bilayer period = 6.4 and 7.2 nm compared to CrN_{HIPIMS}/TiN_{DCMS} coatings deposited with additional CrN_{HIPIMS} (CrN/TiN/CrN) and TiN_{HIPIMS} (CrN/TiN/TiN) layers.

The XRD pattern, shown in Figure 3, of the CrN/TiN multilayer coatings indicate that with decreasing bilayer periods from 7.2 to 6.4 nm the negative and positive first and second order satellite peaks of the (200) and (111) primary reflections became more pronounced. This confirms the formation of a superlattice structure for the CrN/TiN multilayer coatings with a value of 6.4 nm [25,26]. Further increase of the bilayer period to values around 7.8 nm indicates no significant change in the XRD pattern compared to 7.2 nm. When a third cathode equipped with a Cr or Ti is introduced, which is operating in HIPIMS mode, to the deposition process of the CrN/TiN multilayer (where the facing Cr and Ti cathodes are fed with 5.5 kW HIPIMS and 4 kW DCMS, respectively) the negative and positive first and second order satellite reflexes of the (200) and (111) primary reflexes decrease in intensity again, see Figure 3. This indicates that the superlattice effect on the XRD patterns decrease as the alteration of HIPIMS CrN and DCMS TiN layers is interrupted by using a two and three fold substrate rotation at deposition and an additional HIPIMS CrN or TiN layer.

According to the dense morphology of our coatings, also the hardness and elastic modulus for CrN/TiN coatings deposited with one, two and three fold rotation are comparable with H values around 26 GPa and E values around 350 GPa, see Figure 4. As shown in former publications [19,20], the mechanical properties are changing drastically if

we change the rotation mode during DCMS deposition. The high ion density of the HIPIMS process, resulting in increased adatom mobility, allows depositions of coatings with high densities and increased properties even with multiple rotations during deposition.

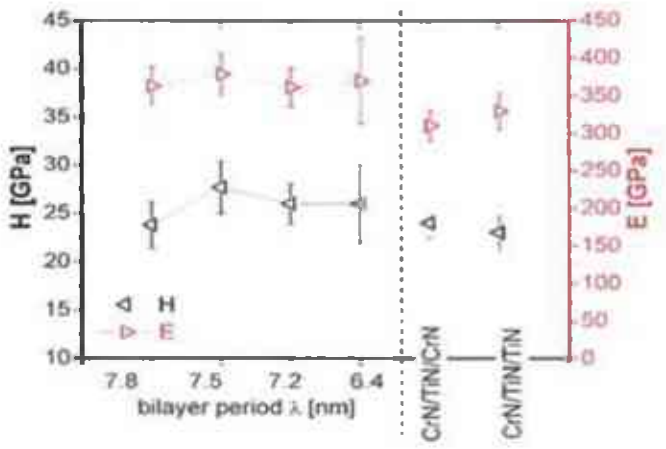

Fig. 4: Indentation hardness (H) and Young's modulus (E) of CrN_{HIPIMS}/TiN_{DCMS} coatings with bilayer periods from 6.4 to 7.8 nm compared to CrN_{HIPIMS}/TiN_{DCMS} coatings deposited with additional CrN_{HIPIMS} (CrN/TiN/CrN) and TiN_{HIPIMS} (CrN/TiN/TiN) layers.

Dense coating structures, as generated by HIPIMS or combined HIPIMS/DCMS deposition, generally provide a better resistance against crack formation and crack growth compared to the open porous structures of coatings prepared by DCMS with substrate rotation. Figure 5 shows RT dry-sliding BOD friction coefficients of the CrN/TiN multilayer coatings deposited by the hybrid HIPIMS/DCMS technique, using a one fold substrate rotation between the facing Cr_{HIPIMS} and Ti_{DCMS} cathodes with a bilayer period of 7.2 and 6.4 nm. The coatings with = 7.6 and 7.8 nm exhibit a comparable friction coefficient to the coating with = 7.2 nm shown in Figure 5. A further decrease in to 6.4 nm, where the CrN_{HIPIMS} and the TiN_{DCMS} layers are of comparable thickness, see Figure 2, causes a further reduction of μ to values around 0.35. The friction coefficient can further be decreased to values around 0.25 when additional CrN_{HIPIMS} layers (CrN/TiN/CrN) are introduced by a third cathode and using a three fold substrate rotation. When instead of these additional CrN_{HIPIMS} layers additional TiN_{HIPIMS} layers (CrN/TiN/TiN) are introduced (by equipping the third cathode with Ti) the friction coefficient can be even further decreased to values as

low as 0.05, which is comparable to DLC coatings [27-29]. The steady state low friction coefficient of 0.05 is obtained after a short running in period of ~100 m, see Figure 5.
The sliding wear coefficient of the CrN/TiN multilayer coatings is approximately $5.1 \cdot 10^{-16}$ m^3/Nm and $3 \cdot 10^{-16}$ m^3/Nm having a bilayer period of 7.2 and 6.4 nm, respectively. The CrN/TiN/CrN and the CrN/TiN/TiN multilayer coatings exhibit sliding wear coefficients of $1.2 \cdot 10^{-16}$ m^3/Nm and $6.17 \cdot 10^{-16}$ m^3/Nm, respectively.

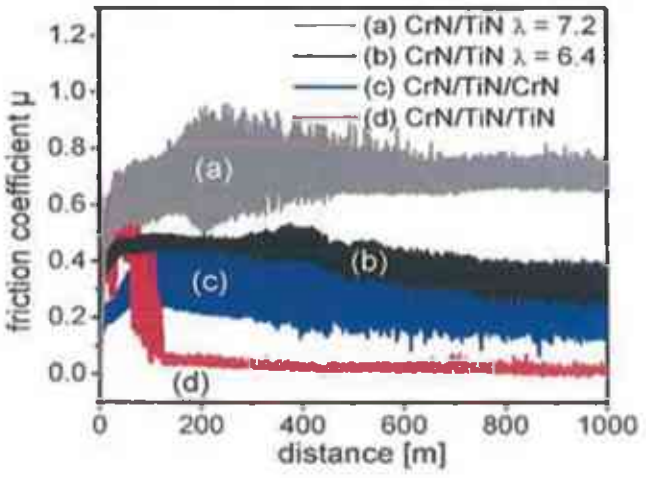

Fig. 5: BOD tests at ambient air conditions (relative humidity ~ 25 %) of CrN_{HIPIMS}/TiN_{DCMS} coatings with bilayer periods = 6.4 and 7.2 nm compared to CrN_{HIPIMS}/TiN_{DCMS} coatings deposited with additional CrN_{HIPIMS} (CrN/TiN/CrN) and TiN_{HIPIMS} (CrN/TiN/TiN) layers.

To investigate the influence of different atmospheric conditions on the tribological behaviour of our coatings, BOD tests were also conducted in dry Ar, N_2 and synthetic air as well as in distilled water, see Figure 6. For the tests in different atmospheres the acrylic box, housing the CSM BOD tester, was filled with Ar, N_2 and synthetic air. Measurements in distilled water were carried out by using a cylindrical sample holder which is especially used for tribological tests in lubricants. For the Ar, N_2 and synthetic air atmospheres the humidity was adjusted at values below 1%.
Figure 6 shows the effect of different atmospheres and humidity during dry sliding BOD tests for the CrN/TiN/TiN multilayer film which exhibit a steady-state friction coefficient of 0.05 in ambient air with ~25 % relative humidity. In Ar, N_2 and synthetic air with a relative humidity below 1 %, friction coefficients μ of 0.65 and 0.75 are obtained. Performing the test in a distilled water bath results in friction coefficient values in the range of 0.05 to

0.1, which is comparable to the tests in ambient air conditions. In non-oxidizing atmospheres (Ar and N_2) dry-sliding wear coefficients are around $4.3 \cdot 10^{-17}$ m^3/Nm, whereas values of $4.5 \cdot 10^{-15}$ m^3/Nm and $2.1 \cdot 10^{-15}$ m^3/Nm are obtained in synthetic air and distilled water, respectively.

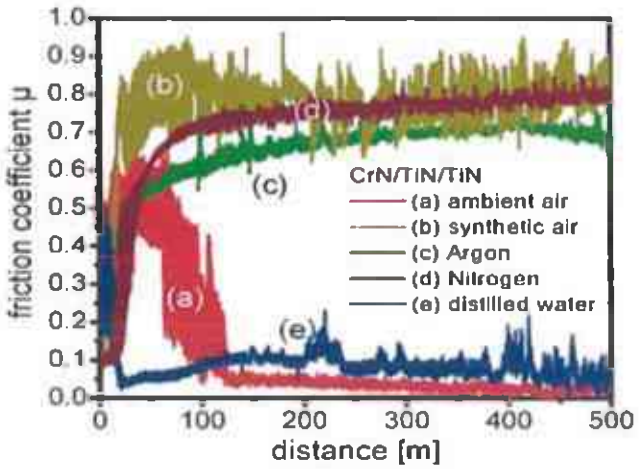

Fig. 6: Friction coefficient μ of CrN/TiN/TiN coatings evaluated after BOD test in different atmospheres: (a) ambient air (relative humidity ~ 25 %), (b) synthetic air, (c) Ar and (d) N_2 atmospheres (relative humidity ~ 1 %) and in (e) distilled water.

These results suggest that in a non-oxidizing atmosphere the wear performance is increased, because of reduced oxidation and formation of abrasive particles. But these conditions results in increased friction coefficients as the formation of solid (or even liquid) lubricants in the wear track is reduced [23].

The low friction behaviour of coatings like DLC or carbo-nitrides are based on forming graphite-like transfer layers, which act as lubricants during sliding [23,27-30]. The experiments in dry and humid atmospheric conditions, see Figure 6, suggest that for our coatings the low friction effect is caused by the formation of humidity-triggered layers during dry-sliding BOD testing. The wettability of these CrN/TiN coatings with different bilayer periods and the CrN/TiN/CrN and CrN/TiN/TiN multilayer coatings is investigated by contact angle measurements between a distilled water drop and the as deposited film surface, see Figure 7.

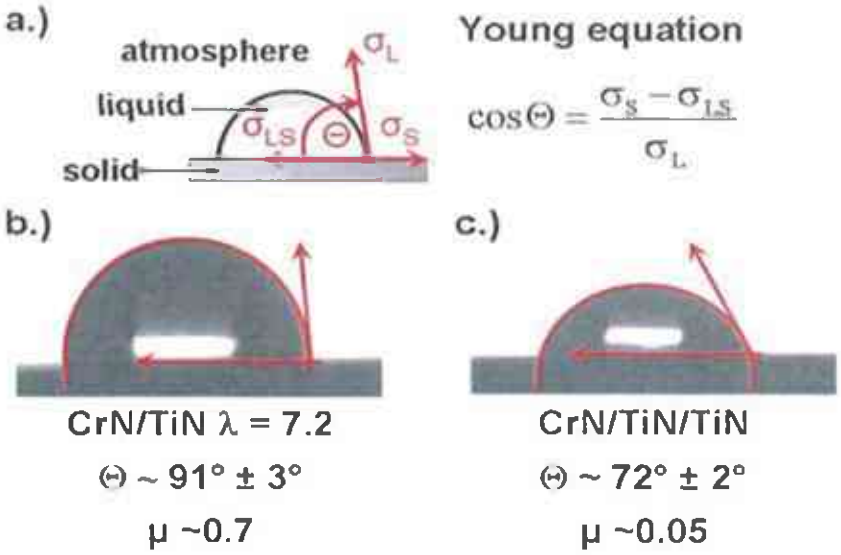

Fig. 7: Measurements of surface tension after Young's equation (a) by evaluating the contact angle of distilled water drops on the surface of the as deposited coating i.e. (b) CrNHIPIMS/TiNDCMS coating with bilayer period = 7.2 and (c) CrN_{HIPIMS}/TiN_{DCMS} coating deposited with addition TiN_{HIPIMS} layers (CrN/TiN/TiN).

According to the Young equation [31], the contact angle can be used to calculate the surface tension, and hence the wettability of the coatings. With increasing contact angle, the surface tension and wettability decreases, and vice versa. To minimize testing errors, between 10 and 15 water drops of constant volume of ~0.015 µl were dropped on the film surfaces having a roughness R_a of 12 ± 2 nm. The surface temperature and the analyzing delay to measure the contact angles was 4 s. Figure 7a shows the simplified Young equation and the contact angles of coatings with the highest friction coefficient (Figure 7b; bilayer period of 7.2 nm) and lowest friction coefficient (Figure 7c, CrN/TiN/TiN).

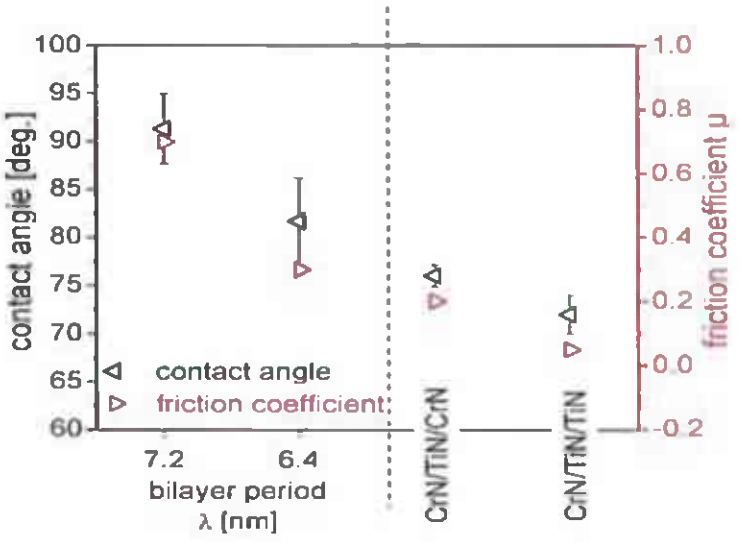

Fig. 8: Friction coefficient and contact angle for CrN_{HIPIMS}/TiN_{DCMS} coatings as a function of the bilayer period = 6.4 and 7.2 compared to CrN_{HIPIMS}/TiN_{DCMS} coatings deposited with additional CrN_{HIPIMS} (CrN/TiN/CrN) and TiN_{HIPIMS} (CrN/TiN/TiN) layers.

Figure 8 compares the evaluated data of the CrN/TiN multilayer coatings and indicates a correlation between their friction coefficient and the wetting angle. With increasing contact angle, hence decreasing surface tension and wettability, the friction coefficient increases. These results suggest that the low friction effect of our coatings during dry-sliding RT BOD testing is due to the formation of a lubricious film in the wear track, which is a result of the humid ambient atmosphere (relative humidity ~25 %) and the low wetting angle.

Summary and conclusions

Multilayered CrN_{HIPIMS}/TiN_{DCMS} coatings with various bilayer periods from 7.8 to 6.4 nm where the CrN_{HIPIMS} layer thickness were set constant at 3.2 nm were deposited with one-fold substrate rotation between two facing Cr and Ti targets operating in HIPIMS and DCMS mode, respectively. Independent of their bilayer period these coatings exhibit dense microstructures with smooth surfaces and hardness values around 25 GPa. Nevertheless during dry-sliding RT BOD tests decreasing friction coefficients from ~0.7 to 0.35 are obtained, when the bilayer period decreases from 7.8 to 6.4 nm, respectively.

When introducing a third HIPIMS operated cathode equipped with a Cr or Ti target to the CrN_{HIPIMS}/TiN_{DCMS} deposition and using a two- and three-fold substrate rotation the hardness is with ~25 GPa unchanged. In contrast, their friction coefficient μ in ambient air conditions (relative humidity around 25%) decreases to values of ~0.25 or 0.05, when equipping the additional HIPIMS operated cathode with a Cr or Ti target (i.e. CrN/TiN/CrN or CrN/TiN/TiN), respectively. Dry-sliding BOD tests of the CrN/TiN/TiN (μ ~ 0.05 in ambient atmosphere) in Ar, N_2 and synthetic air atmospheres (with a relative humidity of 1%) as well as in a distilled water bath clearly correlate the low friction coefficient with the humidity as values around 0.7 are obtained for tests in Ar, N_2 and synthetic air, whereas the tests in distilled water exhibit again μ values around 0.1. Measurements of the contact angle between a distilled water droplet and the coating surfaces show that with decreasing values, hence increasing wettability, also the friction coefficient decreases.

Based on our results we can conclude that by combining HIPIMS with conventional DCMS during deposition, CrN/TiN multilayer coatings with friction coefficients as low as 0.05, high hardness of ~ 25 GPa, and reasonable deposition rate can be obtained even for multi-fold substrate rotation. Especially the latter is of utmost importance to meet industrial requirements of uniform deposition on complex shaped specimens.

Acknowledgement

Financial support by the Austrian Federal Government and the Styrian Provincial Government, represented by Österreichische Forschungsförderungsgesellschaft mbH and Steirische Wirtschaftsförderungsgesellschaft mbH, within the research activities of the K2 Competence Centre on "Integrated Research in Materials, Processing and Product Engineering", operated by the Materials Center Leoben Forschung GmbH under the frame of the Austrian COMET Competence Centre Program, is gratefully acknowledged.

References

[1] J.-E. Sundgren, Thin Solid Films 128 (1985) 21

[2] I. Petrov, L. Hultman, J.-E. Sundgren, J. E. Greene, Journal of Vacuum Science and Technology A 10 (2) (1992) 265

[3] L. Hultmann, J.-E. Sundgren, L.C. Markert, J.E. Greene, Journal of Vacuum Science and Technology A 7 (3) (1989) 1187

[4] I. Petrov, P. B. Barna, L. Hultman, J. E. Greene, Journal of Vacuum Science and Technology A 21(5) (2003) 117

[5] P.H. Mayrhofer, M. Geier, C. Löcker, L. Chen, International Journal of Materials Research 100 (2009) 8

[6] I. Petrov, P. B. Barna, L. Hultman, J. E. Greene, Journal of Vacuum Science and Technology A 21(5) (2003) 117

[7] P. H. Mayrhofer, F. Kunc, J. Musil, C. Mitterer, Thin Solid Films 415 (2002) 151

[8] M. Lattemann, A. P. Ehiasarian, J. Bohlmark, P. Å. O. Persson, U. Helmersson, Surface and Coatings Technology 200 (2006) 6495

[9] P. H. Mayrhofer, G. Tischler, C. Mitterer, Surface and Coatings Technology 142-144 (2001) 78

[10] A. P. Ehiasarian, W.-D. Münz, L. Hultman, U. Helmersson, I. Petrov, Surface and Coatings Technology 163-164 (2003) 267

[11] J. E. Greene, S. A. Barnett, Journal of Vacuum Science and Technology 21(2) (1982) 285

[12] I. Petrov, L. Hultman, U. Helmersson, J. E. Sundgren, J. E. Greene, Thin Solid Films 169(2) (1989) 299

[13] L. Hultman, W.-D. Münz, J. Musil, S. Kadlec, I. Petrov, J. E.Greene, Journal of Vacuum Science and Technology A 9(3) (1991) 434

[14] A. P. Ehiasarian, R. New, W.-D. Münz, L. Hultman, U. Helmersson, V. Kouznetsov, Vacuum 65 (2002) 147

[15] V. Kouznetsov, K. Macák, J. M. Schneider, U. Helmersson, I Petrov, Surface and Coatings Technology, Volume 122 (1999) 290

[16] A. P. Ehiasarian, P. Eh. Hovsepian, L. Hultman, U. Helmersson, Thin Solid Films 457 (2004) 270

[17] C. Schönjahn, L. Donohue, D.B. Lewis, W.-D. Münz, I. Petrov, J, Journal of Vacuum Science and Technology A 18(4) (2000) 1718

[18] G. Hakansson, L. Hultman, J.-E. Sundgren, J.E. Greene, W.-D. Münz, Surface and Coatings Technology 48 (1991) 51

[19] J. Paulitsch, P.H. Mayhofer, W.-D. Münz, M. Schenkel, Thin Solid Films 517 (2008) 1239

[20] J. Paulitsch, P. Mayrhofer, W.-D. Münz, M. Schenkel, SVC - 50th Annual Technical Conference Proceedings, ISBN: 0737-5921 (ISSN) (2007) 150

[21] W.-D. Münz, M. Schenkel, S. Kunkel, K. Bewilogua, M. Keunecke, R. Wittorf, SVC - 50th Annual Technical Conference Proceedings, ISBN: 0737-5921 (ISSN) (2007) 155

[22] G. M. P. W.C. Oliver, Journal of Materials Research 7 (1992) 1564

[23] M. Rebelo de Figueiredo, J. Neidhardt, R. Kaindl, A. Reiter, R. Tessardi, C. Mitterer, Wear 265 (2008) 525

[24] VDI guideline 3842 (2001)

[25] J. Birch, T. Joelsson, F. Eriksson, N. Ghafoor, L. Hultman, Thin Solid Films 514 (2006) 10

[26] H. C. Barshilia, A. Jain, K. S. Rajam, Vacuum 72 (2004) 241

[27] P.H. Mayrhofer, C. Mitterer, L. Hultmann, H. Clemens, Progress in Material Science 51 (2006) 1032

[28] A. Grill, Diamond related Materials 8 (1999) 428

[29] C. Donnet, Surface and Coatings Technology 100-101 (1998) 180

[30] A.A. Voevodin, S.D. Walck, J.S. Zabinski, Wear 203-204 (1997) 516

[31] T. Young, Philosophical Transaction of the Royal Society London 95 (1805) 65